Die approbierte gedruckte Originalversion dieser Diplomarbeit ist an der TU Wien Bibliothek verfügbar
The approved original version of this thesis is available in print at TU Wien Bibliothek.

Die approbierte gedruckte Originalversion dieser Diplomarbeit ist an der TU Wien Bibliothek verfügbar
The approved original version of this thesis is available in print at TU Wien Bibliothek.

Technical University of Vienna

Development of a sensor-integrated organ-on-chip platform for the investigation of size-dependent effects on neural differentiation of P19 embryoid bodies

Master's Thesis

Daniel Rieger

11731664

Supervisors
Prof. Dr. rer. nat. Heinz Wanzenböck
Department of Electrical and Computer Engineering

Prof. Dipl.-Ing. Dr. Peter Ertl
Department of Applied Synthetic Chemistry

submitted Oct 02nd, 2022

Die approbierte gedruckte Originalversion dieser Diplomarbeit ist an der TU Wien Bibliothek verfügbar
The approved original version of this thesis is available in print at TU Wien Bibliothek.

Kurzfassung

Neuronale Zellkulturen werden häufig als Forschungsmodelle für die Untersuchung der Entwicklung des Nervensystems oder für Neuropathien verwendet. Damit davon abgeleitete Erkenntnisse auf den Menschen angewandt und Therapien entwickeln werden können, ist eine möglichst realitätsnahe Zellkultur für die Validität dieser Modelle entscheidend. Organ-on-Chip (OOC) Systeme mit drei-dimensionalen Zellkulturtechniken gelten dabei als innovative Ansätze für solche Modelle.

Diese Diplomarbeit behandelt die Planung, Herstellung, Charakterisierung und Erprobung einer mikrofluidischen Organ-on-a-Chip (OOC) - Plattform für die Untersuchung von größenbedingten Unterschieden in der neuronalen Differenzierung von muralen P19 Embryonalkarzinomzellen. Zellen dieser Linie durchlaufen bei Exposition mit Retinsäure eine dem Menschen auf zellulärer und signalmolekularer Ebene ähnliche embryogenetische Entwicklung, wenn sie in multizellulären Spheroiden, auch Embryoid Bodies genannt, angeordnet sind. Im Rahmen dieses Projekts wurde der Einfluss verschiedener Zellsaatdichten der Embryoid Bodies auf Wachstum, Größe, Morphologie, elektrischer Aktivität sowie Differenzierungseffizienz systematisch untersucht. Langfristig kann dieses Modell darüber hinaus zur Untersuchung des Nervensystems und der Erforschung neurologischer Krankheiten dienen. Es wurde ein Multielektrodenarray (MEA) zur Messung elektrophysiologischer Signale wie Aktionspotentiale integriert wurde, wobei drei verschiedene Herstellungsprozesse des MEAs erprobt wurden. Die Entwicklung dieses OOC in-vitro Modells ist motiviert durch Hindernisse in der aktuellen wissenschaftlichen Praxis aufgrund hoher Kosten, ethischer Bedenken oder schwacher Aussagekraft der Ergebnisse bisher existierender in-vitro Modelle.

Das Multielektrodenarray wurde durch photolithographische Herstellungsprozesse im Reinraum hergestellt und auf elektrischer Leitfähigkeit getestet. Es wurden Mikroelektroden mit verschieden dicken Ti/Au - Beschichtungsprozessen sowie einer optisch transparenten Ti/ITO/Au - Schicht aufgesputtert. Die elektrische Charakterisierung ergab beim Ti/Au-MEA mit erhöhter Leitschichtdicke die beste Leitfähigkeit. In der Folge wurde das mikrofluidische Zellreservoirsystem mit vier getrennten Saatkammern per 3D-Modellierung designed, flussmechanisch simuliert, aus PDMS hergestellt und auf dem MEA positioniert und gebondet. Zur Untersuchung der P19 Krebszelllinie wurden verschiedene Färbetechniken und optische Analysemethoden herangezogen sowie elektrophysiologische Messungen der differenzierten P19-Zellen auf dem MEA-PDMS-Chip durchgeführt.

Die P19-Spheroide zeigten gute Viabilität, Differenzierungsfähigkeit und elektrische Aktivität und konnten erfolgreich am Chip überleben und Neuriten bilden. Bei den P19-Zellspheroiden wurde die Größenentwicklung in Abhängigkeit der Saatzelldichte sowie eine Obergrenze der Saatdichte von 5000 Zellen/Titer festgestellt, da darüber liegende Saatdichten zu hohem Auftreten von toten Zellbestandteilen sowie veränderter Morphologie der Spheroide führt. Weiterhin wurde ein Ansteigen der Differenzierungseffizienz mit höherer Saatzahl gefunden mit einem Maximum bei 1000 Zellen/Titer, weshalb diese Dichte für weitere Untersuchungen empfohlen wird. Außerdem wurde bei größeren Spheroiden die Varianz der Differenzierungsrate immer größer, sodass kleinere Spheroide reproduzierbarere Ergebnisse liefern, sodass unter Beachtung dieser Parameter eine optimale Validität erwartet werden kann. Die Messung der elektrischen Aktivität ergab keine nachweisbaren elektrischen Signale, wobei in einer Fehleranalyse mehrere potentielle Problemquellen identifiziert wurden. Anschließend wurde eine optimierte Designiteration des PDMS-Chips vorgestellt.

Die im Rahmen dieses Projektes hergestellte mikrofluidische OoC-Plattform kann erfolgreich zur Zucht von P19 Embryoid Bodies und in zukünftigen Projekten zur Untersuchung größenabhängiger Unterschiede in der neuronalen Differenzierung eingesetzt werden. Langfristig kann diese als in-vitro Modell zur Erforschung des Nervensystems und neurologische Erkrankungen benutzt werden.

Die approbierte gedruckte Originalversion dieser Diplomarbeit ist an der TU Wien Bibliothek verfügbar
The approved original version of this thesis is available in print at TU Wien Bibliothek.
TU WIEN Bibliothek Your knowledge hub

Abstract (EN)

Neural cell cultures are commonly used as research models for the investigation of the development of the nervous system and neurological diseases. To ensure high validity of the results derived by such models, cell cultures need to be designed as realistic as possible. Organ-on-chip (OOC) systems with three-dimensional (3D) cell culture techniques are regarded as an innovative approach for such models.

This master's thesis deals with the planning, designing, producing and evaluation of a microfluidic organ-on-chip platform with an integrated multielectrode array and the investigation of size-dependent influence on the differentiation of P19 embryonal carcinoma cell line, organised in a multicellular spheroid called embryoid body. In detail, the influence of the seeding density of P19 embryoid bodies on growth, size, morphology, electrical activity and differentiation efficiency has been examined.

This cell line shows embryogenetic and neurogenetic similarities in terms of molecular expression and signalling pathways and is ideal for modelling neurodevelopmental diseases when cultured as a multicellular spheroid in exposition to retinoic acid. The resulting in vitro research model can aid in the investigation of neurological diseases on a cellular and molecular level and can function as an alternative to animal models or other in vitro models, which suffer from rising costs, ethical concerns and low translatability of the results.

The multielectrode array was produced with microfabrication technology using photolithographic thin film deposition processes in the cleanroom. Two thin film processes with titanium and gold (Ti/Au) as conduction layer with varying thickness and one optically transparent microelectrode array with titanium, indium tin oxid and gold (Ti/ITO/Au) thin film design were produced. In the following assessment of their electrical conductivities the Ti/Au-MEA with increased conduction layer thickness yielded the lowest resistivity. The microfluidic cell culturing chip with four seeding chambers was designed in 3D, fluid-mechanically characterised, produced with PDMS and bonded to the MEA. For the investigation of the P19 embryoid bodies various dyeing techniques and optical analysis methods have been used. Finally, an electrophysiological measurement of neurophysiological activity of the differentiated P19 embryoid bodies on the self-built MEA-PDMS-system has been executed.

The P19 spheroids demonstrated high viability, differentiation capability towards neural tissue and calcium ion-channel activity, which points towards spontaneous action potential generation. The embryoid bodies yielded a positive correlation between size and initial seeding density with a reasonable cut-off density of 5000 cells per well. Above this seeding density morphological malformations and high amounts of floating cell debris occur. The P19 cell spheroids showed a significant correlation between high differentiation efficiency and high seeding density with increasing variance, so that smaller spheroids yield lower differentiation rates but higher reproducibility. Therefore, high validity of results can be expected under consideration of these parameters. The P19 embryoid bodies could successfully be seeded on the chip, where they proliferated and formed neural processes. Continuous fluid mechanical examination displayed neglectable fluid shear stresses. The electrophysiological measurements yielded inconclusive recordings. An error analysis revealed possible sites of optimisation, and a redesign with improved parameters of the PDMS chip is presented.

The microfluidic organ-on-chip platform, which was designed and built in this thesis, can be used for growing P19 embryoid bodies and investigate size-dependent differences in the neural differentiation. It can serve as an in vitro model for future investigations around diseases of the central nervous system, like neurodevelopmental diseases.

Die approbierte gedruckte Originalversion dieser Diplomarbeit ist an der TU Wien Bibliothek verfügbar
The approved original version of this thesis is available in print at TU Wien Bibliothek.

Erklärung

Hiermit erkläre ich, dass die vorliegende Arbeit gemäß dem Code of Conduct – Regeln zur Sicherung guter wissenschaftlicher Praxis (in der aktuellen Fassung des jeweiligen Mitteilungsblattes der TU Wien), insbesondere ohne unzulässige Hilfe Dritter und ohne Benutzung anderer als der angegebenen Hilfsmittel, angefertigt wurde. Die aus anderen Quellen direkt oder indirekt übernommenen Daten und Konzepte sind unter Angabe der Quelle gekennzeichnet. Die Arbeit wurde bisher weder im In– noch im Ausland in gleicher oder in ähnlicher Form in anderen Prüfungsverfahren vorgelegt.

Ort, Datum

Unterschrift

Die approbierte gedruckte Originalversion dieser Diplomarbeit ist an der TU Wien Bibliothek verfügbar
The approved original version of this thesis is available in print at TU Wien Bibliothek.
TU WIEN Bibliothek Your knowledge hub

Die approbierte gedruckte Originalversion dieser Diplomarbeit ist an der TU Wien Bibliothek verfügbar
The approved original version of this thesis is available in print at TU Wien Bibliothek.

Contents

Die approbierte gedruckte Originalversion dieser Diplomarbeit ist an der TU Wien Bibliothek verfügbar
The approved original version of this thesis is available in print at TU Wien Bibliothek.

Die approbierte gedruckte Originalversion dieser Diplomarbeit ist an der TU Wien Bibliothek verfügbar
The approved original version of this thesis is available in print at TU Wien Bibliothek.
TU Bibliothek WIEN Your knowledge hub

List of Figures

Die approbierte gedruckte Originalversion dieser Diplomarbeit ist an der TU Wien Bibliothek verfügbar
The approved original version of this thesis is available in print at TU Wien Bibliothek.

List of Tables

Die approbierte gedruckte Originalversion dieser Diplomarbeit ist an der TU Wien Bibliothek verfügbar
The approved original version of this thesis is available in print at TU Wien Bibliothek.

Die approbierte gedruckte Originalversion dieser Diplomarbeit ist an der TU Wien Bibliothek verfügbar
The approved original version of this thesis is available in print at TU Wien Bibliothek.

List of Abbreviations

2D	Two-Dimensional
3D	Three-Dimensional
ADME	Absorption, Distribution, Metabolism, Excretion
BFM	Brightfield Microscopy
CNS	Central Nervous System
CFD	Continuous Fluid Dynamics
DI	Deionised Water
EB	Embryoid Body
ECM	Extracellular Matrix
ETHD	Ethidium Homodimer
ESC	Embryonal Stem Cell
ICP	Inductively Coupled Plasma:
IHC	Immunohistochemistry
iPSC	induced Pluripotent Stem Cells
ITO	Indium Tin Oxide
HP	Hotplate
MEA	Multielectrode Array
MCS	Multichannel Systems
OOC	Organ-on-Chip
PDMS	Polydimethylsiloxan
PECVD	Plasma-Enhanced Chemical Vapour Deposition
RIE	Reactive Ion Etching
RT	Roomtemperature
Ti/Au	Titanium-gold

Die approbierte gedruckte Originalversion dieser Diplomarbeit ist an der TU Wien Bibliothek verfügbar
The approved original version of this thesis is available in print at TU Wien Bibliothek.

Die approbierte gedruckte Originalversion dieser Diplomarbeit ist an der TU Wien Bibliothek verfügbar
The approved original version of this thesis is available in print at TU Wien Bibliothek.

Die approbierte gedruckte Originalversion dieser Diplomarbeit ist an der TU Wien Bibliothek verfügbar
The approved original version of this thesis is available in print at TU Wien Bibliothek.

Chapter 1

Aims of the thesis

The pursuit of innovative diagnostic and therapeutic approaches for diseases is limited by the ability of research models to mimic the complexity of organisms. Especially in neuroscience, finding suitable, practical and rapidly adaptable models that mimic the development of the human nervous system and enable the investigation of genetic cues and signalling pathways impose enormous challenges to the scientific community due to the vast complexity of the central nervous system (CNS). A majority of current efforts in medical and clinical research focuses intensely on in vivo animal models as well as in vitro models with animal or human cell lines.

Classical research models like animal models suffer e.g. from ethical concerns, high husbandry costs and limited applicability to humans, while current in vitro approaches with animal or human cell lines are often oversimplified and can not mimic physiological conditions well enough to be translated to both animal or human in vivo. Due to the significant phylogenetic differences, it is generally challenging to gain knowledge about the human nervous system from e.g. a mouse in vitro model directly. Despite some limitations of animal in vivo models, the results allow to understand the link between human in vitro to human in vivo models. Therefore, as an intermediary transfer model, a mouse cell model will still give fundamental insights.

As an alternative to in vivo or conventional cell culture models, organ-on-a-chip technology has been developed to mimic tissues, single organs and even multiple organs with growing complexity under approximate physiological conditions. These combined approaches of in vitro OOC devices benefit from their rapid adaptability, reproducibility, low costs and advanced imaging possibilities. For this reason, they are especially valuable for early-stage pharmaceutical research.

One promising candidate for the investigation of vertebrate embryogenesis and particularly neurogenesis is the P19 embryonal carcinoma cell (ESC) line. A multitude of publications report the directed differentiation of P19 ESC line into neural tissue in a 3D cell culture by the generation of multicellular aggregates. The formation of cell aggregates leads to a spatial multicellular structure called embryoid bodies (EBs), which recapitulates the early stages of embryonic development on a cellular and molecular level. These neural spheroids are also widely used to produce electrically active neural tissue. [1] They have been shown to simulate certain aspects of human neurogenesis and exhibit similarities to human midbrain tissue. [2] Furthermore, the P19 ESC is known to be a stable, quickly differentiating and thoroughly examined cell line. It offers a fast iteration cycle in design, production, examination and reevaluation of experimental setups, which all account to the fact that the P19 cell line is one of the most well-researched cell lines, with widespread contributions around the mechanics of differentiation, agglomeration and embryogenesis. [3]

The application of the P19 embryoid bodies in a research model for neurogenetic studies requires precise control over size, morphology and reliable differentiation mechanics and thus gene expression profiles. P19 cells are especially well-known to differentiate towards different kind of tissue depending on the size of the EB, as the gene expression of cytokines varies with the size of the EB. [4] Therefore, size control enables a better-defined cell fate determination of EBs. [5] Also, the influence of the cell location within an EB on the cell type determination during differentiation is well-established due to local differences in cytokine generation.

Despite this, little is known about the interplay between the amount of cells seeded per culturing well and its influence on the differentiation efficiency, which denotes the ratio of differentiated to undifferentiated cells within the embryoid body. The cell density influences the chemical cell-cell communication, which regulates cell growth, metabolism and differentiation. Previous studies implemented differing P19 cultivation protocols in their experiments with contradictory results. Precise control of the properties of the produced P19 embryoid bodies in terms of size, morphology and cell differentiation is crucial for their reproducible production. This is necessary for a well-defined scientific model, especially for its intended use in modelling neurogenetic events on a molecular level or for other advanced applications like drug screenings. Therefore, the correlations between cell seeding quantity per well and size, morphology and differentiation efficiency of the embryoid bodies will be examined in a systematic series of experiments in the course of this thesis.

In order to achieve this, a combined approach of microfluidics and multielectrode array (MEA) techniques is used in the development of the OOC device. The MEA offers non-invasive electrical sensors to measure changes in the electrical field caused by the cells. The microfluidic system offers precise control over chemical gradients like biochemical triggers and an environment for the cells to proliferate, differentiate and adhere to. The use of a transparent microfluidic system also aids in the analysis of a three-dimensional (3D) cultivated structure for two-dimensional (2D) monitoring in real-time. The P19 ESC line is not only very promising as a model cell line for neurogenetic research. Due to their high popularity and validity in biological and medical research, it is very suitable as a test cell line for the evaluation of the microfluidic OOC platform.

To summarise, this thesis aims to develop a microfluidic OOC-MEA platform to investigate size-dependent differences in the neural differentiation of P19 ESC embryoid bodies, which is an established cell line for research of embryogenesis and neurogenesis. Further goals of this project include the investigation of the influence of the cell seeding density on growth and morphology of the EBs, the ideal seeding density for the reliable production of healthy EBs as well as the ability of the P19 EBs to adhere to the OOC platform and to form neurite projections. In order to achieve this, all the individual biological and the technical components were thoroughly characterised and investigated. The P19 embryoid bodies' ability to adhere, grow, proliferate and generate neurites on a 2D surface after being cultivated in a 3D manner were tested. The results prove the aptitude of the chip as an investigation environment for model cell lines. Finally, an electrophysiological measurement to assess spontaneous and chemically stimulated neural activity was executed.

In the future, this OOC device can not only be used to study embryogenetic events or developmental diseases of the central nervous system with the P19 cell line. The developed platform also allows to study and compare genetically engineered versions of the P19 ESC, human neural tissue or advanced models including induced pluripotent stem cell (iPSC)-derived microtissues.

Die approbierte gedruckte Originalversion dieser Diplomarbeit ist an der TU Wien Bibliothek verfügbar
The approved original version of this thesis is available in print at TU Wien Bibliothek.

Die approbierte gedruckte Originalversion dieser Diplomarbeit ist an der TU Wien Bibliothek verfügbar
The approved original version of this thesis is available in print at TU Wien Bibliothek.
TU WIEN Bibliothek Your knowledge hub

Chapter 2

Theory

This thesis unites a multitude of different scientific disciplines ranging from cell biology, fluid mechanics, electrophysiology and cleanroom process technology. Therefore a complete, in-depth presentation of the underlying theoretical content would go beyond the scope of this work. For this reason, short general introductions with a broad view into the respective scientific areas with a subsequent focus on the relevant information will be given.

ESC lines are claimed to be a valuable tool to generate nervous tissue and simulate neural development in vitro, therefore the development and structure of our neural system and its cellular components will be briefly discussed in the next chapter, followed by a short introduction into stem cells. The P19 ESC line as a member of the stem cell family used in this thesis will be thoroughly described. Subsequently, an introduction to current in vivo and in vitro research models, their respective applicability and relevance to biomedical science until today with focus on multicellular spheroids will be given. Lastly, an overview of the current state of the art of neuron-on-a-chip technologies will be given.

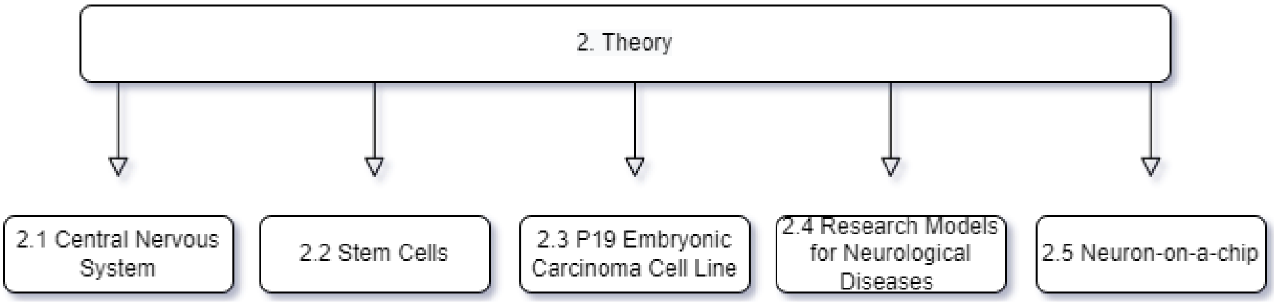

2.1 The central nervous system

In order to not only understand the biological theory but also grasp the relevance of this thesis, a quick introduction to the central nervous system of mammals, its cell types and its embryonal development or neurogenesis will be described in the following section.

The notoriously complex nervous system as the main control centre of the human body consists of two parts: the CNS and the peripheral nervous system or short PNS. The PNS consists primarily of bundles of long fibres or axons that connect the CNS to the peripheral nervous system, located in the distal regions of the body: limbs, organs and extremities. The two systems are interconnected and make up the nervous system as a whole. The CNS denominates the part of the nervous system located in the brain and the spinal cord. Generally, it acts as the main receiving and information processing unit and controls the body's activity via electrochemical communication. Anatomically, the brain and spinal cord are housed within a triple-layered membrane called the meninges, which are protected by the skeleton. [6]

Figure 2.1: Schematic visualisation of the human central nervous system [7]

Neurogenesis

The nervous system begins to build during the intrauterine development of the embryo in a process called neurulation. During the first month of pregnancy, the ectoderm, one of the three germ layers, develops in stages from the neuroectoderm into the neural tube. Finally, the process terminates with the proliferation and differentiation of neural tube cells into mesenchymal and epithelial cells. [8] The same steps of embryonic development have also been proven to occur in vitro using embryonic stem cells when cells aggregate to form an embryoid body. This will be discussed more deeply in section 2.4.3. As these multicellular aggregates mimic in vivo embryonal development and physiological functions, they start to build functioning neural tissue consisting of many different kinds of cells. For this reason, the cells of the nervous system will be presented in the following subsection.

Cells of the central nervous system

On a cellular level, two functionally and morphologically distinct groups of cells arise from the neuroectoderm, which builds up the nervous system. The neurons constitute the main signalling pathways, while the neuroglia or glial cells form tissue around the neurons with various supporting functions. [9][10]
The following section offers a short overview of those two different groups and their functions in the CNS. Some of the cells exist in the CNS but not in the peripheral nervous system and vice versa.

Glial cells

The term glia depicts all the cells of the CNS, which are not electrically excitable, but still participate in maintaining its functionality, usually by offering mechanical, biochemical and immunological support to the neurons. The amount of cells in a human body is estimated to be around 85 billion glial cells, approximately as many as neural cells. [11][12] They can be broadly divided into different groups of cells. An overview of these cells is displayed in Figure 2.2.

Die approbierte gedruckte Originalversion dieser Diplomarbeit ist an der TU Wien Bibliothek verfügbar
The approved original version of this thesis is available in print at TU Wien Bibliothek.

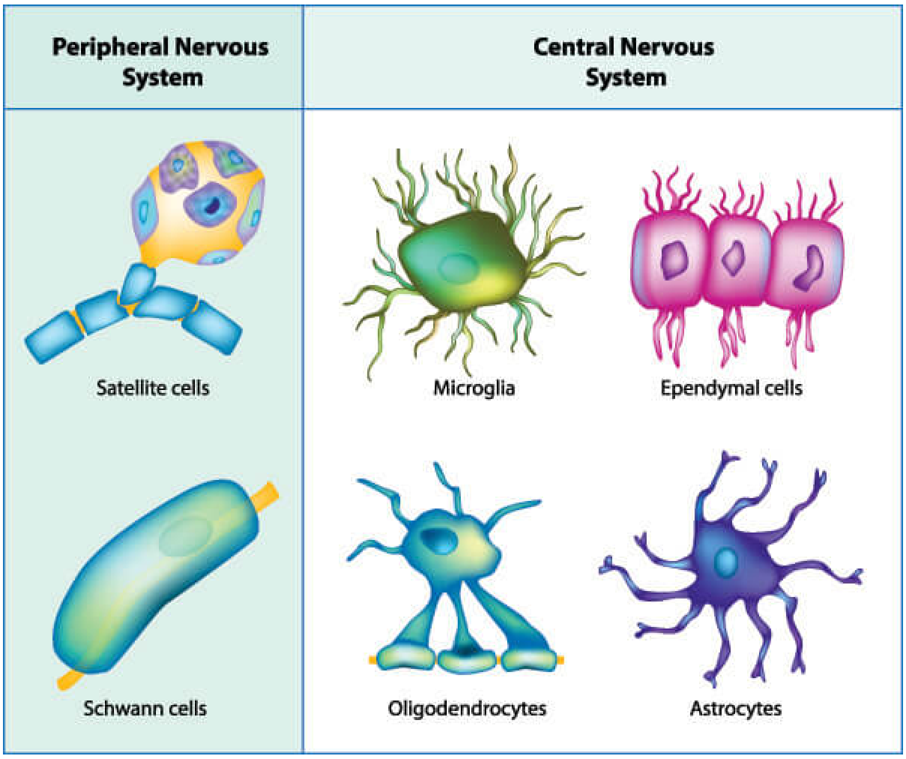

Figure 2.2: Schematic overview of different cell types of the CNS [13]

Glial cells support neural tissue by providing structural fortification, supplying nutrients and oxygen, maintaining the blood-brain barrier and insulating neurons. The macroglia in the CNS are generally divided into four different groups.

- Microglia: act like macrophages in the brain with the function of destroying pathogens and remove dead cell debris by phagocytosis
- Astrocytes: exhibit a broad range of functions, which are yet to be resolved. Examples of functions incorporate the maintenance of the blood-brain barrier, various immunological functions within the CNS, regulation of blood supply in the brain to enable hyperemia, which denotes the increase in blood flow due to electrical activity of neurons[14], etc.
- Oligodendrocytes: create the myelin sheath, which enables faster conduction of electrical signals along neural axons
- Ependymal Cells: line the spinal cord and the ventricular system of the brain

Cells like astrocytes have also been shown to display complex behaviours. In addition to above-mentioned functions, they remove excess ions, take up and release or "recycle" neurotransmitters, directly influencing the breathing process. [15] Another noteworthy cell type is the radial glia. These cells constitute neuronal progenitor cells and are crucial for neurogenesis, as they scaffold new nerve cells during the creation of the embryo's nervous system by travelling along radial glial fibres to reach their final usage site. [16]

Die approbierte gedruckte Originalversion dieser Diplomarbeit ist an der TU Wien Bibliothek verfügbar
The approved original version of this thesis is available in print at TU Wien Bibliothek.
TU WIEN Bibliothek Your knowledge hub

Neurons

Neural cells constitute the nervous system's main function, as they offer electrical pathways for intercellular communication. This is based on the intra- and extracellular exchange of ions.

Neurons are, with few exceptions, typically comprised of three cardinal regions: the soma, the axon and the dendrites, which end with synaptic terminals. A depiction of a typical neuron is shown in Figure 2.3. Apart from the soma, which contains the typical cell organelles, the neuron's most prominent morphological features are the projections, also called neurites, that arise from the cell body. These projections connect many cells with each other to communicate: the dendrites act as the site for inputs from other nerve cells and the cell's axon as the signal output. Axons has been shown in the past to grow along gradients of neural growth factors. [17] The myelin sheaths provided by olygodendrocytes in the CNS or Schwann cells in the PNS increase the travel velocity and offer electrical insulation. [6]

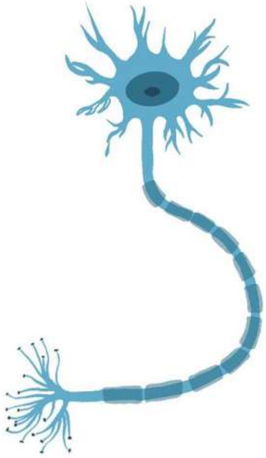

Figure 2.3: Depiction of a typical neuron, created in Procreate©

2.2 Stem Cells

As the cell line used in the experiments of this thesis is an embryonic stem cell line, a short overview over stem cells, relevant mechanisms for their differentiation and their potential in past research is presented in the following section. Since their discovery in the 1960s' by Ernest McCulloch and James Till with the blood-forming hematopoietic stem cell[18], they have been in the focus of biomedical research ever since. [19] Stem cells have the unique ability of self-renewal and indefinite proliferation. The most prominent feature of stem cells is the ability to differentiate irreversibly into various cell types, depending on the individual potency or differentiation potential of the stem cell. They are found in practically every multicellular organism and are essential for the development, maintenance and repair of all kinds of organs and tissues. [20] More detailed information about the differentiation of stem cells can be found in Section 2.3

There are multiple ways of classifying and organising stem cells according to different categories the most popular classifications being stem cell potency and stem cell source. The latter relates solely to embryonic stem cells or "early" stem cells, which are derived during early development of the embryo at the blastocyst stage, in contrast to adult or somatic stem cells, which reside among differentiated cells in a tissue or organ of a developed organism. [21]

The potency, on the other hand, refers to the ability or limitations of the cells to differentiate into a variety of specialized cell types. The main four classifications are presented below:

- Totipotency: The ability to differentiate into every possible cell type and reconstruct a fully functional organism
- Pluripotency: The ability to differentiate into every cell type of the three embryonic germ layers, but no extra-embryonic cell types
- Multipotency: The ability to differentiate into a specific set or family of cells
- Unipotency: The ability only to self-renew and proliferate indefinitely

Die approbierte gedruckte Originalversion dieser Diplomarbeit ist an der TU Wien Bibliothek verfügbar
The approved original version of this thesis is available in print at TU Wien Bibliothek.
TU WIEN Bibliothek Your knowledge hub

Die approbierte gedruckte Originalversion dieser Diplomarbeit ist an der TU Wien Bibliothek verfügbar
The approved original version of this thesis is available in print at TU Wien Bibliothek.

Embryonic Stem Cells in Biomedical Research

Embryonic stem cells are pluripotent, which means that they can differentiate into any tissue of the three embryonic germ layers (endoderm, mesoderm and ectoderm). In contrast, adult stem cells can differentiate only into a specific tissue type, depending on the lineage.

Figure 2.4 displays the capability of ESCs to differentiate into various cell types within the three embryonic germ layers. ESC lines have been isolated from the blastocyst's inner cell mass, which refers to a shortlived cell aggregation three to four days after insemination during embryogenesis. [22] The first successful derivation of an ESC line was executed in 1981 from a murine teratocarcinoma. [23] 17 years later, the first human ESC (hESC) was extracted from the inner cell mass of a pre-implantation human blastocyst. [24] This enabled new possibilities for researchers in biology and medicine worldwide and prompted widespread ethical discussions and international jurisdictions about the acquisition and use of ESCs in biomedical research and therapy.

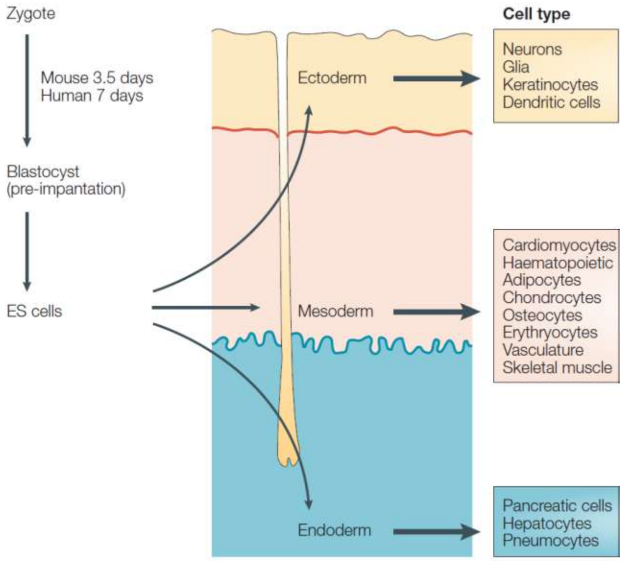

Figure 2.4: The differentiation potential of ESCs into cell types of the three embryonic germ layers.

In 2006, Takahashi *et al.* showed that mouse adult fibroblasts could be reprogrammed into cells with all ESC characteristics by introducing selected transcription factors known to be expressed in ESCs. This gave rise to the so-called induced pluripotent stem cells (iPSCs), bypassing the ethical concerns towards ESCs. [25]

Despite those concerns, the ability to differentiate into any kind of cell of an organism made ESCs a highly valuable tool for various clinical applications. In a study from 2010, it was firstly used in a therapeutical sense in a transplantation to cure spinal cord injury[26], but also as a tool in tissue engineering to rebuild and model human tissue and organs or to simulate organisms as a whole in vitro. [27] As an example, Kawasaki *et al.* demonstrated the induction of dopaminergic midbrain neurons by stroma-derived inducing from mouse ESCs. [28]

Today, the usage of ESC has become a standard in the field of in vitro drug discovery, toxicity examination, high-throughput screenings and safety pharmacology. The psychotropic compound trifluoperazine, for example, has been tested on ESCs to inhibit cancer stem cell growth. ESCs enabled the generation of models for neurodegenerative disease, genetically altered cardiomyocytes with a predisposition to heart failure or hepatocytes for metabolic profiling. [29] [30]

In the context of neurogenesis, research around the development of neurons and neurulation has been pursued intensely using three different cell types. [31] Research around neural progenitor cells derived from adult nervous tissue or nonneural organs contributed much progress on this topic. [32][33] Additionally, stem cells and specifically ESCs, have been prevalent cell types for studying neurogenic events in the past. As an important member of the ESC family, the mural P19 embryonal carcinoma cell line offers a robust model culture[34] and will be presented in the following section.

2.3 The P19 embryonic carcinoma stem cell

The P19 cell line was extracted for the first time in 1982 after McBurney *et al.* induced teratocarcinoma, a rare form of cancer, in the testis of a mouse. They transplanted a 7.5-day-old murine embryo and harvested the embryonal carcinoma cells out of the resulting primary tumour tissue. The resulting cell line showed high genetical stability with a low mutational rate and exhibited both spontaneous immortalization or pluripotency, typical properties of cancer cells and stem cells within one cell. These carcinomic stem cells were subsequently named P19 cells. [35]

The P19 cell line possesses pluripotency, which was demonstrated by transplanting single undifferentiated P19 cells into blastocytes of another strain of mice. This resulted in mouse chimeras with P19 derived, differentiated successor cells. Also, the cell line showed doubling rates around 15 hours, depending on the culturing conditions without the necessity of feeder cells. [36] Furthermore, the P19 cell line inherits a male euploid karyotype (40:XY). P19 cells are easy to maintain in an undifferentiated state compared to other cell lines. In contrast, solely changing the chemical composition of the culture media initiates fast and efficient differentiation of the cells. [3]

Die approbierte gedruckte Originalversion dieser Diplomarbeit ist an der TU Wien Bibliothek verfügbar
The approved original version of this thesis is available in print at TU Wien Bibliothek.
TU Bibliothek WIEN Your knowledge hub

Similarities between the P19 ESC line and human early embryo cells

As mentioned before, the P19 ESC line as a descendent of a germ tumour and the cells of the early embryo display notable similarities. This is based on the pluripotency of the P19 ESC, derived from its teratocarcinomic origin. According to Martin *et al.*, early embryo cells and teratocarcinoma-derived cells share at least one antigen, which so far has only been observed for sperm cells. [37] These two cell types share significant immunologic properties, like the shared absence or presence of highly specific molecular markers. Examples are the absence of major histocompatibility H-2 antigens in a study by Artzt *et al.*[38] or the specific detection with an antiserum, which showed activity only against mural ESCs, mural sperm and early embryo cells, but not against non-teratocarcinoma or somatic teratocarcinoma cells. [39] Further similarities encompass biochemical, morphological and functional properties. Detailed information can be found, e.g. in mentioned the article by Martin *et al.*. [37]

The P19 ESC in neurogenic research

The P19 cell has been one of the first cell lines investigated around its ability to differentiate to cardiomyocytes with dimethyl sulfoxide as well as to neural tissue with retinoic acid. It has thus been intensively researched in the past 40 years. The high reproducibility of the generated cells of the differentiation protocols has been used in studying molecular and cellular processes. The high affinity of P19 cells to transgenic interference also fueled their research progress. The transfection of recombinant DNA via calcium phosphate or electropermeabilisation in the cells and its integration into the genetic code of the cell line opened up many new experimental possibilities. For these reasons, the P19 cell line contributed to progress in the analysis of upstream signalling pathways and transcription factors, as well as epigenetic and molecular variations in protein and ion channel regulation. [35][40]

P19 neuronal differentiation

Various molecules can trigger the directed differentiation of P19 ESCs. Directed differentiation describes the controlled differentiation of stem cells by influencing environmental factors like temperature, chemical composition, ph-value or the number of seeded cells with the intent to generate a targeted type of cell or tissue. [41] Retinoic acid and dimethyl sulfoxid in non-toxic concentrations are the most effective differentiation agents of P19 ESCs. Although both compounds are considered toxic in higher doses, typical concentrations to trigger effective differentiation have been shown to be non-toxic. This implies true differentiation of the P19 instead of selection. Selection, in this case, would mean that already existing differentiated cells would be selected to be the sole survivors in the cell culture. Therefore, no actual triggered differentiation process would be happening. [42] The exposition of P19 ESCs to dimethyl sulfoxide triggers the formation of cardiomyocytes, while the introduction of RA into the metabolism of P19 cells induces the formation of neurons, glia and fibroblast-like cells, which will be explained below. This enables the P19 cells to differentiate into cells of the ectodermal, endodermal and mesodermal lineage. [42][43]

Retinoic acid (RA)

As mentioned before, retinoic acid is a well-known chemical suitable for triggering directed differentiation of P19 ESCs to neurons. All-*trans*-retinoic acid (ATRA), abbreviated retinoic acid (RA), is a metabolite of Vitamin A_1 or all-*trans*-retinol, as depicted in Figure 2.5. Both belong to the group of the essential Vitamin A, which strongly influences growth, development and vision in organisms. [44] RA binds to RARα, RARβ, and RARγ receptors and induces a change in conformation. This leads to either epigenetic up- or downregulation of gene expression profiles of morphogenic genes[45], e.g. of the homeotic Hox genes, which control growth of body segments. [46] It has a profound influence on the anatomical development in the chordate phylum during the early embryogenesis in vertebrates. RA determines the direction of the cell growth along the posterior axis (embryonic anterior/posterior axis), guiding the embryo's development. [47] More detailed information about the functions, metabolism and molecular effects of RA can be found in various textbooks. [48]

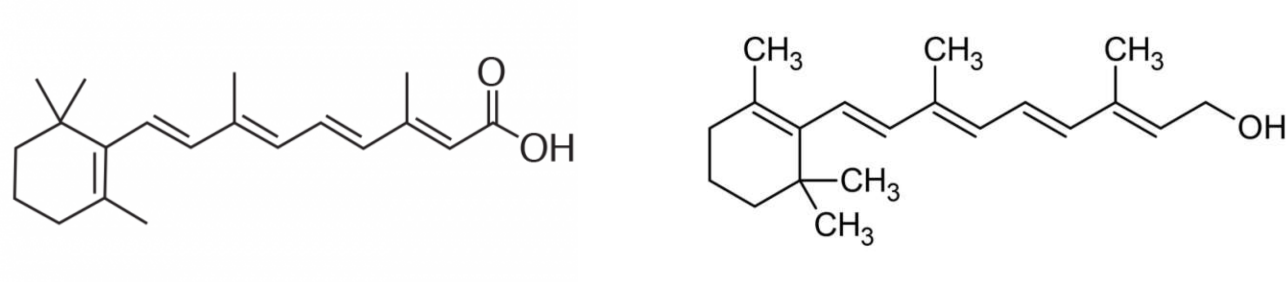

Figure 2.5: The molecular structures of all-*trans*-retinoic acid (left) and all-*trans*-retinol (right) [49][50]

In the RA-triggered differentiation process of the P19, several proteins belonging to different families participate, which is subject of current research. To name an example, Morii *et al.* measured histone deacetylase 8 (HDAC8) activity using an HDAC8 inhibitor and HDAC8-knockout P19 cells. They discovered, that inhibition of HDAC8 enzymatic activity suppressed neuronal differentiation, while the HDAC8-knockout cell line showed immature differentiation compared to the original cell line, so that a direct influence of the HDAC8 activity on neuronal differentiation of P19 ESCs was concluded. [51] Generally, it has been discovered that the undifferentiated P19 ESC monoculture turns into a heterogeneous spectrum of differentiated cells,[34] although it is more narrowly limited compared to spontaneous differentiation in P19 cells. [3] As mentioned before, it has also been shown that the concentration of RA determines the type of resulting differentiated cells. Low concentrations around 10×10^{-9} M generate a large amount of endodermal skeletal muscle cells, while higher doses around 10×10^{-7} M to 10×10^{-5} M produce mostly neuroectodermal neurons, astroglia and microglia. [52][53]

Generally, rigid cell-cell contact is conducive but not an absolute necessity to effective differentiation. This is fulfilled sufficiently in spatial aggregations of cells like embryoid bodies, which is a 3D in vitro research model that will be presented in the next section over research models in biomedical sciences.

Similarities of P19 ESC neurons to human neurons

Differentiated P19 neurons and human neurons of the CNS share many typical properties of mature mammalian neurons, like neuronal polarity and functional synaptic transmission. [54] Results of a study by Wu *et*

Die approbierte gedruckte Originalversion dieser Diplomarbeit ist an der TU Wien Bibliothek verfügbar
The approved original version of this thesis is available in print at TU Wien Bibliothek.
TU WIEN Bibliothek Your knowledge hub

al. suggest that differentiated P19 neurons display a dopaminergic phenotype. Interestingly, this is upregulated in hypoxic culture conditions, demonstrating the importance of oxygen concentration for neurogenesis. [55] Furthermore, they express various human glutamate receptors, including GluR1/4 and NMDAR1,[56] as well as CB1 cannabinoid receptors, gamma-aminobutyric acid (GABA), acetylcholine, somatostatin, neuropeptide Y, catecholamines and survival motor neuron (SMN) promoter. These are also expressed within the human organism. [57][58][59][60] Lastly, they also exhibit microtubule-associated protein 2 (MAP-2) and Glial Fibrillary Acidic Protein (GFAP), typical mammalian markers of neurons and astrocytes. [61][62] However, a more recent study revealed a "similar to stronger" sensitivity to toxins of the P19 ESCs than human neuroblastoma cells. [63] To summarise, the differentiated P19 neurons exhibit fairly similar properties to neurons of the developing mammalian forebrain, which increases the translativity of results and therefore caused the rise of interest into the P19 cell line as a research model.

Die approbierte gedruckte Originalversion dieser Diplomarbeit ist an der TU Wien Bibliothek verfügbar
The approved original version of this thesis is available in print at TU Wien Bibliothek.

2.4 Research models for neurological diseases

As the overall aim of this thesis is the development of a microfluidic device for the investigation of three-dimensional in vitro models, it is imperative to question its legitimacy, validity and efficiency in contrast to other research models. What information can we extract from those models, and how can we synthesize them to find new therapies for neurodevelopmental disorders? This is a fundamental topic within biology and biomedical sciences, which gained worldwide public interest due to broad ethical discussions, e.g. about genetic alterations or the (mis-)use of animals in scientific research. Therefore, this chapter will introduce a selection of the most important in vivo and in vitro research models and carve out their properties with a narrowed focus on the techniques used in this thesis.

Translatability of biological models

How much worth is the information we can gain from in vivo or in vitro models? The explanatory power of empirical models needs to be handled with care, as differences in size, anatomy, metabolic rate, diet and phylogenetic distance may limit their validity. This led to the distinguishment of three categories for animal models: predictive, isomorphic and homologous.

Predictive animal models yield some translational value or gain of information towards human pathology or certain features of diseases while no further resemblance between the animal and the human disorder can be found. Isomorphic animal models state high similarity of the animal disorder to the human disorder, but the etiology between both differ. Homologous animal models offer a complete analogy, which means that insights of an animal disorder can be linked directly to the human disorder. [64] [65] [66] More detailed information about phylogenetic relatedness between animals and animal models can be found in various textbooks. [67]

2.4.1 Animal models

The study of animals to gain information about humans or other species is no new concept: The earliest records date back to Alcmaeon of Croton in ancient Greece around the fifth century BC, who used a dog model to draw one of the first anecdoted, animal-model based neuroscientific conclusions on human anatomy: "The brain houses human intelligence." [68] Since then, animal models have been a research standard for centuries in evolutionary and behavioural biology. They were used in the analysis of diseases in order to comprehend underlying processes and factors used in the pursuit of diagnostics and therapies without risking to harm a human.

Nowadays, the variety of animal models has narrowed down to a couple of intensely researched species, which dominate today's scientific research.

Drosophila Melanogaster: Firstly described in 1830 by Johann Wilhelm Meigen[69] is generally portrayed as the most intensely researched organism in the world and used as a classic subject matter organism for case study because of its simple genetics and inexpensive husbandry. [70] Despite the enormous anatomical and physiological differences, its genome and the human are 60% congruent. Around 75% conformity to human disease-related genes have been identified. Thus the model has contributed to progress in genetics, investigation of the endocrine system and cancer research. [71][72][73][74][75]

Danio Rerio: The Zebrafish has emerged as a powerful model for high-throughput chemical and toxicological hazard assessments to predict neurotoxic effects of chemicals and drugs on humans. Zebrafish embryos and larvae are convenient research models due to their small size, transparency, low cost and easy maintenance. [76][77] Zebrafish are homologous to many higher-order vertebrates in terms of molecular signalling processes, tissue/organ structures as well as neurodevelopment. [78]

Mus: The most popular mammalian model species within biological research is the mouse. It has been investigated around endocrine, nervous, cardiovascular, genetic and immunological processes. Techniques to specifically target and modify genes led to a wide range of over 2700 different genetically engineered mouse strains just at the National Human Genome Research Institute. [79] The ability to manipulate the genome of a model species allows for the design of animal models uniquely susceptible or resistant to a certain disease and enables the study of altered gene expression and protein coding within the physiological environment in an organism. [80] Some diseases that would not exist naturally in mice like Alzheimer's, SLE or alopecia areata could now be introduced into the genome and investigated thoroughly. [81][82][83][79][64]

A quick overview and comparison of these three dominant animal models versus conventional cell cultures is visualised in Figure 2.6. It must be mentioned that there are a multitude of other model organisms in use.

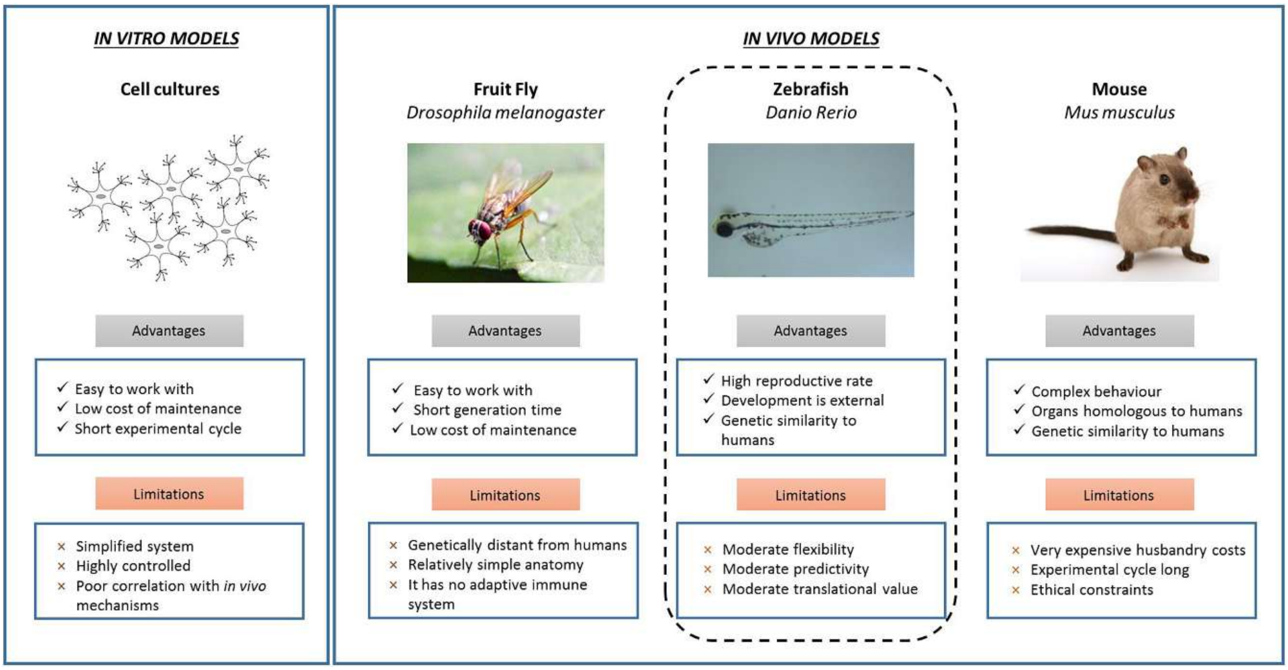

Figure 2.6: Broad comparison of scientific history's most intensely researched and widely used animal models, contrasted by cell culture models. Excerpt from Moraes *et al.* (2018)[78]

Die approbierte gedruckte Originalversion dieser Diplomarbeit ist an der TU Wien Bibliothek verfügbar
The approved original version of this thesis is available in print at TU Wien Bibliothek.

Animal models in neuroscience

Animal models contributed strongly to neuroscientific research. The rodent model contributed notably to progress in Alzheimer's disease research. For example, in a study conducted by Olabarria *et al.*, the interactions between astrocytes and neuritic plaques and their consequences on cytoskeletal atrophy of the CNS were investigated by use of a triple transgenic animal model. [84] Despite these efforts, recent systematic studies on the predictive value of animal models have demonstrated poor correlations between human data and animal outcomes, e.g. in psychiatric research[85] or neurodegenerative diseases[86], because of grave differences in disease pathways. [87] This underlines the critical need for new approaches to model complex human-relevant conditions.

> *"If you have cancer and you are a mouse, we can take good care of you."* – Judah Folkman[88]

However, the average rate of successful translation of therapies from animal models to clinical cancer trials is less than 8%. [89]

2.4.2 In vitro models

How is it possible to circumvent mentioned ethical problems, high-cost factors and disputable efficiency in providing progress in human medicine? In vitro cell culture techniques are very common as they can offer a low-cost, low-maintenance, high-throughput and relatively efficient alternative to animal models. Cells are arranged around a glass surface, a plastic dish or suspended in a medium. The physiology of the living cell usually is attempted to be maintained, depending on the precise culturing mode, while (almost) no sacrifice of animals is required. [90] This motivated the extraction and in vitro investigation of a huge variety of cell lines with various culturing techniques. The resulting cell cultures can either be categorised according to their origin (primary or secondary cells), their phylogenicity (human or animal) or other properties like their potency (stem cells). Growing cells in vitro opens up new possibilities, as experiments can now be automated and visualised in real-time with otherwise unavailable quantitative analytical methods in high resolution. The optical transparency of cell culturing devices is another key advantage over animal models. [27] Despite this, data and conclusions derived from in vitro models usually need to be extrapolated and retested in vivo in order to be applicable.

2D vs 3D cell culturing

2D cell culture methods can be defined as a monolayer culturing method on a usually coated surface to facilitate cell-surface binding. It is generally known as a low-cost, high-throughput procedure with easily interpretable and highly reproducible results. Its applications have led to valuable insights in the fields of carcino-, embryo-, and neurogenesis. [91]

However, the culturing conditions are far from a physiological environment, as information about biochemical, electrical, mechanical or biological cues to and from the environment of the cell is lost. In an organism, cells are in contact with a variety of extracellular matrix (ECM) components, cell-secreted factors and interacting heterogeneous cell populations, whereas the monolayer inherently implies constant and unlimited exposition to cell medium and its ingredients. The arrangement, composition and number of connections with surrounding cells influence the cells' ability to regulate fundamental cellular behaviours and cycle, including survival, differentiation, proliferation, migration and cell morphology. The influence of the ECM on the physiological state of the cell therefore can not be stressed enough. [92]

Die approbierte gedruckte Originalversion dieser Diplomarbeit ist an der TU Wien Bibliothek verfügbar
The approved original version of this thesis is available in print at TU Wien Bibliothek.
TU Bibliothek Your knowledge hub WIEN

TU WIEN Bibliothek Your knowledge hub
Die approbierte gedruckte Originalversion dieser Diplomarbeit ist an der TU Wien Bibliothek verfügbar
The approved original version of this thesis is available in print at TU Wien Bibliothek.

Generally, adhesive interactions with the surrounding ECM and neighbouring cells define cell shape and organisation. In planar culturing modes, the polarity of the cells has been shown in a study to develop an apical-basal-like polarity resembling epithelial cells[93]. This has been proven to correlate with a higher rate of apoptotic signals. [94] In addition, adherent cultures are monocultures and only allow for the study of a single cell type. [95] Cell signalling, expression of genes and proteins, responsiveness to external stimuli and other cellular functions are also altered by the synthetic culture environment. As an example, it has been shown that mammary epithelial cells upregulate the expression of $\beta 1$ integrins in 2D culture, which does not occur in 3D cultures nor in vivo. Differences in the distribution of transmembrane adhesion proteins in 2D and 3D cultures also impact cell migration. [96] Even the loss of phenotype occurs, as has been shown in another study, where chondrocytes lose their cartilage phenotype. [97]

3D cell cultures techniques address these limitations by simulating in vivo tissue with artificial spatial agglomerations of cells. They can be categorized into three different culture types: suspension cultures e.g. in non-adherent, ultra-low attachment (ULA) plates to generate spheroids like e.g. neurospheroids, which are agglomerations of neural stem cells. [98] Moreover, cultures with concentrated medium or gels as well as scaffolded cultures. An example of the latter are organoids, self-assembling clusters on scaffolds of organ-specific cells to model e.g. a whole liver. [99] These cultures display higher resemblance to natural tissue and provided another alternative to 2D cultures and animal models since their first experimental implementations in the 1970s. Here, cells are arranged in anisotropic, spheroidal layers. Inside these spherical agglomeration, cells are shielded from the medium and microenvironments are created. This enables physiological cell-cell and cell-medium interactions, limited access to metabolites, oxygen and cytokines leading to nutrient gradients and as a consequence, roughly physiological gene expression profiles. [100] Also, in comparison to 2D cell cultures, cell morphology, cell cycle and polarity can be maintained in a physiological state. [94]

Apart from that, 3D cultures are very suitable for measuring absorption, distribution, metabolism and excretion (ADME) of drugs. [101][102] Especially cancer cells are less sensitive to drugs cultured in 3D than in 2D, which is derived from the differences in access to medium and cell signalling. 3D cell culturing and the condition of the same cell density as in vivo tissue facilitates the generation of a drug response comparable to that of a solid, natural tumour. [103] Finally, the extension from planar to spatial culturing as a more physiological culturing mode enables the in vitro simulation and modelling of embryogenesis.

On the other side, the increase in complexity of 3D cultures also creates more challenges in culturing, imaging and analysis. Polylayered cultures reach a thickness of several hundred micrometres. They are highly scattering samples, which prompted the development of advanced imaging techniques with the ability to penetrate such advanced types of samples, like confocal microscopy, multiphoton microscopy or optical coherence tomography. [104]

To summarise, the emergence of new scientific possibilities with increased predictive power of experimental results brought by more complex 3D models comes at the cost of increased difficulty in monitoring, reproducing and interpreting obtained results. [91] Still, regarding the ongoing improvements in automation, high-resolution monitoring technologies and cost reductions, 3D cultures will function as an intermediary technique between animal and 2D models, depending on the context of research and will aid in reducing the need for animal models in the near future.Current developments around 3D cell culture techniques aim to close the gap to in vivo by modelling physiological conditions of organisms with ever increasing preciseness in vitro. One promising 3D research model specialized in modelling differentiation mechanics or embryo- and neurogenesis among others are the already mentioned spherical agglomerations of cells or embryoid bodies, which will be presented in the following chapter.

Die approbierte gedruckte Originalversion dieser Diplomarbeit ist an der TU Wien Bibliothek verfügbar
The approved original version of this thesis is available in print at TU Wien Bibliothek.
TU WIEN Bibliothek Your knowledge hub

2.4.3 Embryoid bodies

In the pursuit of developing advanced therapies for neurodevelopmental disorders, it is imperative to fully simulate tissue in all its complexity in vitro. For this reason, cell agglomerates called embryoid bodies have gained increased interest in the past decades. [105] ESCs like the P19 cells can organise themselves to spheroidal EBs, when cultured in a suspension or with so-called hanging drop techniques. [106]

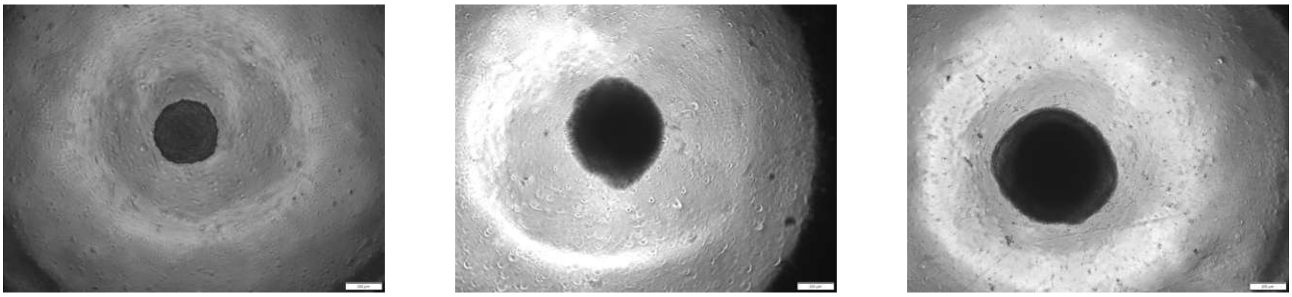

Figure 2.7: Depiction of a P19 embryoid body at different time stamps in culture. From left to right: Day 2, day 5 and day 8. Seeding Density per well: 5000.

Agglomeration and generation of multicellular aggregates

The formation of Cell-cell contacts and their interactions are commenced by cadherins, a group of Ca_2^+-dependent transmembrane adhesion receptors. The agglomeration is facilitated by the composition of an ECM, offering mechanical stability and cell-cell signalling pathways. [107] Lin *et al.* defined three steps in building the ECM of multicellular spheroids, beginning with long-chain ECM fibres providing rapid initial aggregation of dispersed cells. After a delay phase showing upregulated cadherin expression, homophilic cadherin-cadherin binding between two cells secures strong cell adhesion. [108] The production of cell adhesion molecules, synaptophysin and extracellular matrix proteins is also increased in EBs when compared to monocultures. [109]

The most common 3D culture methods are suspension 3D cultures and plastic or hydrogel scaffold cultures, which anchor the cells and offer stability simulating a synthetic ECM. [105] Suspension or scaffold-free 3D cultures are performed using hanging drops or culture well plates with low-attachment wall coating (using hydrophobic polymers or agarose[110]), leading to a spontaneous agglomeration of cells in the medium without any contact to a solid structure. This method is easier to facilitate but yields a higher variance in size and morphology of the EBs. [111] Microfabricated microstructures and microfluidic channel systems have been integrated for improved control of the properties of EBs. [112] Also, large-scale production protocols of EBs in a bioreactor using oscillating spinner flasks have already been realised. [113]

Applications of embryoid bodies

Generally, embryoid bodies are used intensively in research for the analysis of cell-cell interactions, the influence of its formation on the cell secretome, gene expression profiles and gene-function mapping[114]. They are also used for research on neurulation or early embryogenesis but also as a model for immunologic assays[115], for avascular cancer tissues [116] or in ADME screenings. [117] Also, they are used in tissue engineering for organ reconstruction, like the bioartificial liver (BAL). [118]

As mentioned, newly formed EBs exhibit partial similarities to the early embryonic development, where cells spontaneously differentiate to progenitor cells of the neuroendoderm. The exact molecular processes occurring during the agglomeration and leading to differentiation are not fully understood yet. [3] Initial differentiation of embryonal carcinoma cells begins in EBs with the differentiation of the outer cells of the aggregate into endoderm-like cells that surround the undifferentiated core. [119] By controlling cell-cell interactions by cell aggregation and combining with mentioned bioreactor culture technique, it was reported to scale the amount of differentiated hematopoietic cells in a controlled way. [120] Recently published papers report the generation of populations of neural progenitors with high purity by using EBs. It is a very common practice today to use EBs in directed differentiation protocols to generate specific cell types from undifferentiated stem cells. In a study conducted by Murry *et al.*, which showed that the location of the cell influences the differentiation process either into mesodermal or endodermal cell types. [41]

Diffusive mass transport in multicellular aggregates

In multicellular spheroids, the spherical sheets of cells act like a biomechanical membrane, which influences permeability and hinders the transport of molecules. This induces a gradient of medium ingredients, molecules and cell waste products between the medium-cell border and the inner core cells of the EB. Said gradient is driven by diffusion of an excess of external molecules to the inside and vice versa. For a better understanding of this issue, which is fundamental for the question of the relationship of seeding size and differentiation efficiency in this thesis, a brief introduction to diffusion physics will be provided next.
Diffusion is a stochastic process describing the natural mixture of several compounds depending on time, creating a net flow of a considered species from regions with a high density of a species into regions with lower density. It is driven by Brownian motion, which is derived from the particles' thermal energy. This time-independent diffusion flow is described by Ficks' first law Equation 2.1

$$\vec{J}_{diff} = -D \cdot \nabla c \tag{2.1}$$

$\vec{J}_{diff}$ corresponds to diffusive flux density, D corresponds to diffusivity and c corresponds to the concentration of the species. The diffusion constant D can be calculated via the Stokes-Einstein Equation 2.2:

$$D = \frac{k_{\mathrm{B}} \cdot T}{6\pi \cdot \eta \cdot r} \tag{2.2}$$

[121] Here k_{B} corresponds to Boltzmann constant, T corresponds to absolute temperature, η corresponds to the mobility and r corresponds to the radius of the considered spherical particle. This means that concentration gradient, particle size and particle mobility are mainly responsible for nutrient exchange in and out of the EB. With bigger EBs and higher distances covered, efficient supply can not be sufficiently maintained after reaching a critical size and necrosis occurs.

Mathematical models facilitated simulations of nutrient, oxygen and waste transport. [122] Mueller-Klieser *et al.* developed a method to determine oxygen diffusion coefficients for EBs: Analogous to tumour tissue, a diffusion limitation for pathways over 150 µm to 200 µm for molecules like O_2 occurs. [123] In addition to hypoxia and waste accumulation in the core due to inefficient mass transport, as metabolic activity by the cells downgrades the nutrients entering the EB, only few nutrients reach the core. As the embryoid body grows, the gradient increases until a point of malnutrition is reached, and the core begins to become necrotic. [124] Spheroids above 500 µm diameter commonly display a necrotic core, an inner zone with quiescent cells and an outer zone with proliferating cells. [125] This is visualised in Figure 2.8.

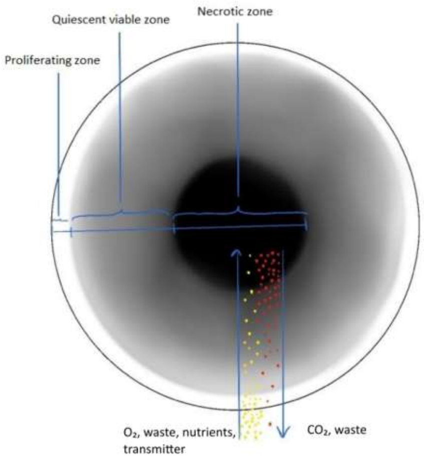

Figure 2.8: Graphical representation of the gradients and cell viability zones in EBs.

Die approbierte gedruckte Originalversion dieser Diplomarbeit ist an der TU Wien Bibliothek verfügbar
The approved original version of this thesis is available in print at TU Wien Bibliothek.

After P19 neurons and embryoid bodies have been presented, the neuronal differentiation of P19 ESCs within EBs will be presented next.

2.4.4 Neuronal RA-directed differentiation of P19 embryoid bodies

While P19 embryonal carcinoma cells grown as a monolayer on a plastic surface have been considered to only differentiate to non-neuronal successor cells when exposed to RA in the past, they have been demonstrated to develop neural tissue in 3D cell agglomerations like embryoid bodies. [3] Some older studies also describe, that the expansion of specific embryonic progenitors and their further differentiation appears to require 3D sphere-like culturing methods,[126][42] while more recent studies reported successful while less efficient neuronal differentiation without the use of EBs. [51] With the introduction of specific cytokines and molecules like retinoic acid, the efficiency of differentiation was found to be increased. The combination of agglomeration and drug application combined is used to induce P19 embryonal carcinoma cells differentiation very efficiently into derivatives of all three germ layers in embryoid bodies. [120] But not only the concentration of the chemical trigger appears to control cell fate, also the size of the cell spheroid plays an essential factor. Livigni *et al.* developed differentiation protocols of mural embryonic stem cells, where differently sized EBs form tissue from different primary germ layers. It was assumed that smaller EBs ensure the required high levels of exposition of cytokines. [4] In 1987, a study also reported the time-varying influence of the cell cycle on the differentiation ability. [1] At low concentrations, RA directs P19 ES cells to differentiate into cells displaying an endodermal phenotype, whereas at higher concentrations it induces the differentiation towards cells of the neuroectoderm. [53]

Correlation of seeding density vs differentiation efficiency in P19 cells

EBs are already well established since decades, but random areal differentiation patterns and heterogeneous microstructures still pose a challenge. As the initial seeding size has strong effects on the development of EBs, one focus of this thesis is to investigate the relationship of the seeded quantity of cells on the differentiation efficiency. "Differentiation efficiency" in this regard is a term, that is defined as the quotient between the amount of differentiated and the amount of undifferentiated cells.
It is imperative to understand and control differentiation in cell culture tissue to simulate the in vivo for applications like drug screening and therapy development for future applications in human medicine more effectively.

The amount of cells seeded is one crucial factor driving the differentiation to a specific type. As mentioned before, smaller EBs with a diameter of 100 µm showed increased ectoderm (HES1) marker expression, while larger with a diameter of 500 µm demonstrated an increased expression of endoderm (AFP) and mesoderm (GATA1)-associated markers. [5] In addition to cell type, the size also has been demonstrated to influence the ratio of differentiated cells. In this regard, it has been shown that the amount of cells seeded per well or the seeding density, which influences the size of the EB, showed correlations with the efficiency of the differentiation in the past. Also, during the directed differentiation of P19 cells with RA, Berg *et al.* demonstrated that the cell seeding density accounts as a major factor in generating differentiated cell types efficiently, as opposed to e.g. the cell cycle. Contrary, cardiac differentiation of hPSCs has been shown to act otherwise, as Laco *et al.* reported a correlation of increased differentiation efficiency with cells in G1 cell cycle phase. [127]

Unfortunately, literature on this topic reveals heterogeneous experimental procedures and results. Kitani *et al.* reported a positive proportionality between high cell seeding densities (more than 2×10^4 cells/cm2) and high differentiation in EBs for neurons and astroglia with P19 embryonal carcinoma cells after 14 days of incubation[128] in serum-free medium, while another study executed by Berg *et al.* revealed exactly the opposite. Here, low-density cultures revealed 75-97%, while high-density samples led to a 10% yield of differentiated

Die approbierte gedruckte Originalversion dieser Diplomarbeit ist an der TU Wien Bibliothek verfügbar
The approved original version of this thesis is available in print at TU Wien Bibliothek.
TU Bibliothek WIEN Your knowledge hub

Study	Range of Cell Seeds (low to high)	Correlation	Cell Type	Differentiation protocol
Kitani	1×10^4 to 5×10^4	Positive	P19	Neuronal, RA, serum-free
Berg	5×10^3 to 5×10^5	Negative	P19	Neuronal, RA
Parnas	1×10^3 to 6×10^3	Positive	P19	Neuronal, RA
Srimasorn	1.75×10^4 to 5×10^4	Positive	Human iPSC	Neuronal, cell-derived

Table 2.1: Comparison of various studies examining the influence of cell seeding density on differentiation efficiency.

cells during exposition of $1\,\mathrm{mM}$ RA. An increase in exposition duration leads to a gradual harmonisation of the differentiation efficiency in low-/and high-density cultures. [43]

As an attempt to give an outlook on literature dealing with this issue, Table 2.1 summarises its results without claiming to be complete. It lists the density range as "low" and "high" in regard to seeding density and the trend between seeding density and differentiation efficiency. Lastly, the used cell type and experimental information are listed, as comparative studies with deviant differentiation protocols or cell types are added. For this reason, the cell seeding quantity is introduced as an adequate measure. Generally, the majority of studies tend to agree on a positive correlation between seeding density and differentiation efficiency, but use differing cell density intervals and cell culturing protocols.

Possible attempts to explain the dependence of differentiation on the seeding density deal with cell-cell and cell-ECM interactions. Parnas *et al.* noticed higher neurite growth rates and earlier release of the neurotransmitter [^{3}H]aspartate for bigger seeding densities. [129] Quick cell metabolism of RA on the EB periphery or inefficient mass transport might explain a tendency of small embryoid bodies with higher efficiency, while the need for higher complexity for the required amount of neural growth factors etc. as a condition for neural development might point to higher efficiencies. Loehle *et al.* showed that neuronal differentiation efficiency decreases when the amount of transcription factors was decreased. [130] Furthermore, it was shown during multicellular hepatic differentiation of iPSCs, that larger multicellular spheroids have enhanced capability to differentiate by increasing the expression marker albumin, CYP3A4 and down-regulation of fetal hepatic marker AFP. [131] One less specific solution to improve differentiation rates of cell cultures is the introduction of gene editing methods like CRISPR/Cas9, as it has been done successfully in a recent study with gene-Corrected Beta-Thalassemia iPSCs. [132] In summary, certain information about molecular interactions in neuronal differentiation mechanics inside embryoid bodies of P19 ESCs is limited.

Die approbierte gedruckte Originalversion dieser Diplomarbeit ist an der TU Wien Bibliothek verfügbar
The approved original version of this thesis is available in print at TU Wien Bibliothek.
TU WIEN Bibliothek Your knowledge hub

2.5 Organ-on-a-chip technology

In the previous chapter it was demonstrated, how much progress was made in the field of emulating tissues or organs with in vitro or in vivo models for basic and pharmaceutical research until today. As a valuable technology that contributed to significant progress in combination with in vitro research models, the following section describes the importance, applications and limitations of organ-on-a-chip devices in medical research. In the past, OOC approaches have been used to simulate, monitor and investigate all kinds of biological tissues, like cardiac tissue[133], whole organs like lungs[134], or combined multi-organ systems like the liver-heart-lung model[135] in vitro by maintaining cells or tissue biopsies in a microfluidic unit. [136] In this context, milestones of neurobiology-on-a-chip technology as an advanced 3D in vitro model for the investigation of nervous tissue by combining a mobile cell culturing environment with integrated data acquisition techniques and its current state-of-the-art will be presented. Prior to that, a brief introduction into microfluidics is provided next.

Die approbierte gedruckte Originalversion dieser Diplomarbeit ist an der TU Wien Bibliothek verfügbar
The approved original version of this thesis is available in print at TU Wien Bibliothek.

Microfluidics in organ-on-chip technologies

Microfluidic devices are microfabricated fluid reservoir systems, which deal with liquids in the nano-scale and below with the objective of investigating cellular and molecular biological or physical events. Due to their versatility, simple and accessible manufacturing techniques, their popularity within biological and medical research increased drastically in the past decades. They usually offer fast production and iteration cycles, so that prototypes can be produced rapidly. In addition to this, only low amounts of liquids and few reagents are required. Due to the dimensions, most microfluidic systems inherently operate with laminar flow, indicated by little or no mixing of fluids and no generation of swirls or eddies, which denotes the swirling of a fluid and the reverse current, e.g. behind an obstacle. This makes flow highly predictable, simplifies fluid simulations and enables the exposition of fluid-sensitive cells or tissues like nervous tissue to medium convection, a crucial condition for many whole organ or multi-organ on-chip research models. [137] Common components of microfluidic systems are channels, valves, pumps and mixers that exert precise control of fluid flow. This makes it possible to control the chemical and physical parameters like ph-value or temperature, giving rise to many experimental possibilities. Various features like the artificial integration of chemical gradients, mechanical barriers and obstacles or electrical and optical stimulation in order to control of microenvironment can be implemented. [138] Their applications make use of the generation of pressure, concentration gradients and precise control over the microenvironment to simulate physiological environments for cell cultures. [139][140] Their integration in OOC device applications also enabled high-resolution and real-time imaging possibilities resulting in substantial advances in the monitoring of otherwise highly scattering three-dimensional tissues and organs in vitro.

Exemplary for the successful implementation of microfluidics within neuron-on-a-chip technologies, a pyramidal setup of interconnected, serpentine microfluidic channels on a chip has been developed to facilitate the control of molecule and signal factor concentration gradients by application flux parameters. [141][142] Furthermore, a laminar flow regime in a microfluidic setup alongside nanostructure patterning assists neuron placement, migration and growth on the chip. Microfluidic technology aids in the control of axonal directionality, growth or precise application of axotomy and cell injury. [143]

TU Bibliothek WIEN Your knowledge hub

Electrophysiological assessment in vitro

The electrophysiological measurement is a type of neuroscientific experiment branch that explores the electrical activity of living neurons to investigate the cellular functionality. It is based on measuring the ion channel flow and the extracellular potential of electrically active cells like neurons or cardiomyocytes. As it is one of the oldest acquisition techniques, today's state of the art ranges from single ion-channel to whole brain imaging technologies like electroencephalography. [144][145]

Single-unit recording describes the small-scale measurement of intracellular action potentials of cells by in-

Die approbierte gedruckte Originalversion dieser Diplomarbeit ist an der TU Wien Bibliothek verfügbar
The approved original version of this thesis is available in print at TU Wien Bibliothek.
TU WIEN Bibliothek Your knowledge hub

serting a microscopic electrode or in close proximity to non-invasive electrodes. Typical signals are 2-5ms long action potentials. Bigger electrodes like the ones used in this thesis in the range of up to several hundred microns are used for multi-unit recordings of simultaneously active neurons, assessing whole-field potentials. [146] In the latter case, various recording sites with synchronous net activity can be simultaneously recorded and analysed. Whole field potentials with a multitude of different signals are measured, which enable the assessment of spatiotemporal patterns of neural networks. They are generated and added up by synaptic currents, fast action potentials, afterpotentials, Na+/Ca2+ spikes and voltage-/ligand-gated intrinsic currents. [147] Filtering and software analysis are required to distinguish and sort out signals of interest from noise, which are identified when the voltage measured by an individual electrode fulfils specific criteria like exceeding a threshold over a specified time or other. Raw electrode data needs data processing to define and sort spikes, which on a higher level of analysis reveals spatiotemporal spike organisation, e.g. for structure-function assignment. [148]

Neuron-on-a-chip: state of the art

A neuron-on-a-chip device is a microfluidic cell culturing device, often equipped with integrated circuits to investigate electrically active biological tissue. It is a member of the recently emerged organ-on-a-chip device family. The primary purpose of OOC approaches with neuron-based systems is to mimic neurological responses in vitro and decrease the demand for in vivo experiments. The introduction of OOC devices into neuroscience enabled new unique features like optical and electrical monitoring techniques during experiments. The data acquisition and analysis of whole neuronal networks were initially restrained due to technical limitations in recording electrical activity of multiple neurons at once. However the first multi-channel chips with limited performance had already been developed back in the 1970s. [149] Since then, macro-scaled brain-on-a-chip devices using either isolated brain tissue or brain slices have been developed. [140] As cell culturing techniques, biocompatible polymers, microfluidics and microscale electronics progressed, single neural cell evaluation advanced into micro-scaled single synapse event[150] or single ion channel monitoring. [151] Today, a multitude of specialised chips exist. Neuron-on-a-chip devices can be divided into six general categories, as depicted in Figure 2.9: in 2D monolayer cultures, in 3D with engineered scaffold systems, organoids like embryoid bodies, tissue explants, neurospheres or bioreactor based models. [152] Lee *et al.* distinguishes multiple techniques for self-assembly of arrayed 3D multicellular spheroids by using microplatforms from hanging-drop, microwell arrays, micropatterned substrates, microfluidic chips to the encapsulation of cells in microfiber or microparticles. [153]

An example of studies with complex combined applications of neural tissue growth and OOC systems are the neurospheroid-on-chip by Chang *et al.*, demonstrating the generation of functional neural connections capable of signaling between artificial nervous tissues. [98] They created artificial 3D nerve-like neural bundles to simulate the formation of certain nervous system growth patterns in vitro. Park *et al.* presented a study about a 3D brain-on-a-chip with neurospheroids and integrated flow to model Alzheimer's disease. The application of a physiological flow regime to mimic in vivo conditions of the interstitial part of the brain was implemented to assess the toxicity of amyloid beta, a major contributor in Alzheimer's disease, on neurospheroids. Furthermore, the influence of flow on size, neural network formation and neural differentiation of neurospheres was measured. [154] Another noteworthy example of neural OOC applications is the 3D-innervated corneal tissue chip for the simulation of anatomy, properties and cellular components of corneal tissue[155] to study innervation-on-a-chip. Zhou *et al.* presented a nanoelectrode-innervated tissue hybrid chip, in which they developed tissue-scaffold-mimicking 3D nanoelectronic arrays for 3D mapping and manipulation of electrical activity in real-time, an example of developing a model to simulate in vitro tissue. [156]

Author/Year	Cell line/type	Species	Description
Wijdeven/2018[160]	DRG	Rat	Structuring axon growth in multi-nodal neural network (MNNN) on-chip
Bobo/2020[138]	PC12	Rat	Neural on-chip calcium response to mechanical stimulation
Zhou/2017[159]	ASH	C.Elegans	Neuro-modulation chip: sensoric-neural response to ultrasound stimulation
Wijdeven/2020[143]	Corticon	Rat	LOC platform for axotomy and electrophysiological neuromodulation in a MNNN
Song/2013[162]	P19	Mouse	LOC impedance flow cytometer to identify differentiation status of P19 cells
Kim/2011[163]	P19	Mouse	On-chip differentiation of P19 cells and cell trapping with microfluidic networks

Table 2.2: Overview on milestones in neuron-on-a-chip applications

In a study conducted by Kato-Neghishi *et al.*, dissociated cortical cells were seeded in microchambers of a microwell array and cultured for 1–2 weeks, during which neurospheroids extended axons to neighboring neurospheroids, forming tight connections between them. [157]

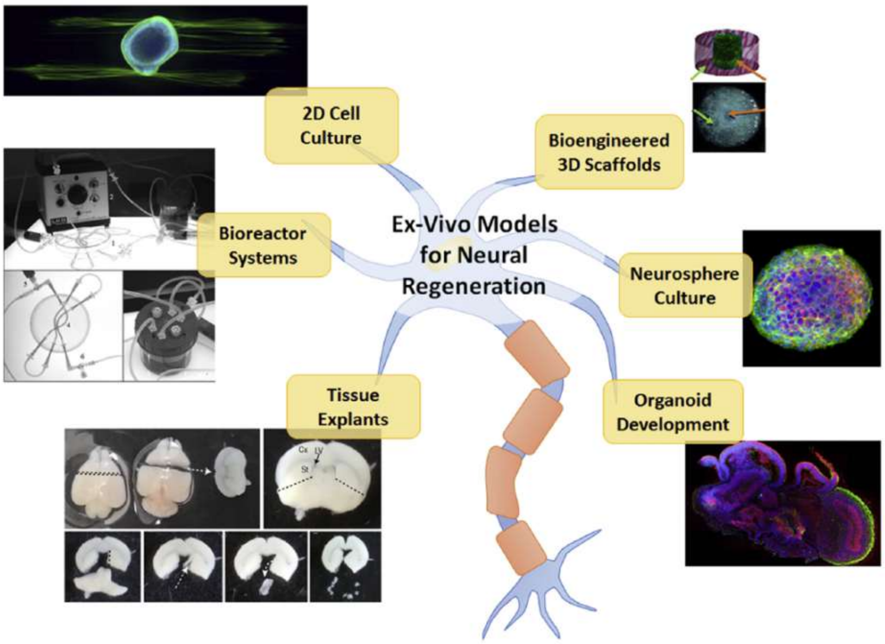

Figure 2.9: Categories of neuron-on-a-chip technologies [158]

In addition to before-mentioned studies, an overview of current state of the art, relevant milestones of OOC applications in neuroscience and specifically of neurons-on-a-chip devices are presented in Table 2.2. The mentioned works from Bobo[138] and Zhou[159] for example used different physical stimulation techniques and protocols to investigate their effects on cell activity on-chip. At the same time, Wijdeven contributed strongly to chip design to neural network. [160][143] The OOC technology is a valuable technology for the structure-function-mapping of neurons and their synaptic connections to the different parts of the neural system: the connectome. [161]

Further presented studies show the progress of OOC applications for P19 cells[162]. The study published in *Lab Chip* by Kim *et al.* [163], presents a chip with the 3D on-chip differentiation of P19 ESC embryoid bodies assessing the early differentiation of ES cells - this thesis can therefore be viewed as an expansion with investigation of size-dependent spheroid proliferation and differentiation efficiency analysis as well as electrophysiological activity measurements.

Die approbierte gedruckte Originalversion dieser Diplomarbeit ist an der TU Wien Bibliothek verfügbar
The approved original version of this thesis is available in print at TU Wien Bibliothek.
TU WIEN Bibliothek Your knowledge hub

Die approbierte gedruckte Originalversion dieser Diplomarbeit ist an der TU Wien Bibliothek verfügbar
The approved original version of this thesis is available in print at TU Wien Bibliothek.

Chapter 3

Materials and Methods

This chapter lists the materials, chemicals, reagents, laboratory equipment and scientific methods used to acquire the data for this thesis.

3.1 Materials

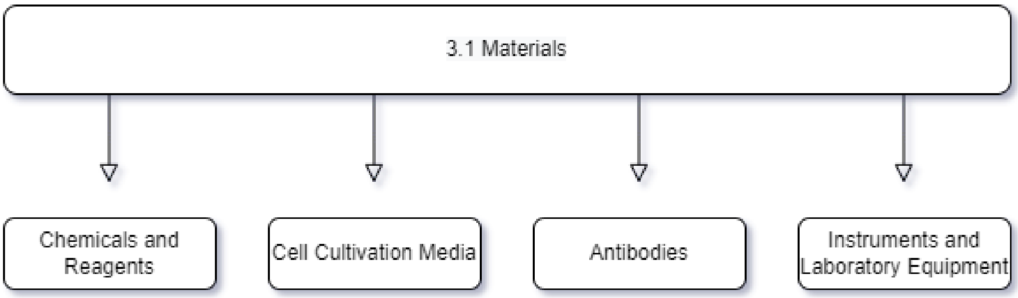

The following lists provides an overview of the chemicals and reagents (Table 3.4), the cell cultivation media (Table 3.1), the used antibodies for stainings (Table 3.3) and the instruments and laboratory equipment (Table 3.2) used in this study.

Cell cultivation media

This section gives a brief overview of the different cell culture formulations that were used for the cultivation and subsequent differentiation of the P19 cell line. The following table lists their precise relative concentrations.

The standard medium

This medium was used for cultivation, passaging and during the first three days (day 0 until 2) of the embryoid body formation and differentiation protocol.

Inducer medium

The inducer medium is an expansion of the standard medium with 1 µM RA used to trigger the cells' differentiation into neurons.

Neurobasal medium

The neurobasal medium was used for the differentiation of the P19 cells.

Die approbierte gedruckte Originalversion dieser Diplomarbeit ist an der TU Wien Bibliothek verfügbar
The approved original version of this thesis is available in print at TU Wien Bibliothek.

The components of the used cell media

Medium	Component	Concentration
Standard medium	α-MEM	89%
	Newborn Calf Serum	7.5%
	Fetal Calf Serum	2.5%
	Antibiotics	1%
Inducer medium	*Like standard + Retinoic Acid*	1µM
Neurobasal medium	Neurobasal® Medium	96.75
	B27	2%
	L-Glutamine	0.25%
	Antibiotics	1%

Table 3.1: The components of the standard, inducer and neurobasal medium

The used laboratory equipment and instruments

Device	Model	Manufacturer
Spin coater	COROS OP15	Siemens, Fairchild Semiconductor
Sputter	LS 320 S	VonArdenne
PECVD	PlasmaPro 100 PECVD	Oxford Instruments
RIE	Plasmalab System 100	Oxford Instruments
Plasma Cleaner	PDC-002-CE	Harrick Plasma
PDMS Cutter	CAMM-1 GS-24	Roland
Microscope for IHC and calcium stainings	cellVivo	Olympus Lifescience
MEA signal acquisition	MEA1060-(Inv/Up/BC), TC02	MultiChannel Systems

Table 3.2: The instruments and laboratory equipment

The used antibodies

Product name	Target	Manufacturer	Cat. No.
Alexa Fluor Plus Goat anti-Rabbit 555 nm IgG	GFAP (astrocytes)	Invitrogen	A32732
Alexa Fluor Goat anti-Chicken 488 nm IgY	MAP2 (neurons)	Invitrogen	A11039

Table 3.3: Overview of the antibodies employed in the evaluation of P19 cell differentiation

The used chemicals and reagents

Chemical	Manufacturer	Catalogue Number
$\alpha - MEM$	Sigma-Aldrich	M4526
α-Lipoic acid	USP Reference Standard	1368201
Antibiotic Antimoycotic solution (100x)	Sigma-Aldrich	A5955
AZ 5214E	MicroChemicals	n.a.
B27	Gibco	17504044
Bovine serum albumin	n.a.	n.a.
Dimethylsulfoxid (DMSO)	Roth	0728.1
Dulbecco's PBS	Sigma-Aldrich	D8537
Dulbecco's PBS with MgCl2 and CaCl2	Sigma-Aldrich	D8662
Ethidium Homodimer	Sigma-Aldrich	46043
Fetal bovine serum	Sigma-Aldrich	F0804
Fluo-4 AM Calcium Imaging Kit	Thermo Fisher Scientific	F10489
Hank's Balanced Salt Solution	R & D Systems	B32150
Hellmanex III	Sigma-Aldrich	20059584
Hoechst 33342 dye	Invitrogen	11544876
L-Glutamine	Gibco	25030
Neurobasal® medium (1x)	Gibco	21203-049
Newborn calf serum	n.a.	n.a.
Paraformaldehyde	VWR	28794.295
Dulbecco's PBS	Sigma-Aldrich	D8537-500ML
Retinoic acid	Sigma-Aldrich	R2625
Sodium chloride	Sigma-Aldrich	71383
TI Prime	MicroChemicals	n.a.
Triton X-100	Sigma-Aldrich	X100
Trypsin–EDTA Solution	Sigma-Aldrich	SLCD2567
Trypsin-EDTA (0.25%), phenol red	Thermo Fisher Scientific	25200056
VECTASHIELD® Antifade Mounting Medium	Vector Laboratories	H-1200-10

Table 3.4: A tabulated overview of the used chemicals and reagents

Die approbierte gedruckte Originalversion dieser Diplomarbeit ist an der TU Wien Bibliothek verfügbar
The approved original version of this thesis is available in print at TU Wien Bibliothek.

Die approbierte gedruckte Originalversion dieser Diplomarbeit ist an der TU Wien Bibliothek verfügbar
The approved original version of this thesis is available in print at TU Wien Bibliothek.

3.2 Methods

This section describes the scientific methods, technical processes and experimental parameters used in this thesis.

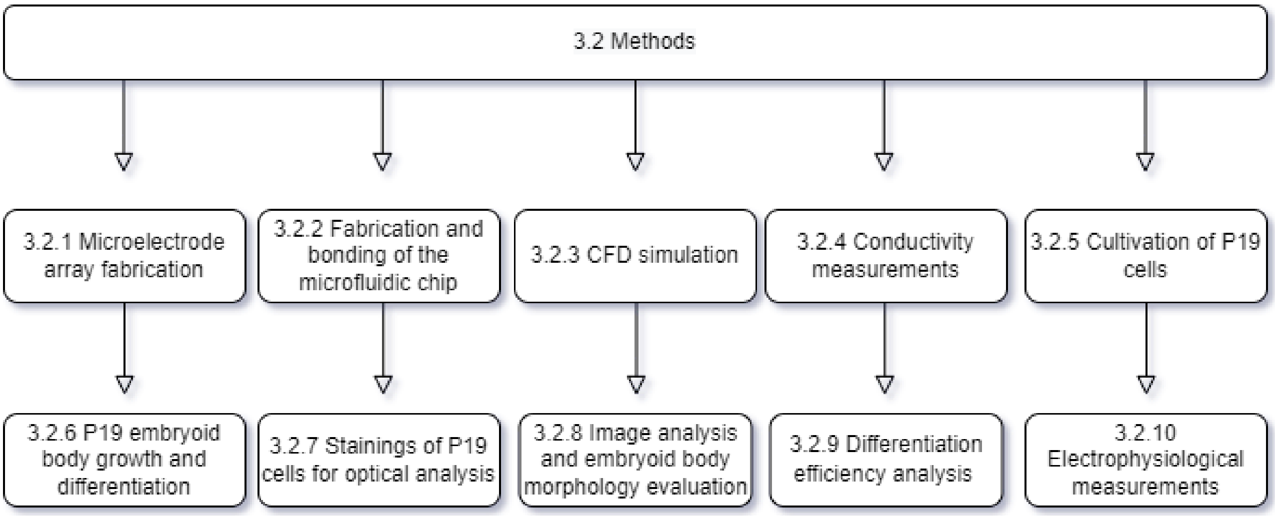

3.2.1 Multielectrode array fabrication

The MEA was built in a cleanroom environment (degree of purity level 5 after ISO 14644-1[164]) in the Center of Micro- and Nanostructures at the Technical University Vienna. Depiction 3.1 presents the individual steps to produce the MEA.

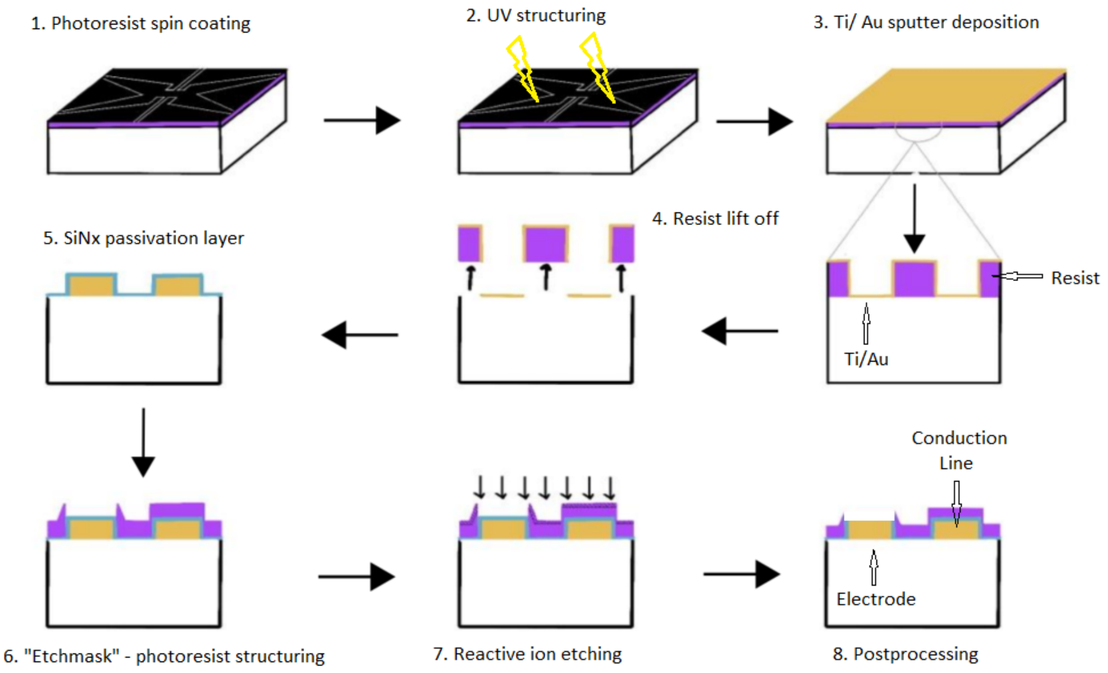

Figure 3.1: The individual MEA production steps

As a quick overview, the steps for the fabrication of the MEA can be summarised in two steps:

Die approbierte gedruckte Originalversion dieser Diplomarbeit ist an der TU Wien Bibliothek verfügbar
The approved original version of this thesis is available in print at TU Wien Bibliothek.

1. Conduction Layer

In the first step, the electrode tabs and conductive connects on the MEA was structured via the sputter deposition technique on a glass substrate. This is accomplished by using thin film lithography with the photoresist AZ5214, depositing a titanium layer, followed by a gold layer via magnetron sputtering and finally removing the metal from undesired areas with a so-called lift-off step using aceton.

2. Passivation Layer

In order to insulate the conduction lines, a dielectric silicon nitride layer was deposited. Since the electrodes would then also be subsurfaced and insulated, the passivation layer over them was removed in the following step via reactive ion etching.

In the following, each step is described in detail.

Preparation of glass substrate

Firstly, the glass substrate was cleaned. For that, it was placed into a glass with acetone and exposed to an ultrasonic bath for 1 min at maximum intensity. Afterwards, the surface of the glass was washed thoroughly with acetone and isopropanol, so that the acetone does not leave any residues on the surface. After that, the rest of the liquid was removed by pressurised air and a short bake on a hotplate (120 ℃) for 2 min.

Lithography

In order to create the patterned structure of the electrodes as well as the conduction lines between inner and outer electrodes, an optical lithographic process was applied. An image reversal photoresist was used, where the light-exposed area became soluble. The exposed areas of the image reversal photoresist, on the other hand, got cross-linked and insoluble in the reversal bake step. The main advantage of this procedure lies within the "undercut" structure at the edges of the exposed-unexposed areas.

As a first step, one layer of TI Prime was added to increase the adhesiveness of the photoresist to the substrate.

Therefore, the glass sample was transferred into the spin coater and then fully covered by pipetting the TI Prime.

After applying the TI Prime, the spinner was accelerated with 2000 $\mathrm{rpm\,s^{-1}}$ to a maximum speed of 4000 rpm. Then, the sample was removed from the spinner and placed on top of a hotplate (120 ℃) for 2 min for a "pre-bake" step, removing the solvents within the resist and increasing the viscosity. Secondly, the photoresist AZ5214 was applied to the glass and the whole process was repeated with the photoresist with an acceleration of 750 $\mathrm{rpm\,s^{-1}}$ to a maximum speed of 3000 rpm and pre-baked on the hotplate (100 ℃) for 60 s.

Chemical	RPM	RPM/s	Time (s)	HP Temp. (℃)	HP Time (s)
AZ 5214E	3000	2000	30	100	60
TI Prime	4000	750	30	120	120

Table 3.5: Production parameters for the spin coater

Next, the sample and the lithographic mask were inserted into the aligner for UV exposure. For that, a laser-printed mask to imprint the patterns on the substrate was used. The sample was manually positioned according to align symbols on the edges of the mask and put into direct contact with the latter. A depiction of the lithographic mask is shown in Figure 3.2.

Then, it was illuminated with UV light for 4 s or 40 $\mathrm{mS\,cm^{-2}}$. Afterwards, the sample was put on a hotplate for the "reversal-bake" step at 120 ℃ for 70 s, for crosslinking the UV-light activated area. Then the sample was

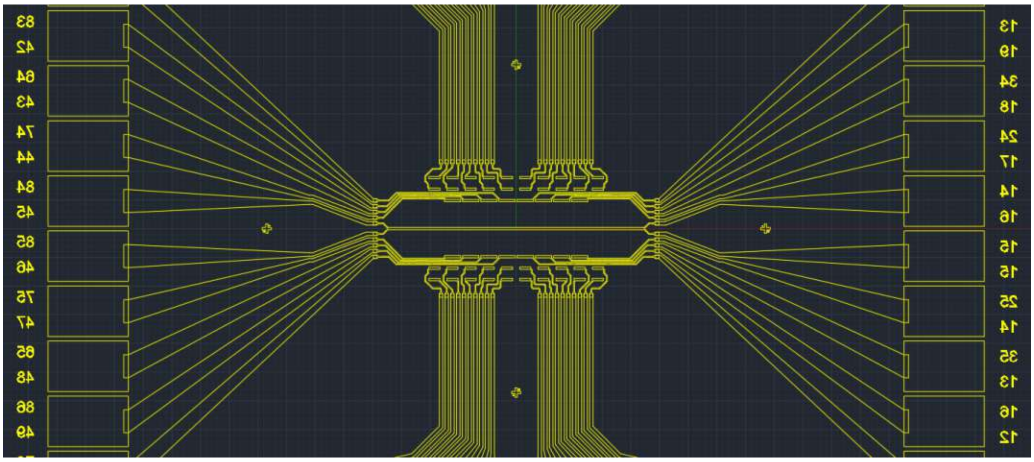

Figure 3.2: Depiction of the lithographic mask

again placed in the aligner and flood exposed for 20 s (equivalent to 250 mS cm^{-2}) without a mask to make the areas which remained unexposed in the first step soluble. In the last step, these areas were removed by gently stirring the sample in the developer (AZ 726MIF) for 70 s. The resulting layer of photoresist had an average thickness of 1.4 µm.

Sputter deposition

After the substrate had been patterned, the conducting metal layer was added in the next step. For this, magnetron sputtering as an anisotropic physical vapour deposition method has been proven suitable. The anisotropy of this technique is important, because the photoresist with the unwanted deposits needed to be removed in a lift-off step with acetone, which can only enter via the undercutted structures. As a first step, a sacrificial layer of titanium was deposited at maximum intensity to remove remaining oxygen in the chamber. Then, a thin middle layer of approximately 15 nm titanium was added before the deposition of gold as the conduction bulk material. This is required since noble metals like gold have bad adhesive properties on glass due to their chemical inertness. [165]

After the samples were introduced in the device, the reaction chamber was evacuated to a pressure of 1×10^{-5} mbar before depositing titanium on the sample. A high vacuum is important not only for the plasma, but also to ensure a low number of oxygen atoms, which react with the titanium to TiO$_2$ and highly degrade the quality of the layer.

Then, the primary bulk conductivity material gold was added. The same pressure, time and energy values were used, resulting in a layer of approximately 160 nm thickness.
Three different deposition protocols have been used in this thesis. The resulting MEAs were named Ti/Au-MEA V1, Ti/Au-MEA V2 and Ti/ITO/Au-MEA. Their process parameters are depicted below in this order in Tables 3.6, 3.7 and 3.8.

Target	Energy (W)	Base Pressure (mbar)	Working Pressure (mbar)	Time (s)	Layers
Ti	50	1×10^{-5}	8×10^{-3}	60	2
Au	50	1×10^{-5}	8×10^{-3}	50	2

Table 3.6: Used production parameters for the sputter for the Ti/Au-MEA "V1"

In order to obtain the desired patterning, the Ti/Au-layer on the undesired areas with the resist below was then removed by the so-called lift-off technique. Since the resist is soluble by acetone-containing reagents, the samples were placed in an acetone bath for 15 min to 25 min on a hotplate (58 ℃) and carefully blown with a

Die approbierte gedruckte Originalversion dieser Diplomarbeit ist an der TU Wien Bibliothek verfügbar
The approved original version of this thesis is available in print at TU Wien Bibliothek.

Target	Energy (W)	Base Pressure (mbar)	Working Pressure (mbar)	Time (s)	Layers
Ti	50	5×10^{-6}	8×10^{-3}	60	5
Au	50	5×10^{-6}	8×10^{-3}	60	3

Table 3.7: Used production parameters for the sputter for the Ti/Au-MEA "V2"

Target	Energy (W)	Base pressure (mbar)	Time (s)	Layers
Ti	50	1×10^{-5}	60	1
ITO	50	1×10^{-5}	60	8
Au	25	1×10^{-5}	30	2

Table 3.8: The parameters in the sputter device for the Ti/ITO/Au-MEA

pipette to remove residual Ti/Au of the surface. The substrate was then placed for 1 min in the ultrasonic bath at the lowest intensity. Lastly, it was carefully rinsed with Isopropanol and dried with pressured nitrogen.

Passivation layer

As mentioned before, the electrodes in the middle of the MEA act as the cell seeding spot for input signals, which are transmitted via the conductive lines to the outer electrodes. Subsequently, an insulating layer of SI_3N_4 was added by the process of PECVD to avoid noise resulting from the unshielded conductive lines.
Prior to that, a spin coating step in order to apply a layer of TI Prime was added to ensure proper adhesion of the SI_3N_4 on the gold layer. This was executed as mentioned before.
After the sample was positioned on the mounting table, the lid was closed and the sample was transferred into the reaction chamber. Then, a vacuum was generated and the mounting table was heated. Summaries of the detailed gas fluxes are depicted in Table 3.9.

SiH_4	NH_3	N_2
875	20	300

Table 3.9: The used gas fluxes (in sccm) for the PECVD

Temp. (°C)	Energy (W)	Pressure (mbar)	Time (min)
875	20	300	50

Table 3.10: Used production parameters for the PECVD

This step was executed for 30 min at 20 W with an additional low frequent sinus wave with a median energy of 20 W and a pressure of 1.333 mbar. Detailed process parameters are provided below in Table 3.10.

Reactive ion etching

Lastly, an etch step with the RIE technique in order to excavate the electrodes, which are buried beneath the dielectric silicon dioxide layer, was executed.

For this, a lithographic mask that is depicted in Figure 3.3 was used in order to transfer the pattern on a photoresist. In the depiction, the big framed areas left and right as well as the small patterned area in the middle are the electrode tabs, the rhomb-shaped areas are alignment markers. Only the contact tabs of the inner and the outer electrode are framed and protected from UV exposure. This means, that in those areas will be no photoresist as a protecting layer for the ion etching. The photolithographic procedure was executed as

Die approbierte gedruckte Originalversion dieser Diplomarbeit ist an der TU Wien Bibliothek verfügbar
The approved original version of this thesis is available in print at TU Wien Bibliothek.

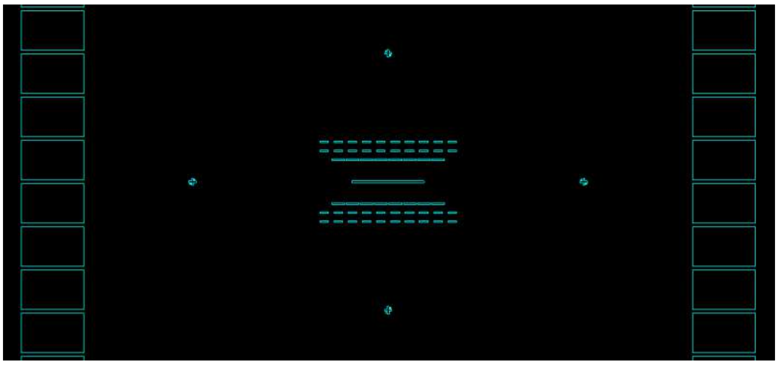

Figure 3.3: Depiction of the etch mask

mentioned before. Then, the sample was inserted into the mounting table of the RIE. The etch process was executed with $20\,\mathrm{c^3m/min}$ of SF6 and $10\,\mathrm{c^3m/min}$ of Ar. A detailed list of the used parameter is given below in Table 3.11.

Energy (RF) (W)	Energy (ICP) (W)	Set Pressure (mbar)	Strike Pressure (mbar)	Time (min)
50	100	6.66×10^{-5}	5.33×10^{-5}	10

Table 3.11: Used production parameters for the RIE

3.2.2 Fabrication and bonding of the microfluidic chip

Design and fabrication The PDMS microfluidic chip was designed with Autodesk applications AutoCAD and Fusion 360 according to the experimental design requirements.

PDMS sheets with a thickness of $500\,\mu\mathrm{m}$ per layer were xurographically plotted. The cutting conditions were set to a cutting speed of $3\,\mathrm{cm\,s^{-1}}$ with a blade offset of $0.25\,\mathrm{mm}$.

Bonding of chip and MEA Prior to the bonding, a three-step-cleaning protocol for the MEA was executed: first, it was immersed in an aqeuous solution with 2% "Hellmanex III" in DI-Water and put in an ultrasonic bath for $15\,\mathrm{min}$. Then, the same procedure was repeated twice with the MEA immersed in 2-Propanol and DI-Water respectively, each time followed by an ultrasonic bath for $15\,\mathrm{min}$. After the PDMS had been cut, the protection foil with the bottom design was removed with tweezers. The PDMS foil and the MEA were put inside the plasma cleaner, the bonding sites facing upward. The vacuum was generated and the plasma was activated for $2\,\mathrm{min}$ with the highest intensity setting for 2 minutes. Then, the activated surfaces of foil and MEA were placed on top of each other, aligned and softly pressed on for $30\,\mathrm{s}$. This was repeated several times depending on the intended design and the number of used PDMS layers. Lastly, the microfluidic device was cured at $80°$ overnight while constantly applying gentle vertical force onto the surface.

3.2.3 CFD simulation

Continuous Fluid Dynamics (CFD) simulation has been executed by implementing a 3D object of the fluid body within the Autodesk software environment to analyse and improve the design. For that, the following boundary constraints and model parameters were chosen as following:

1. Water was chosen as the fluid with density $1\,\mathrm{g\,cm^{-3}}$.

Die approbierte gedruckte Originalversion dieser Diplomarbeit ist an der TU Wien Bibliothek verfügbar
The approved original version of this thesis is available in print at TU Wien Bibliothek.
TU WIEN Bibliothek Your knowledge hub

2. As an input, a homogenously distributed volumetric flow $10\,\mathrm{mm}^3/\,\mathrm{min}$ was set directed downwards on the surface of the inlet.
3. Only the in-/outlet are in contact with the atmosphere and wells have closed lids. A homogeneously distributed gauge pressure of $1\,\mathrm{bar}$ was set on the outlet of the design on the right.

3.2.4 Conductivity measurements

The conductivity measurements have been executed at a probe station using a two-point measurement with gold pins. A four-point measurement would reduce the measurement error by the exclusion of the contact resistance of the pins. However, the small dimensions of the electrodes hindered the realisation of this technique. The pins of the probe station were positioned in the middle of the contact pads very carefully to not break through the thin material layers. Next, a voltage sweep was introduced from $-1V$ to $+1V$ with a resolution of $0.02V$. Due to the inevitable zero crossing, which arises by dividing through the decreasing denominator of Ohms' law, only the first and the last 30% of data points have been used for later examination.

The specific bulk resistance ρ was calculated using the following equation:

$$\rho = R \cdot \frac{A_{el}}{L} \tag{3.1}$$

R is the resistance, A_{el} is the cross-sectional area, L is the length of the conduction line.

3.2.5 Cultivation of P19 cells

After the production and examination processes of the OOC device has been described, the cell cultivation protocols for the P19 ESC line are presented next. Generally, the cells were frozen in a solution of 90% Fetal Calf Serum and 10% DMSO. They were stored at -120 ℃, with an intermediate step at -80 ℃ for 24 h before freezing.

Cell passaging

In order to ensure the viability of the cell culture, the cell cultures were split regularly. According to the grade of confluency, this process was repeated every second day. Before beginning, the laminar and all listed consumables were thoroughly sterilised by spraying with 70% ethanol. Trypsin, PBS and cell medium were heated to 37 ℃ in a water bath. Firstly, the cell medium was aspirated carefully. The cell layer was washed by adding 5 ml of PBS and gently shaking. Then, 3 ml of trypsin were added and incubated for $5\,\mathrm{min}$ to demount the extracellular matrix holding the cells in position. Next, 6 ml cell medium were added again to deactivate the trypsin. The mixture was centrifuged for $5\,\mathrm{min}$ at 140 rcf and the liquid phase was removed. Next, 1ml of cell medium was added again and resuspended carefully using a pipette. Lastly, the cells were seeded in a new T75 flask with 15 ml cell medium.

Cell counting

In order to be able to seed different cell densities, cell counting was performed. First, the cells were passaged as mentioned above in 3.2.5, but prior to centrifuging, an aliquot of 10 µl was aspirated and mixed 1:1 with Trypan Blue. The living cells were counted in a hemocytometer chamber by Neubauer. Since one chamber has a volume of 0.1 µl, the following formula was used for the calculation of the cell number:

$$2 * 9ml * 10^4 = \textit{Number of cells}$$

Die approbierte gedruckte Originalversion dieser Diplomarbeit ist an der TU Wien Bibliothek verfügbar
The approved original version of this thesis is available in print at TU Wien Bibliothek.

3.2.6 P19 embryoid body growth and differentiation

All experiments were executed following a strict cell preparation protocol. Throughout the whole protocol, the cell medium was changed at least every second day if not stated otherwise. The medium was exchanged by aspirating cautiously from the side walls with a pipette in order to avoid mechanical damage to the ground coating of the microplate.

After the P19 cells had been cultivated in a cell culturing flask and counted (if required), the undifferentiated cells were seeded at various densities with 200 µl standard medium in a 96-well Spheroid Microplate with Ultra-Low-Attachment (ULA) walls. Generally, the differentiation process consists of three phases.

In phase one, the cell proliferation and aggregation toward a spheroid body is supported with the basic medium from day 0 until day 3.

In phase two, the cells are exposed to inducer medium with RA, where the cell differentiation is triggered from day 3 until day 6.

In phase three, the differentiated embryoid body is ready to be transferred onto a chip and used in an experiment. The cells are exposed to neurobasal medium beginning with day 7. Figure 3.4 depicts a timeframe of this protocol.

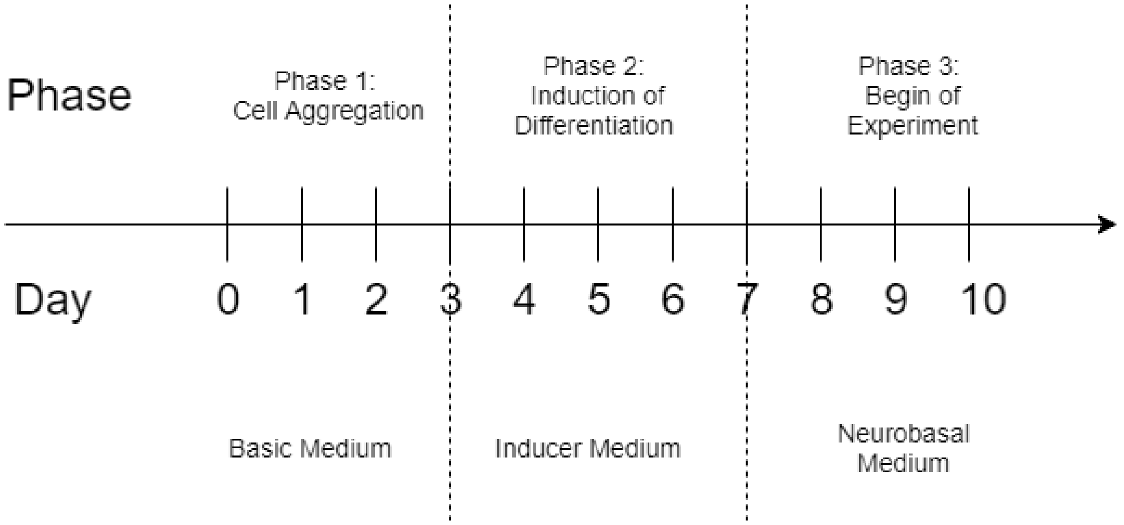

Figure 3.4: A timeframe visualizing the phases of the embryoid body generation and differentiation process

Cell seeding on chip

Prior to the cell seeding on D5 in the well plate, the surface of the chips was sterilised with 70% ethanol and a UV bath for 10 min. Next, the chips were coated in poly-l-lysine on D6 for enhanced cell-chip adhesion for one hour at RT, washed three times with DI and put in the incubator for 15 min. On day seven, the chips were prefilled with neurobasal medium. The cell spheroids were then carefully moved to the coated chips positioned in petri dishes:

In detail, cell aggregates were aspirated with a pipette with a truncated pipette tip, which was employed to transfer the embryoid bodies from the 96 well plate into the chambers of the microfluidic device. Here it is important to mention, that the pipette was held in a vertical position until the embryoid body sank to the bottom into the well only by gravitation. Avoiding medium convection reduces the risk of generating bubbles, potentially causing shear stresses and wrong positioning of the other previously transferred cell aggregates. Lastly, the wells of the chips were sealed with a PCR foil and the chips were placed in a petri dish together with several PBS-filled containers to prevent drying.

Die approbierte gedruckte Originalversion dieser Diplomarbeit ist an der TU Wien Bibliothek verfügbar
The approved original version of this thesis is available in print at TU Wien Bibliothek.
TU WIEN Bibliothek Your knowledge hub

3.2.7 Stainings of P19 cells for optical analysis

Cell stainings have been done to verify cell viability, quantify cell differentiation efficiency and show the existence of electrical signalling between the cells. Pictures and videos were taken with an Olympus cellVivo. Before any staining was applied, the cells were always cultivated in a Corning 96-Well Microplate. Also, it was paid attention to shielding the samples and dyes from light to avoid signal bleaching.

The platform, that a fraction of the stainings has been performed on, was a straightforward, simplified chip design. The design consisted of a PDMS slide of 500 µm in height with a cylindric hole (with a diameter d=17 mm) bonded on a standard microscope slide as the culturing area for the P19 ESCs. The cylinder was coated with poly-l-lysine to ensure cell-surface adhesion, and the cell medium with three EBs was carefully dropped inside.

Live dead staining

Live dead cell stainings were performed to examine the cultures' viability in different experiments. Generally, within each resolution the same exposure times were kept to ensure comparability of the different pictures. The samples were exposed to the dyes diluted in basic cell medium at RT for approximately 15 min and then washed with PBS before analysis.

2D stainings: Calcein-AM and ethidium homodimer (EtHD) were used to stain live cells and dead cells, respectively, for the planar arrangement of the cells on the PDMS slides. Calcein-AM was applied at a concentration of 1:2000 and EtHD at 1:500 in neurobasal medium. A representative section of the cells was chosen, and the number of live cells was divided by the amount of dead cells.

3D stainings: For the spatial viability monitoring of the cells in the PDMS chips and the microwells, Höchst was used to stain all cells, living or dead, while Ethidium Bromide was used for staining the dead cells only. Here, both chemicals only stain the nucleus. Since, in a 3D arrangement, it is impossible to count cells via two-dimensional graphical examination as there could be several targeted epitopes behind each other in a row, images were analyzed by using a positive reference control generated by treating cells with 1% Triton-X over night. Here, since only dead cells were in the control group, the intensity ratio between the Ethidium and the Höchst signals defines zero viability.

Immunofluorescence staining

Immunohistochemistry staining (IHC) was performed to assess the efficiency of differentiation of the EBs in the neuronal lineage. The cells were fixated in 4% paraformaldehyde in PBS and stored in the fridge before the staining. Samples were washed washed three times with PBS $MgCl_2$ enriched PBS. The stainings have been executed on chip with the before-mentioned simplified chip design as well as off-chip in an ultra-low attachment wellplate with equal staining procedures.

On the first day, the microscope slides with the PDMS chip containing the cells were washed with PBS for 5 min. Then the cells were immersed in permeabilisation buffer containing 0.2 % Triton, which enables the antibodies to invade the cell spheroids and bind to the respective epitopes. Next, the embryoid bodies were exposed for 2 h at RT to the blocking buffer, a mixture that blocks other epitopes of the cells and thus increases the specificity of the antibodies. The primary MAP2 antibody for neurons was diluted in the blocking buffer at a concentration of 1:1000 as well as the primary GFAP antibody for the astrocytes, which had a concentration of 1:250. The blocking buffer was then washed away with HBSS, wrapped into aluminium foil for light protection and put into the fridge.

On day two, the samples were taken out of the fridge and washed twice in a row for 15 min. Then, the two secondary immunoconjugated antibodies Alexa Fluor 488 nm and 555 nm, diluted in blocking buffer with a concentration of 1:1000 respectively, were added and left to be absorbed by the samples for 1 h at RT. Lastly, the

Die approbierte gedruckte Originalversion dieser Diplomarbeit ist an der TU Wien Bibliothek verfügbar
The approved original version of this thesis is available in print at TU Wien Bibliothek.

samples were again washed twice for 15 min and a counterstaining (in DAPI) was added. After incubating for 1 h at RT, cells were washed once for 15 min and placed upon a microscope slide. The remaining PBS around the EBs was dried and sufficient Mounting Medium was dropped upon the EBs. Lastly, glass slides were placed upon the EBs and sealed with nail polish remover to prevent drying of the samples. Finally, the EBs were imaged using a fluorescence microscope.

Ingredient	Function
PBS + CA^{2+} + 1% BSA + 5% FCS	Blocks undesired antigen binding on epitopes
PBS + 0,2% Triton X-100	Increases cell membrane permeability

Table 3.12: The used buffers and their components

Calcium staining

The calcium staining was executed to show neuronal signalling between the cells.
Firstly, the samples were washed with HBSS. Then, they were exposed to a mixture containing 2.5 ml HBSS as a buffer, 25 µl of power load and 2.5 µl Fluo-4 firstly in the incubator and then outside at RT for an exposure time of 15 min, respectively. Lastly, they were again thoroughly washed with HBSS before inserting them into the cellVivo for analysis.

3.2.8 Image analysis and evaluation of embryoid body morphology

Diameter and area

Prior to the electrophysiological measurements, the growth and size of the spheroids for various seeding densities were examined in order to define reasonable dimensions for the cell compartments on the chip. Differently sized EBs were generated by employing different starting seeding densities of 200, 500, 1000, 5000, 10.000 and 20.000 cells. On day 7, size and morphology were documented by means of optical analysis. The image analysis of the cell spheroids was executed within Fiji, an open-source image processing software. For the area analysis, an elliptic morphology of the EBs was assumed and measured by manually applying an elliptic overlay. The average of the longest and the shortest diameters or major and minor axis was defined as its diameter. Generally, disruption of parts of embryoid bodies of bigger sizes were ignored, as their influence on the difference in size in a two-dimensional depiction of a spherical object is neglectable. The results were collected, analysed and plotted with a Matlab script.

Circularity

Additionally, the circularity of the spheroids was calculated and compared according to the different seeding densities. It was calculated by a FIJI plug-in using the following formula:

$$Circularity = 4pi(area/perimeter^2),$$

assigning a relative value between 0 and 1, where 1 indicates a perfect circle and 0 indicates an increasingly elongated polygon. [166] After the perimeter was calculated by generating a binary image using a java macro in ImageJ from Palmieri *et al.*, the perimeter pixels were extracted and summed up. [167] The resulting perimeter length for each embryoid body was then calculated by converting the pixels back to micrometer, according to scale. The final circularity was calculated with the mean area of each seeding density.

Die approbierte gedruckte Originalversion dieser Diplomarbeit ist an der TU Wien Bibliothek verfügbar
The approved original version of this thesis is available in print at TU Wien Bibliothek.

3.2.9 Differentiation efficiency analysis

The P19 EBs were cultivated as described above and fixed on day 14. After that, the immunofluorescence staining was executed according to the protocol described in section 3.2.7.

The pictures of the samples were taken with the same exposure time specific for each magnification. Generally, the ratio between the signal of the neurons (FITC) and all cells, realised by the Hoechst staining as a counterstain, was calculated. Therefore, a low green/blue signal ratio corresponds to a low abundance of neurons, low differentiation efficiency and vice versa. The signal strength was calculated by the "Mean grey value" function, which is the sum of the values at all pixels divided by the number of pixels.

3.2.10 Electrophysiological measurements

The MEA with the seeded cells was integrated into the signal acquisition device with its gold pins positioned on the outer electrode tabs. A silver/silver chloride reference electrode was placed in one of the in-/outlets of the microfluidic system and connected to ground. The plate below the MEA was heated to 37.6 ℃. A 16 bits A/D conversion and 20 kHz sampling rate for all 60 electrodes was used. The gold pins were cleaned with ethanol before use. A test chip with a defined signal was used to calibrate and test the setup. Before inserting the actual MEA, the relevant electrode positions were determined by the location of each embryoid body. The cells were immersed in neurobasal medium during the measurements. The top of the chip was covered with aluminium foil to prevent resistive coupling of 50 Hz noise of surrounding electronic devices in the laboratory. Stimulants were pipetted directly into the wells for instant measurable effect.

Die approbierte gedruckte Originalversion dieser Diplomarbeit ist an der TU Wien Bibliothek verfügbar
The approved original version of this thesis is available in print at TU Wien Bibliothek.
TU WIEN Bibliothek Your knowledge hub

Die approbierte gedruckte Originalversion dieser Diplomarbeit ist an der TU Wien Bibliothek verfügbar
The approved original version of this thesis is available in print at TU Wien Bibliothek.

Die approbierte gedruckte Originalversion dieser Diplomarbeit ist an der TU Wien Bibliothek verfügbar
The approved original version of this thesis is available in print at TU Wien Bibliothek.
TU WIEN Bibliothek Your knowledge hub

Chapter 4

Results and Discussion

The following chapter demonstrates the experimental results of this thesis, and presents a discussion and interpretation of the empirical observations.

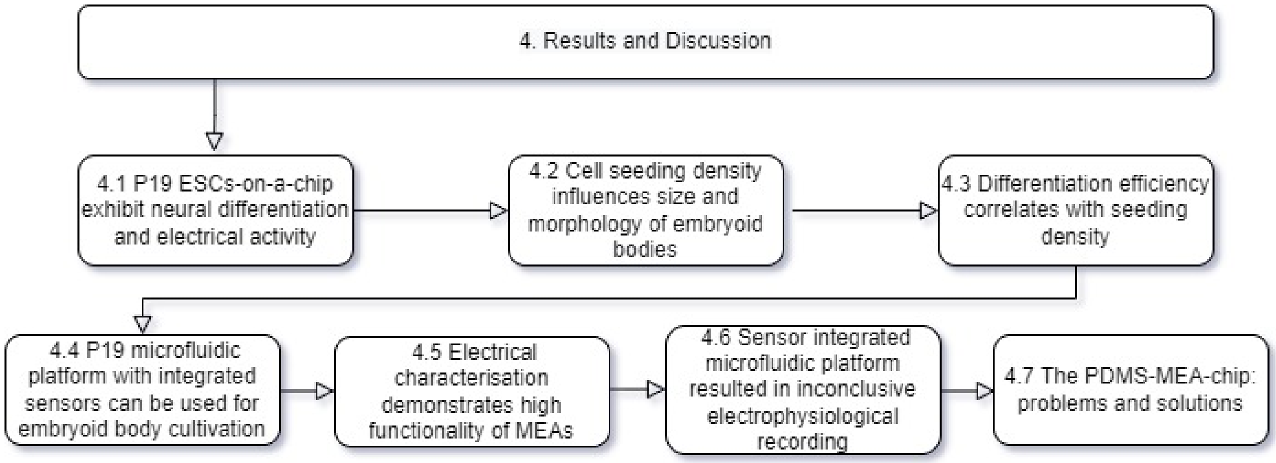

4.1 P19 ESCs-on-a-chip exhibit neural differentiation and calcium ion-channel activity

Initially, the viability of the cells, the generation of differentiated neural cells and the presence of spontaneous neural activity using the protocol presented in 3.2.6 were assessed. A depiction of the cells before differentiation is presented in the appendix in Figure 4.4.

Brightfield pictures of the cell spheroids and outgrowing neurites on a simplified chip design with a cylindric hole in a PDMS slide, bonded on a standard microscope slide, are shown in Figure 4.1. This demonstrates the ability of the P19 cells to agglomerate and to form tight spheroidal superstructures.

As depicted in Figures 4.1, the EBs tend to attach themselves preferably at the edges. There, the area of contact between the cells and the coated glass/PDMS surface and therefore stable adhesion of the cells to the device is maximised. It was concluded that strategic positioning of the wells in the chip design aids in maintaining a controlled position of the EBs over the electrode tabs. Also, the generation of outgrowing neurites is displayed. This already points towards successful neuronal maturation on-a-chip.

Die approbierte gedruckte Originalversion dieser Diplomarbeit ist an der TU Wien Bibliothek verfügbar
The approved original version of this thesis is available in print at TU Wien Bibliothek.
TU WIEN Bibliothek Your knowledge hub

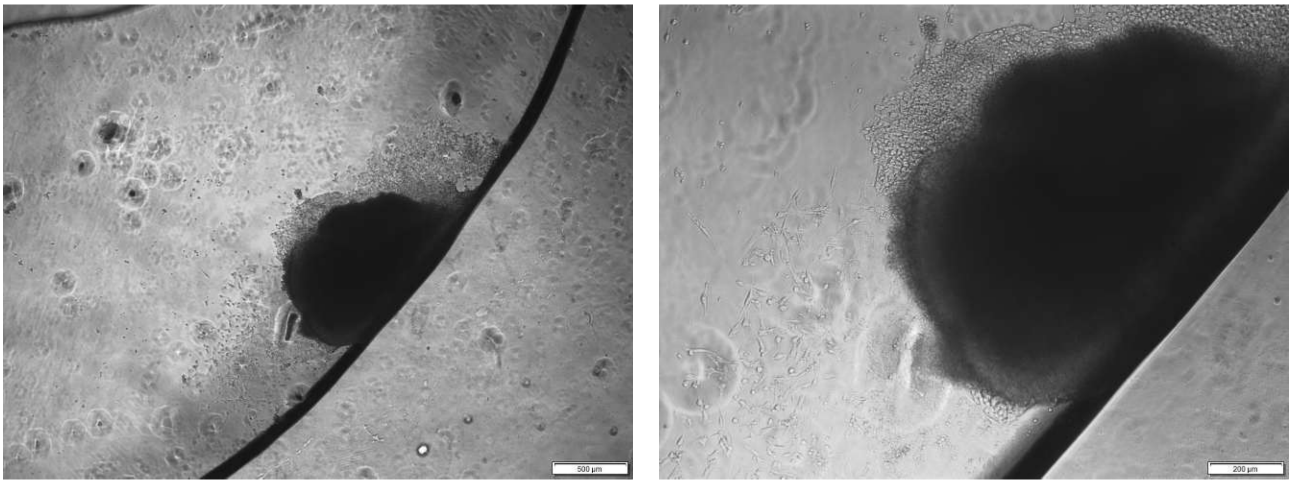

Figure 4.1: An embryoid body attached to the edge of the circular droplet with a magnified depiction demonstrating the outgrowth of neurites

4.1.1 P19 ESCs-on-a-chip display high viability

High viability is one of the most important properties a successful neural cell culturing and testing environment needs to fulfil. The depictions of the live dead staining that was executed with simplified PDMS-on-glass-slide design to show the viability of the cells, and the suitability of the used methods are shown in 4.2.

The pictures of the staining display only a small amount of dead cells, with a viability of at least 90% when comparing the green/red signal ratio. This shows high viability of cells and proves its suitability for the use in culturing P19 cells. Figure 4.2 depicts a high amount of green signal with few red points or dead cells. The depiction on the right also shows dead cells floating outside of the EB.

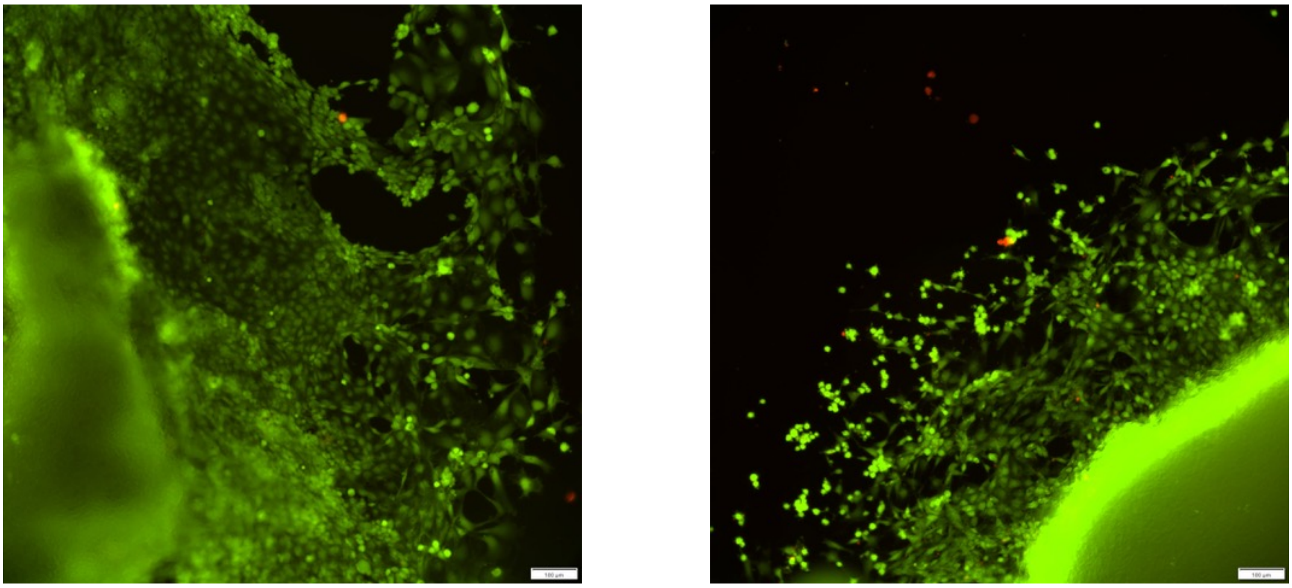

Figure 4.2: Live - dead staining of P19 EB (D10), live cells: green (Calcein-AM), dead cells: red (Ethidium bromide)

4.1.2 P19 ESCs-on-a-chip differentiate to neurons and glia cells

Immunofluorescence analysis was performed to assess the differentiation efficiency of P19 cells after 14 days. Herein specific focus was directed towards the differentiation into MAP2 positive neurons and GFAP positive astrocytes. Figure 4.3 shows recordings in the fluorescent microscope of the grown EBs after initial cultivation in a well plate and continuing growth on a chip for seven days each. Here, the green signal corresponds to the neurons with outgrowth of neurites and dendritic branches on the lower right. The red signal corresponds to the astrocytes with their typical "star"-like morphology. Additional pictures are added in the appendix in Figures 5.2 and 5.3. The blue signal is the counterstaining with Hoechst. The generation of distinct neural cells and glial cells proves the capability of the P19 ESC line to differentiate into neural tissue using the presented chip.

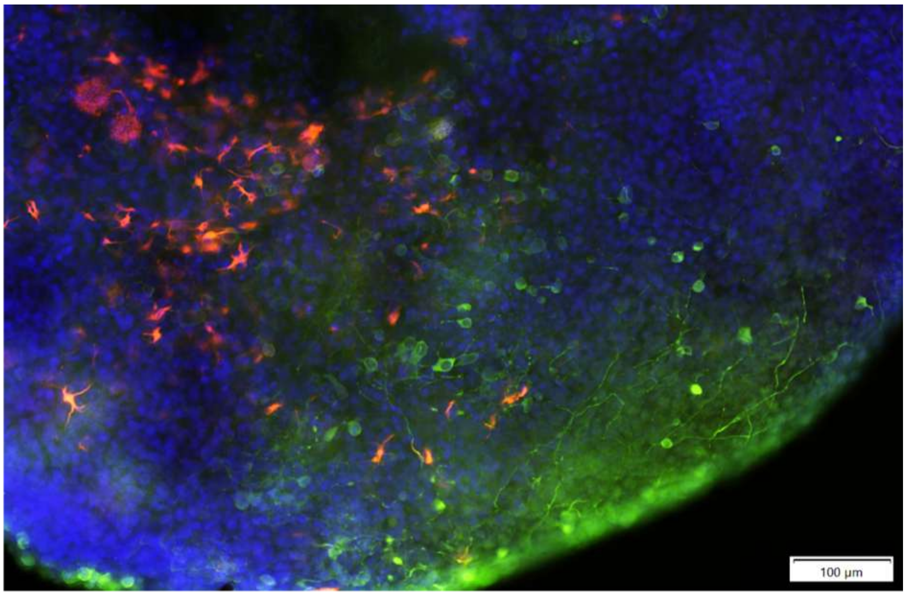

Figure 4.3: 3D-IHC-staining of P19 EB (D14), neurons: green, astrocytes: red

The P19 neurons exhibit a distinctive morphology with long projections from the soma, as shown in the brightfield depictions of Figure 4.5. They differ strongly from the undifferentiated P19 cells, which display a more heterogeneous appearance, typical for cancer cell lines, as shown in Figure 4.4.

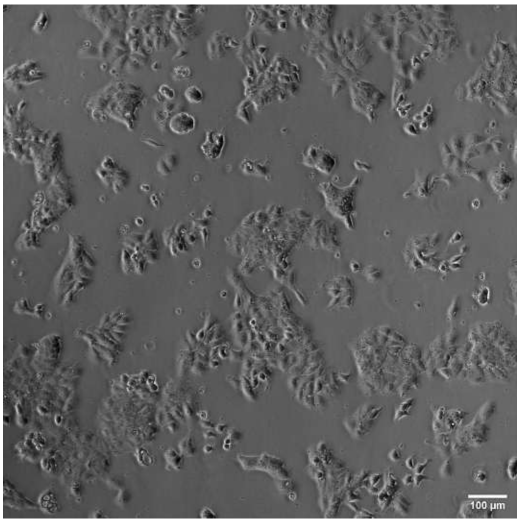

Figure 4.4: A brightfield microscope (BFM) picture of undifferentiated P19 cells with typical heterogeneous morphology of carcinoma cells

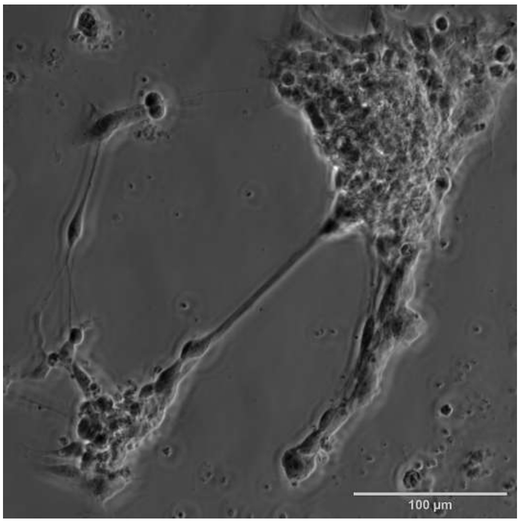

Figure 4.5: A BFM picture of differentiated P19 neural cells with neurites forming connections after RA exposure

Die approbierte gedruckte Originalversion dieser Diplomarbeit ist an der TU Wien Bibliothek verfügbar
The approved original version of this thesis is available in print at TU Wien Bibliothek.

4.1.3 P19 ESCs-on-a-chip show calcium ion channel activity

Next, a calcium staining was performed to display neural activity, as the marker highlights flux of calcium ions, which indicates the appearance of spontaneous action potentials. Here, the embryoid bodies have been stained with Fluo-4 AM in a three-dimensional ultra-low attachment well plate culturing device for the experiment. Figure 4.6 to the right depicts an excerpt of the Fluo 4-AM staining, which shows time-dependent ion channel activity by brief flaring up of green signals. This demonstrates the controlled generation of electrically active neural tissue in the embryoid bodies.

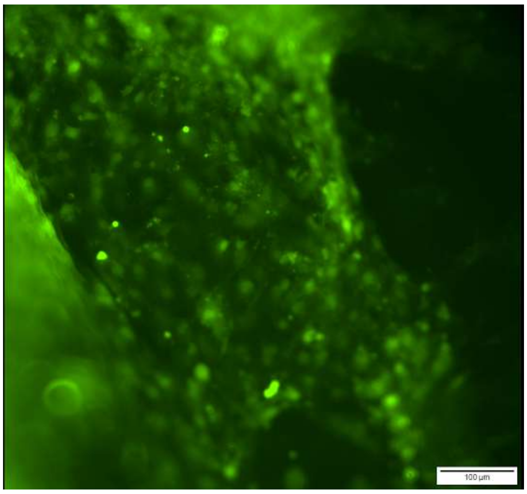

Figure 4.6: The Fluo 4-AM staining shows occurring ion channel activity

4.2 Cell seeding density influences size and morphology of embryoid bodies

As mentioned in chapter 2.4.3, the size of EBs greatly influences the cells' overall viability. Oversized EBs develop a necrotic core, while on the other side, too small EBs might entail inefficient differentiation rates. Recently emerged culturing methods have evolved to control the size, growth, cellular composition and organisation of EBs more precisely, e.g. by adding morphogens or specific extracellular matrix molecules. As functioning cell-cell communication via the expression of signalling molecules is considered crucial for the formation of embryoid bodies, a lower boundary for the size due to low complexity might exist for differentiation to be effective at all with given parameters. Finally, if a correlation between initial seeding density and the number of electrically active cells as well as a correlation between active neurons and the event rate of spontaneous action potentials is proven e.g. by electrophysiological measurements, then initial seeding density and spontaneous action potential rate can be directly linked.

Therefore, in order to produce viable embryoid bodies with reasonable size, the diameter and area of embryoid bodies of a selection of seeding densities have been examined. Also, the circularity of the EBs of the different densities were determined and compared, because this variable also functions as an indicator for the viability of the EBs.

4.2.1 Area and diameter increases with cell seeding density

In the first experiment, the influence of initial cell seeding quantities per well on area and diameter was investigated. For that, an interval of chosen initial cell densities was assessed qualitatively between 200 to 20,000 cells per well. In total, seven data points out of this interval with a sample size of at least n = 3 have been cultured. The points were chosen, so that factor between all sizes is limited to 2.5 to refrain from data interpolation.

A microscopic depiction of a seeding population of 20,000 is shown in Figure 4.8, representative of the majority of samples of the two biggest sizes 10,000 and 20,000. It shows strong occurrence of cell debris

Die approbierte gedruckte Originalversion dieser Diplomarbeit ist an der TU Wien Bibliothek verfügbar
The approved original version of this thesis is available in print at TU Wien Bibliothek.

in the medium as well as bulges in its morphology. The bulges might have occurred due to spontaneous outbreaks of tissue, similar to the appearance of "floating cells" in a cell culture flask, which refers to dead cells that lost the ability to adhere to surfaces. An alternative theory would be that the bulges are caused by (fluid-)mechanical damages by manual handling of the laboratory worker, e.g. during the medium change step, which is implausible due to an abundance of intact spheroids of smaller sizes.

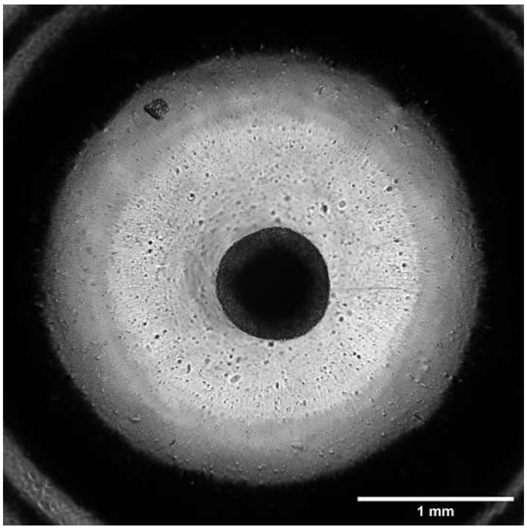

Figure 4.7: BFM depiction of an EB with a seeding size of 200 showing a circular morphology

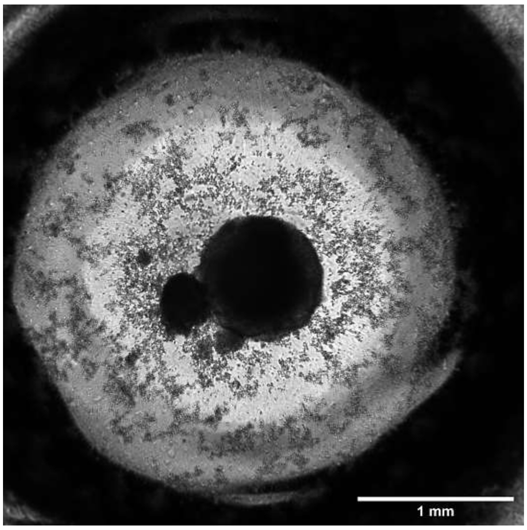

Figure 4.8: BFM depiction of an EB with a seeding size of 20,000 displaying bulges and cell debris

In comparison to this, the depiction of the EB with a starting population size of 200 in Figure 4.7 shows a spheroidal EB with a very low amount of cell debris and no bulges or other abnormalities, which generally was the case for spheroids with a starting density of 5000 or lower.

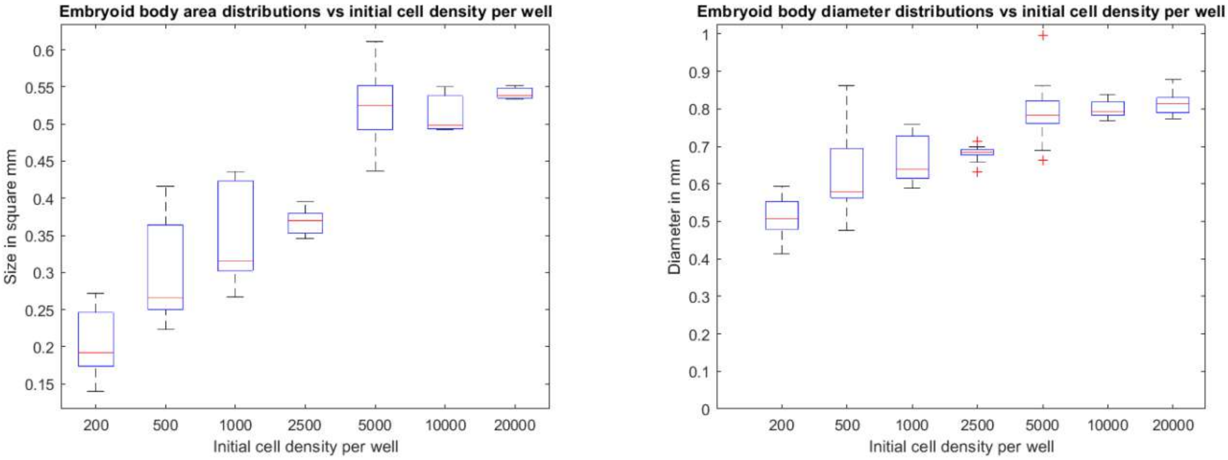

Figure 4.9: Diameter and area distributions vs their seeding densities per well

Figure 4.9 shows the corresponding boxplot graphs of size and diameter averages. Here, one can observe a steady increase in correlation with growing seeding densities up to size 5000, from which area and diameter seem to stagnate for the three biggest densities, indicating an upper size limit for P19 embryoid bodies. The average upper size limit of the three biggest densities yields an area of $0.526\,\mathrm{mm}^2$ and a diameter of $0.801\,\mathrm{mm}$. The graph with reduced density interval from 200 to 5000 in 4.10 yields a quasi-linear trend which in this graphic is slightly adulterated due to the x-axis not being true to scale.

Die approbierte gedruckte Originalversion dieser Diplomarbeit ist an der TU Wien Bibliothek verfügbar
The approved original version of this thesis is available in print at TU Wien Bibliothek.

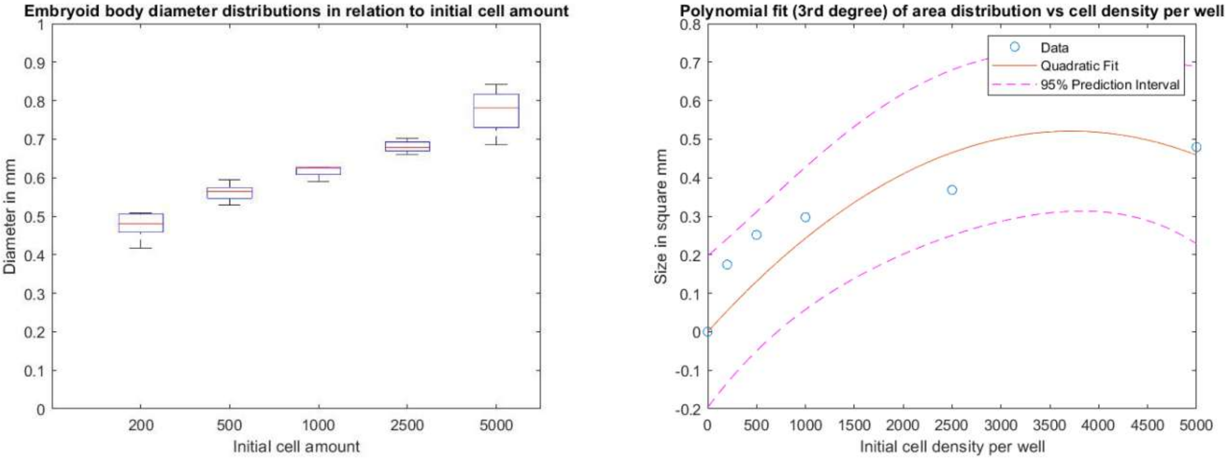

Figure 4.10: Depiction of the area of the EBs depending on their initial seeding amount (left) and a polynomial fitting curve to model the data (right)

Coefficients	a	b	c
Area	-3.77e-08	2,80e-04	0
Diameter	-8.87e-08	5.88e-04	0

Table 4.1: The coefficients for modelling the area and diameter of P19 EBs using a quadratic function with the form $ax^2 + bx + c$

The plot with correct scaled axes reveals a positive gradient with a convex slope. The data can be modelled with a negative quadratic function $f(x) = ax^2 + bx + c$, where x denotes the density of cells per well and coefficients a and b denoted below in table 4.1. C was set to zero to account for the origin as a precondition.

In summary, increasing seeding densities ranged from 200 up to 20.000 cells per well result in increased area and diameter averages after seven days in culture in microwell plate. The positive gradient stagnates for densities above 5000 cells/well. The average radius at density 5000 ranges between 294 µm to 379 µm, with a median of 320 µm.

Here, the data shows two different growth regimes: Firstly, a growth regime for the interval 200 to 5000, defined by a functioning supply of the intraspheroidal cells and a stagnation regime from 5000 to 20.000 cells/well, where no significant increase in area or diameter was recorded. Additional investigation via microscope reveals a huge amount of dead cells floating in the wells of densities over 5000 cells per well. Also, malformations or bulges in the morphology of the EBs were observed. This stagnation towards the existence of an upper size limit and a critical size at which the rate of newly generated cells equals the rate of dying cells. As a trend of increasingly malformed EBs was assumed to correlate with increasing density values, the circularity was quantified.

Die approbierte gedruckte Originalversion dieser Diplomarbeit ist an der TU Wien Bibliothek verfügbar
The approved original version of this thesis is available in print at TU Wien Bibliothek.

4.2.2 Circularity decreases with cell seeding density

The bulges in the morphology of an embryoid body, as presented above in Figure 4.8, represent clear morphological abnormalities. This indicates the generation of a growing necrotic core due to undernourished cells. It is established that an epithelial-like cell sheet covers the surface of EB's to maintain strong cell-cell adhesions, which are extremely sensitive to mechanical stresses. [168] The ECM of dead cells in the multicellular spheroid can burst due to failing renewal of attachment proteins, which leads to a break-out and a potential rupturing of the dead core out of the viable rim of a embryoid body. [5] Therefore it is possible that mechanical stresses interferes with cell-cell adhesion, which leads to out-breaks of cell agglomerations out of the main EB (as expounded in 2.4.3). These broken parts in return have been observed to build new spherically growing microcenters.

This leads to bulges in the EB, a decrease in stability and potentially the release of cell debris in the channels of the microfluidic system. Therefore, the roundness of multicellular spheroids can act as an indicator of the cells' overall viability and the necrotic core's size. The results of the analysis are shown in 4.11, where 1 corresponds to perfect circle and 0 to an increasingly elongated polygon. The graphic shows, that densities above a certain threshold exhibit lower roundness, derived from an increased amount of bulges of dead cell clusters. Despite this it is important to point out that high circularity does not reveal any direct, causal information about the viability of EBs.

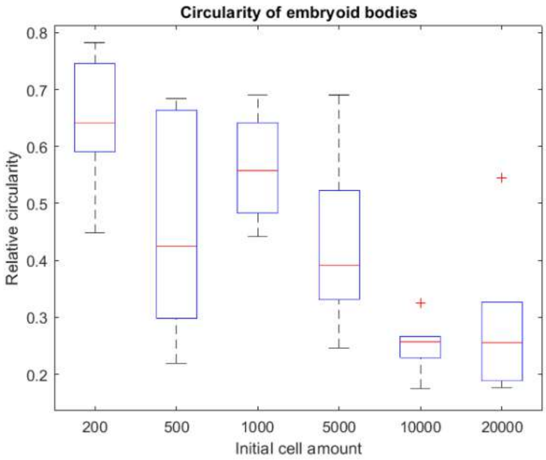

Figure 4.11: Circularity of the embryoid bodies)

To conclude, a constant increase in diameter and area can be observed for increasing seeding densities. From 200 to 5000 cells seeded per well, visual observation shows no occurrence of indicators of low viability like cell debris or bulges derived from dead core outbreaks. Densities above 5000 yielded lower circularities due to these bulges. Also a maximum of 5000 cells is recommended to avoid the latter according to the given data. Therefore, these densities are qualified to be used in future experiments.

The decrease in viability of the EBs correlates to the stagnation in size and the morphological malformation of the higher densities. The high amount of dead cells needs to correlate with the size of the EB, since an undersupply of nutrients in the well can be excluded due to its volume.

One reason for the reduced circularity could be mechanical damages to the ECM. The forced aggregation of an enormous number of cells leads to tension between the cells. [169] Also, epithelial cells and neural tissues are known to be especially sensitive to mechanical forces, which could lead to the disruption of cell-cell formations and trigger apoptotic signal cascades.

Bad diffusivity of the nutrients and waste products into and out of the spheroid might impose another obstacle. Since nutrition molecules like e.g. glucose possess higher complexity and inherently have a lower diffusivity constant, it can be assumed, that their transport into the EB is more problematic than downgraded waste molecules. Also competition between the cells for nutrients until oversaturation is reached which slows the diffusion process might account to that. A study from Hribar *et al.* proved mass hypoxia in the dead core region by staining of the spheroid cross-sections for hypoxic marker HIF-1α[170]. Also a study by Barzegari *et al.* described an alteration of metabolic pathways of LDH, tricarboxylic acid or lactate in the core of EB[169], but little to no information about the diffusive behaviour of those molecules in embryoid bodies is available. More specific metabolic screenings could fuel oncologic research around tumor-induced angiogenesis and

Die approbierte gedruckte Originalversion dieser Diplomarbeit ist an der TU Wien Bibliothek verfügbar
The approved original version of this thesis is available in print at TU Wien Bibliothek.

vascularisation since ESC- and iPSC-derived embryoid bodies are also used to model avascular tumor tissues. [116]

4.3 Differentiation efficiency correlates with seeding density

The size of embryoid bodies influences the viability of the cells and shows huge effects on their differentiative properties. While the influence of size on the resulting cell types has been studied thoroughly, the data on its influence on the abundance or share of differentiated to undifferentiated cells has remained incomplete and unclear, as described in Section 2.4.4. The differentiation efficiency of each size was determined by immunofluorescence stainings and calculating the share of the neural signal intensity to the signal intensity of all cells. The ratio's mean value and standard deviation were calculated and plotted as Gaussian distributions. The results are shown in Figure 4.12. High values on the x-axis correspond to higher portion of neural signal and higher efficiency, while the y-axis describes the statistical density of the distribution.

In summary, the analysis revealed a preponderant portion of the green signal (corresponding to a higher abundance of neural cells) with increasing seeding sizes. The highest signal strength was reached at the seeding density of 1000 cells per well. This statement is visualised in detail in Figure 4.13, which ranks the average differentiation efficiencies from smallest to biggest. The density of 5000 displays the biggest, and 500 the smallest variance within each population. This shows that bigger embryoids generally pose a better environment for the efficient differentiation of P19 ESCs with a significant difference between the data points below and above 1000 cells per well.

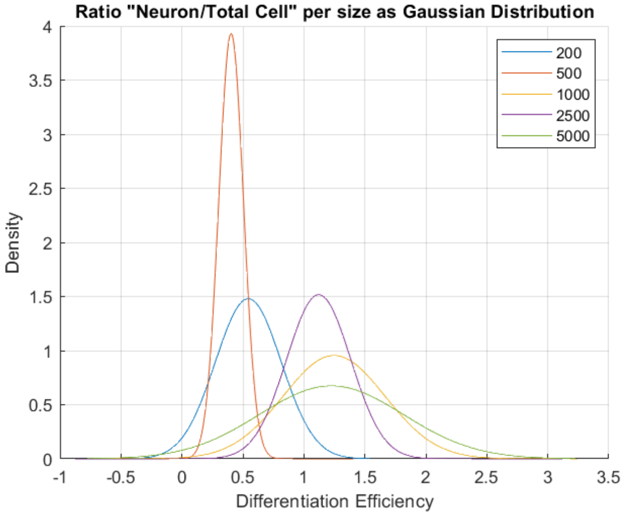

Figure 4.12: Differentiation efficiency plotted as Gaussian distributions

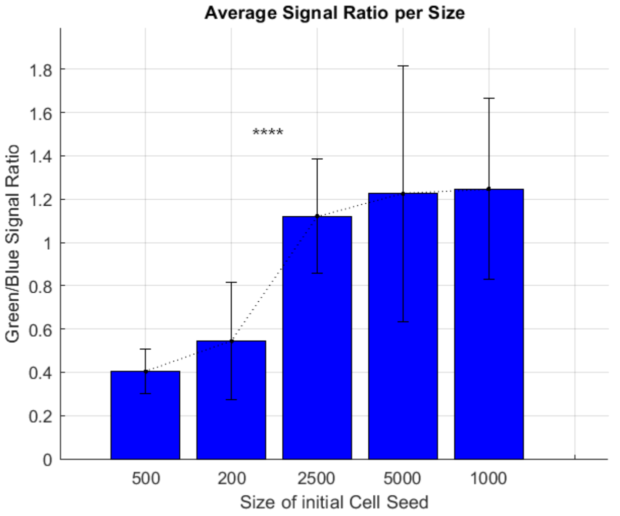

Figure 4.13: Average signal ratio per size as a barplot from smallest to biggest

In regard to the results it is reasonable to assume, that insufficient supply of RA, which has been given in the exact same concentration for each size, does not diminish the differentiation efficiencies for bigger EBs as much. Also, diffusive mass transport of RA or other molecules for higher pathways does not impose such restrictions as initially expected. Bigger embryoid bodies could offer a more suitable microenvironment to cells to trigger neural differentiation, probably due to their increased intraspheroidal complexity and therefore altered expression of biochemical signals. Berg *et al.* assumed that the differentiation with RA is "not rigidly preprogrammed" in P19 cells, but mostly influenced by cell-cell crosstalk and cell position. [43] In future studies, an in-depth screening of molecular signalling molecules like e.g. neural growth factor generation and transmission

Die approbierte gedruckte Originalversion dieser Diplomarbeit ist an der TU Wien Bibliothek verfügbar
The approved original version of this thesis is available in print at TU Wien Bibliothek.

rate can aid in clarifying these assumptions. Park *et al.* already demonstrated that the size of an EB influences the global gene expression profiles and leads to differentiation towards different cell species. [171] Lastly, the seeding density of 1000 cells per well showed the highest efficiency in total. Therefore, this density is the recommended starting size for future experiments in case a high amount of neurons is required. The EBs of this density also offered comparatively well morphological features in terms of circularity, as shown in 4.11.

The statistical analysis executed by using a Welch t-test reveals high significance ($P < 0,0001$) between the distributions of two smallest seeding densities, 200 and 500. The similarity of the three biggest distributions in regard to the mean value and the variance is also peculiar. This is evident due to a similar mean of green/blue signal ratio. Another noteworthy observation is the correlation between growing variance with increasing density numbers. This means, that the distribution of neurons within bigger embryoid bodies is more heterogeneous than in smaller EBs.

	200	**500**	**1000**	**2500**	**5000**
200	x	0,067	<0,0001	<0,0001	<0,0001
500		x	<0,0001	<0,0001	<0,0001
1000			x	0,1112	0,8767
2500				x	0,4377
5000					x

Table 4.2: The P-values between the distributions of the respective seeding densities.

The increase in variance over growing size can be traced in the width of the distribution curve in Figure 4.12, where more width contributes to more heterogeneous results within one density. The distribution of the bigger seeding densities therefore can be described as probabilistic, which in conclusion would make the targeted generation of EBs with a constantly high neural ratio difficult with these densities.

Finally, it was observed that a majority of embryoid bodies exhibits an accumulation of green signals in a confined space within the embryoid body. Therefore it was hypothesised that most neural populations occurred spatially confined, meaning inhomogeneously distributed over the whole spheroid. This statement is visualised exemplary in the Figure 4.14 on the right: A sizeable neural population can be seen on the upper left part of the pictured EB with seeding density of 5000 cells per well, while the lower right region consists of more non-neural cells. As mentioned in the introduction, the influence of the cell location within EBs on the cell type determination during differentiation due to local differences in cytokine generation is well-established. This observation also could point towards morphogenetic gradients, a group of signalling molecules whose concentration gradients control cell fate specification in developing tissue in regionally confined areas. [172]

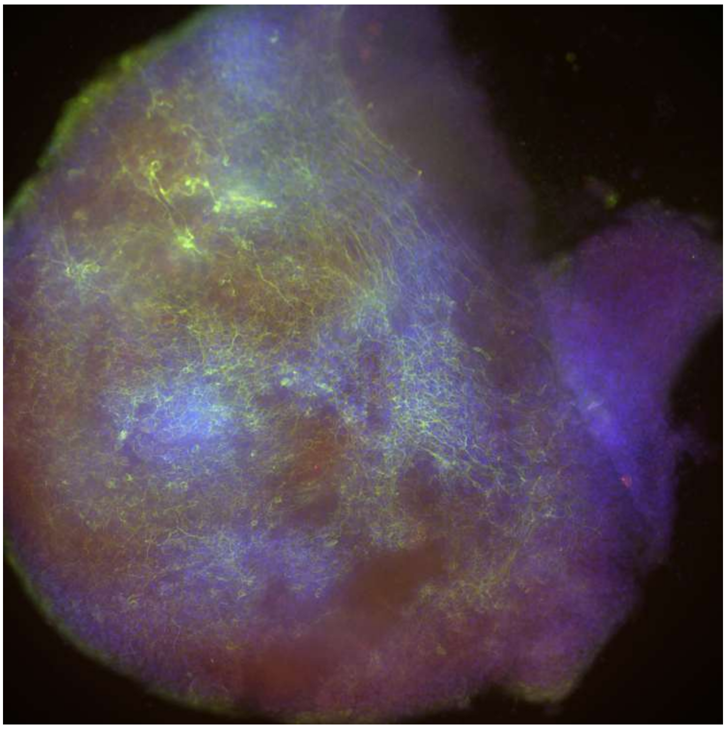

Figure 4.14: Depiction of an immunostained embryoid body with heterogeneous occurrence of neural tissue. (Density: 5000 cells/well)

Die approbierte gedruckte Originalversion dieser Diplomarbeit ist an der TU Wien Bibliothek verfügbar
The approved original version of this thesis is available in print at TU Wien Bibliothek.

These results demonstrate in conclusion, that strong cell-cell interactions in a complex organised and heterogeneous differentiation structures illustrate an essential factor on the development of nervous systems. The investigation of gene expression profiles of signalling molecules in dependence of embryoid body size could yield progress in predicting local differentiation patterns to explain such observations in the future.

4.4 Microfluidic platform on MEA with integrated sensors can be used for embryoid body cultivation

After the P19 embryoid bodies have been investigated, the LOC device with integrated sensors for the cell line-independent cultivation and investigation of in vitro models is presented next. This section presents the design requirements, features and limitations of the sensor-integrated microfluidic device built in the course of the thesis.

4.4.1 Microfluidic PDMS chip design

Main Requirements

A controlled environment for cells to adhere, grow and proliferate is required. For this reason, a microfluidic channel system bonded on top of the data acquisition system needs to seal the cells and cell medium from the surrounding air. The primary purpose of the design with the cell wells used in this thesis is to hold the embryoid bodies in separate compartments. The design needs to offer supply channels for nutrients, which can be added and removed via in-/ and outlets.

It is well-known that adequate mechanical stress could aid neural cells in growing, while extreme forces influences such a molecular expression of neurons leading to damage in neuronal organisation and proliferation. Therefore, the dimensions of the channels are chosen to minimise fluid mechanical forces, induced by adding or aspirating liquids via the in-/outlets.

The electrophysiological recording of the EBs requires close proximity of the cells to the electrodes to enable strong signals and reduced noise. Therefore, they are placed in cylindric wells positioned directly over the electrodes during seeding.

The only contact points with air are located on top of the wells and the in-/outlet cylinders. This enables control over the chemical microenvironment, e.g. for stimulation of the cells. Reagents can be added indirectly via the in-/outlets, which takes some time until it reaches the cells via diffusive motion due to increased distance or directly via the well openings for instant stimulation, which is not recommended as this creates fluid stress and signal falsification.

Next, the microfluidic chip design offers four different, independent wells for simultaneously investigating various cell spheroids.

Lastly, biochemical gradients of nutrients and signal molecules like growth factors are known to guide the growth of neurites. Therefore, it was intented to implement small dimensions at the bottleneck to maintain high gradients between the well and the outer reservoir.

These requirements were realised by xurographically cutting single layers of PDMS with standardised height and bonding on top of each other. PDMS is a biocompatible polymer and a standard for various cell applications because of its rapid prototyping possibilities. [139] In total, three different designs with varying functions have been designed and integrated into a functioning microfluidic chip. The resulting designs are shown in Figure 4.15.

Die approbierte gedruckte Originalversion dieser Diplomarbeit ist an der TU Wien Bibliothek verfügbar
The approved original version of this thesis is available in print at TU Wien Bibliothek.
TU WIEN Bibliothek Your knowledge hub

Die approbierte gedruckte Originalversion dieser Diplomarbeit ist an der TU Wien Bibliothek verfügbar
The approved original version of this thesis is available in print at TU Wien Bibliothek.

The designs are combinations of three different building blocks. First, a top layer for medium storage and for sealing the system from air except at the in-/outlets. This layer was stacked three times to offer more storage volume for the cell medium. Then, the channel design connected the wells with the channel and is the only passage for medium to flow in and out of the well. The bottom design's purpose is to implement a mechanical restrictor between the well and the channel, to avoid undesired displacement of the spheroids. The obstacle helps to prevent this and therefore facilitates long-term adhesion of the EBs inside the well.

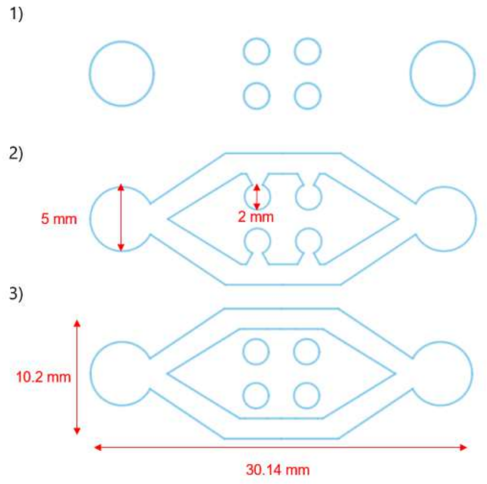

Figure 4.15: The single layers constituting the whole PDMS microfluidic system

Since neurons are known to grow along biochemical gradients of signalling molecules like neural growth factors[17], the axonal growth of the neurons is expected to be in a direction towards the region of higher concentration of cytokines and nutrients. This effect can be utilised in OOC applications to direct cell growth. Therefore as another feature of this design, a gradient in the bottleneck area, as depicted on the right in Figure 4.16, between the well and the channel is generated with objective to guide neural growth towards the channel. At its narrowest point, all media components have to pass through a rectangular area of $0,785mm * 1,5mm = 1,1775mm^2$.

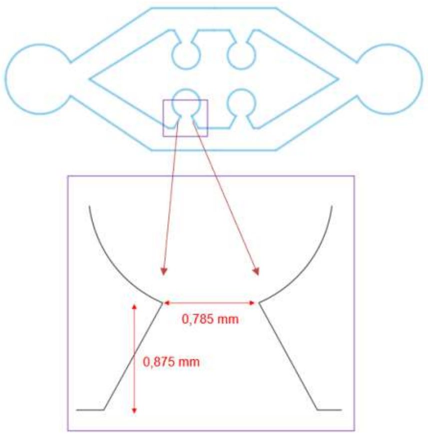

Figure 4.16: A zoom on the bottleneck region between channel and EB well

The final design comprises five layers which are stacked up as shown in Figure 4.17. This results in an overall height of 2.5 mm of the PDMS chip. The organ-on-chip device contains four individual chambers with a diameter of 2 mm and a volume of 7.85×10^{-3} ml for each well, where the embryoid bodies were placed in order to position them above the electrodes. The medium in- and outlets have a diameter of 5 mm and a volume of 49.09 mm^3. Figure 4.18 visualises the final 3D object.

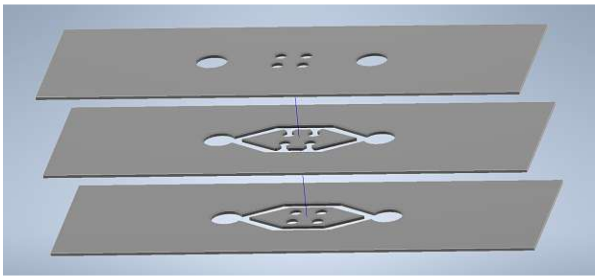

Figure 4.17: "Exploded view" of the three slide designs

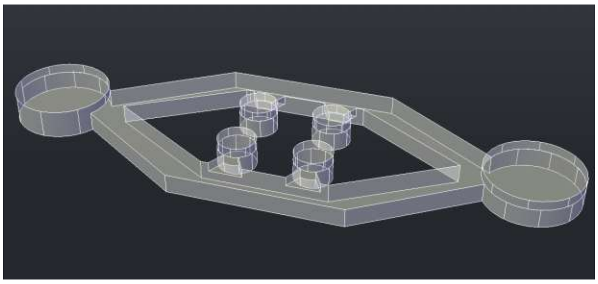

Figure 4.18: 3D animation of microfluidic system

Die approbierte gedruckte Originalversion dieser Diplomarbeit ist an der TU Wien Bibliothek verfügbar
The approved original version of this thesis is available in print at TU Wien Bibliothek.

4.4.2 CFD simulations demonstrate low fluid force generation at cell proximity

The CFD simulations' scope was to find the design option with the lowest shear stresses for the cells inside the wells, since neurons are sensitive to shear forces.

Figure 4.19 depicts 3D mappings of shear stresses of three different design options which were implemented, simulated and compared. The shear stress vectors are displayed on a xy-plane with the height z=0, defined by the centre of mass of the fluid body. The amplitude of the force vectors is shown via colouring.

The three different designs are constituted of different combinations of PDMS layers, as described above in Figure 4.15

- Design 1, a four-layer design with another top layer at the bottom, which adds another obstacle layer,
- Design 2, like design 1 but replaced the bottom layer with another channel layer, removing the restrictor at the bottleneck and doubling the channel height to 1000 µm,
- Design 3, which denotes the design with all three layers as presented before ("bottom", "channel", "top"),

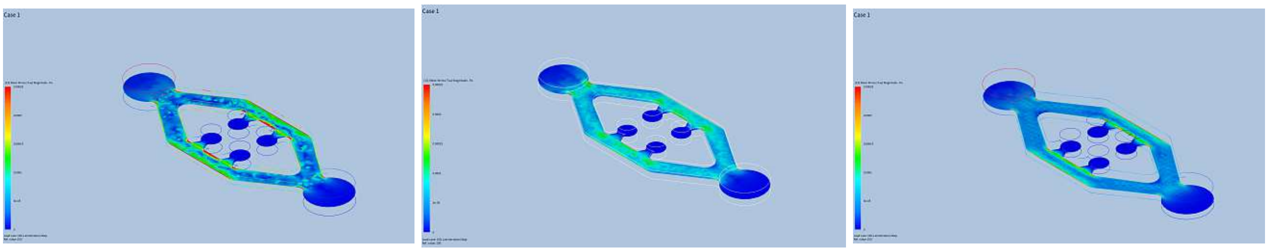

Figure 4.19: CFD simulation of three different designs depicting shear stresses distributed over a X-Y-plane with z=0 (blue colour corresponds to low, red to high shear stress amplitudes)

Generally, as one can see in Figure 4.19, all designs show neglectable shear stress in the middle of wells, where the P19 cells are located. Design 1 exhibits the highest shear stress values of all three design choices, with maxima distributed close to the bottleneck regions and regions with heterogeneous shear force occurrence at close cell proximity. Design 2 displays a more homogeneous distribution of shear forces with lower maxima than design 1, which is why design 1 was excluded for further investigation. Design 3 exhibits a crystal-shaped shear stress profile in the channel. The amplitude of the shear forces within the channel is rather low. At the bottleneck region right before the wells a maxima with values around 0.15 mPa can be observed. Based on the results as well as the handling characteristics, In the end, design 3 was concluded to be the preferred design. In addition, it entails a very feasible production process.

Figure 4.20 on the right visualises the final design with simulated particle traces from the inlet to the outlet. This demonstrates again the protective effect of the well positioning on the cells from fluid-mechanical forces. As a consequence, the supply of nutrients and other molecules to the EBs in the wells is almost entirely driven by diffusion and creates a biochemical gradient for the neurites to grow along.

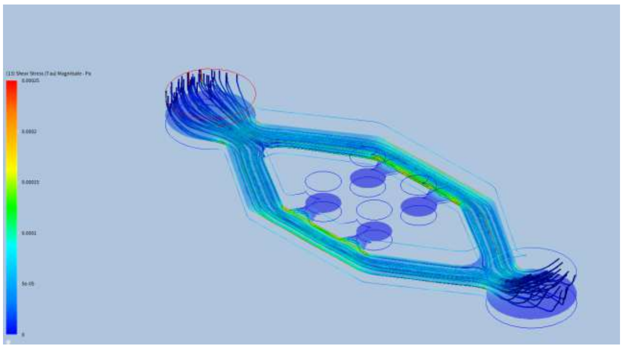

Figure 4.20: Final design simulated with particle traces in the fluid channels.

4.4.3 Multielectrode array design supports simultaneous measurements of whole field potentials

In order to measure the electrophysiological activity of the P19 cells, a MEA was integrated into the microfluidic device. It provides an electrical connection between the area of interest underneath the cells and the signal readout system in order to offer data acquisition of spontaneous action potentials. Figure 4.21 depicts the symmetric layout, which was designed to be photolithographically printed on a substrate with dimensions 4.9x4.9 mm^2. A zoom into the middle part of the multielectrode array is also shown to visualise the smaller structures containing the input electrodes.
Overall, the MEA contains sixty readout electrodes with equally lengthed conduction lines. The tabs on the outer edges are the readout electrodes transferring the signals via an interface to the MCS acquisition system.

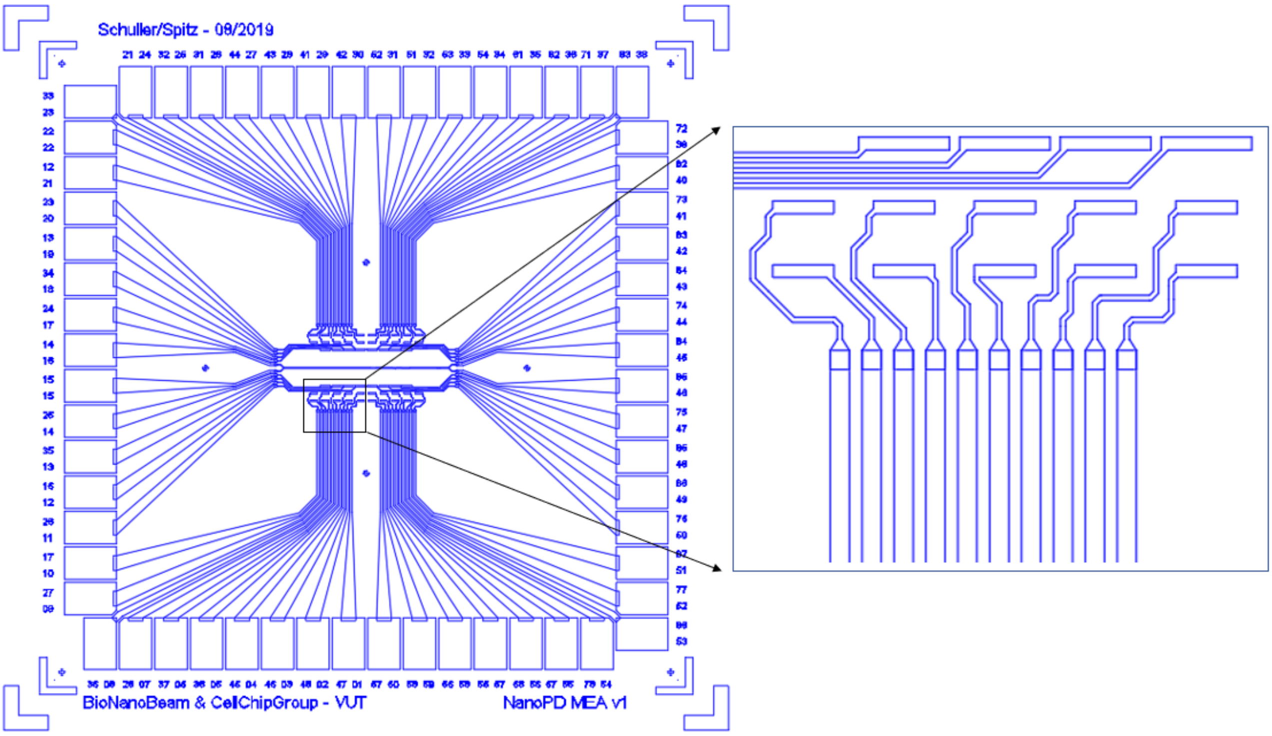

Figure 4.21: Layout of the MEA in AutoCAD, with additional zoom on the inner electrodes

The layout of the inner electrodes consists of 28 electrodes on each side and a big, drawn-out electrode with four parallel conduction lines in the middle, which are horizontally aligned. The electrode in the middle has been designed to act as a reference electrode. While an external Ag/AgCl electrode was employed for electrophysiological recordings, the integration of a central electrode in the MEA design provides the opportunity for on chip reference measurement. The main recording electrodes are structured into three rows of electrodes. The dimensions of the smaller electrodes in the two lower rows with five electrodes measure 100 µm x 480 µm, and the four bigger electrodes on the upper third row measure 100 µm x 710 µm.

Figure 4.22 below shows a 3D exploded view of the PDMS chip bonded upon the MEA.

Die approbierte gedruckte Originalversion dieser Diplomarbeit ist an der TU Wien Bibliothek verfügbar
The approved original version of this thesis is available in print at TU Wien Bibliothek.

Die approbierte gedruckte Originalversion dieser Diplomarbeit ist an der TU Wien Bibliothek verfügbar
The approved original version of this thesis is available in print at TU Wien Bibliothek.

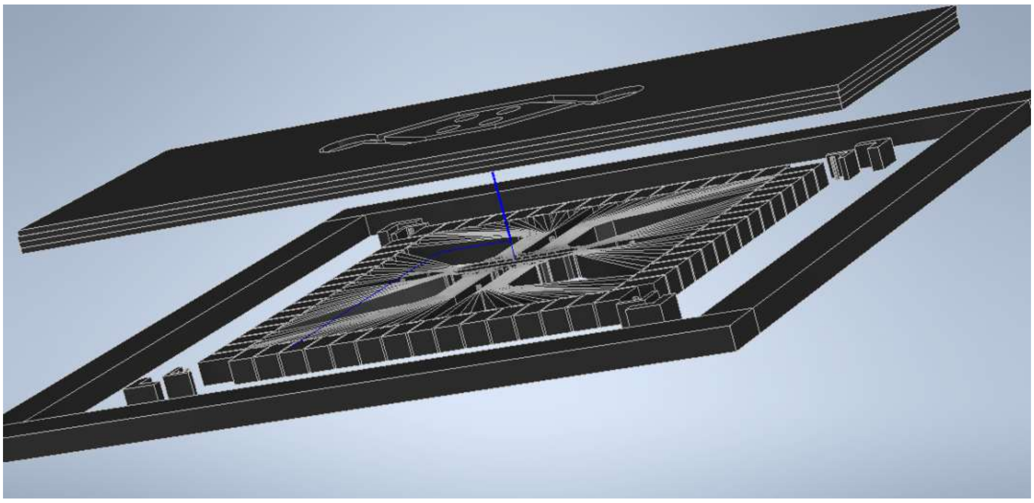

Figure 4.22: Exploded View of the MEA with the chip on top

P19 ESCs display on-chip formation of neuronal processes

The growth of distinctive neural projections starting from the spheroid has been documented on microscope glass chips and on MEAs.

Figure 4.23 shows an embryoid body inside the well of the simplified PDMS chip on the left. The morphology of these neurites indicates the gradual composition of two-dimensional neural networks. The cells organise and build connections over a long distance circularly outwards from the EB via extending neurites, as it can be observed on the right depiction.

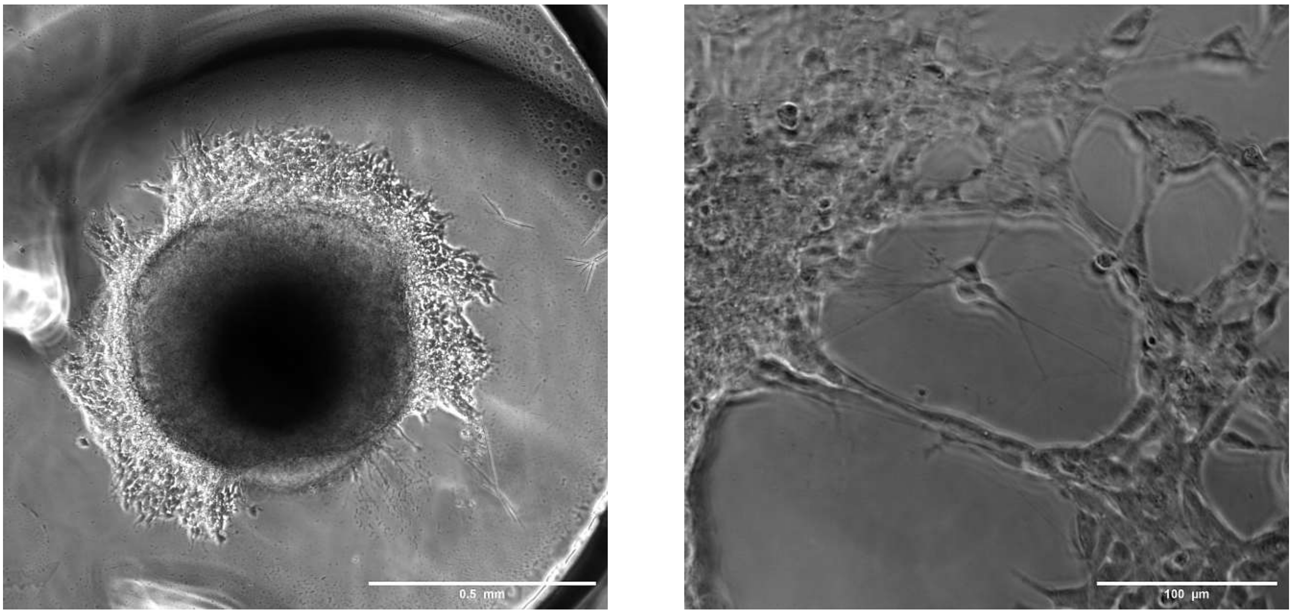

Figure 4.23: Depiction of an embryoid body after seeding on a VWR glass slide and neurites growing on-chip (D2 on chip)

This has also been documented to be the case for embryoid bodies on the microfluidic MEA-PDMS-chip, as depicted in Figure 4.24.

More depictions of neural growth are found in the appendix, for example in Figure 5.1.

In conclusion, the protocol produces viable embryoid bodies and generates differentiated neural and glial tissue. The embryoid bodies build neural distinctions on the PDMS-MEA chip after being cultivated in a wellplate without any cell-surface contact. This indicates, that the generation of spontaneous action poten-

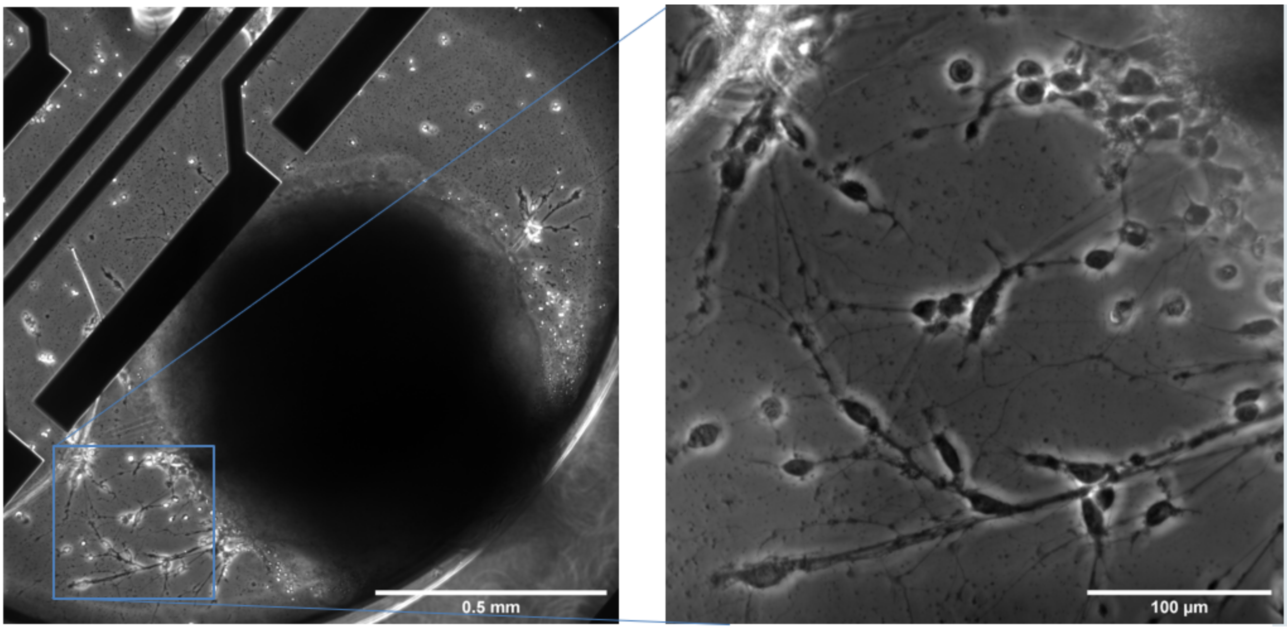

Figure 4.24: Depiction of neurite projections on a MEA surface (D5 on chip, density: 2500, Ti/Au MEA)

tials on-chip can be expected and recorded in electrophysiological experiments.

4.5 Electrical characterisation demonstrates functionality of MEAs

For most lab-on-a-chip applications, certain electrical properties of the readout instrumentation like low signal-to-noise (SNR) ratio are crucial for many applications. To ensure a low SNR, high conductivity and functioning passivation layers are required. This section presents preliminary tests with the intent to define the electrical performance of the used MEAs and evaluate the quality of the used deposition processes. The overall goal was to characterise the influence of the electrical properties on the ability to measure action potentials and find one preferred chip design, which satisfies these requirements the most. The electrical signals in the standard MEA are transported via a Ti/Au double layer. It was assumed, that the gold layer carries the biggest part of the current for three reasons:

Thickness: According to profilometric measurements, the gold layer is at least ten times thicker than the titanium.

Distance: The gold layer is in direct contact with the current source.

Specific conductivity: Gold has a significantly higher conductivity. Literature describes values of $2.56 \times 10^6\,\mathrm{S\,m^{-1}}$ for titanium and $48.8 \times 10^6\,\mathrm{S\,m^{-1}}$ for gold. [173]

4.5.1 Profilometric measurements exhibit low thin film layer thickness

The sputtered layer thickness was examined first to determine the sputter efficiency and to calculate the specific conductivity. Figure 4.25 shows a profilometric measurement of the Dektak over the area of several electrodes and conduction lines, showing the total height of the combined Ti/Au layer (MEA "V1") of approximately $170\,\mathrm{nm}$.

Die approbierte gedruckte Originalversion dieser Diplomarbeit ist an der TU Wien Bibliothek verfügbar
The approved original version of this thesis is available in print at TU Wien Bibliothek.
TU Bibliothek WIEN Your knowledge hub

Furthermore, one sample with twenty layers of titanium with parameters as described in 3.2.1 was sputtered and measured. Height differences were assessed at six representative locations. The result was averaged and scaled down to a single layer resulting in a thickness of approximately 3.23 nm per layer. This means that a pure gold layer thickness of 163.4 nm was sputtered.

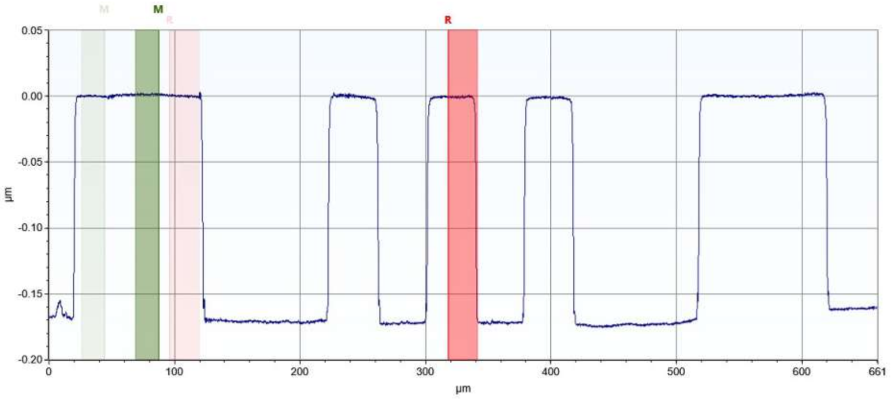

Figure 4.25: Depiction of a profilometric measurement over an electrode tab, three conduction lines and another electrode (from left to right)

4.5.2 Ti-MEA displays non-linear electrical performance due to titanium oxide layer formation

Titanium is part of most standard thin film chip production processes, not because of its conductivity but as a cheap and reliable bonding agent since gold does not adhere well to glass surfaces. Although its influence on the conductivity is expected to be of little to no impact to the total conductivity in theory, impurities due to production processes can have a significant influence in reality. For this reason, a MEA was produced with titanium only (Parameters: 2x60s at 100W) and measured. The results of the voltage sweeps are shown in Figures 4.26 and 4.27.

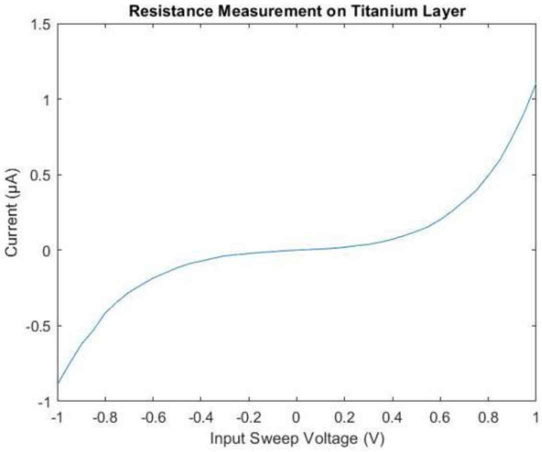

Figure 4.26: Input voltage vs current

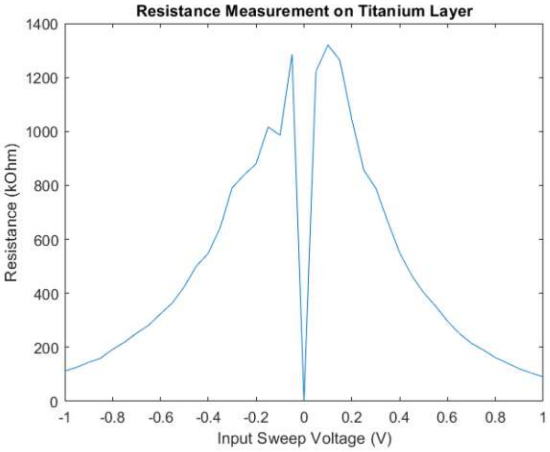

Figure 4.27: Input voltage vs resistance

The graph shows very high resistivity values and a striking nonlinearity, which can be described with a polynomial function of the third degree, $f(x) = x^3$. This can be interpreted as a consequence of the spontaneous formation of an oxide layer, which naturally occurs for pure titanium in the atmosphere that can be burst through when reaching a critical breakdown voltage. This explains the decreasing resistance for increasing absolute

Die approbierte gedruckte Originalversion dieser Diplomarbeit ist an der TU Wien Bibliothek verfügbar
The approved original version of this thesis is available in print at TU Wien Bibliothek.

values of the voltage. This situation can be approximated with an electrical equivalent circuit consisting of a parallel connection with the resistance of gold and titanium layer as R_G and R_T.

$$\frac{1}{R_{ges}} = \frac{1}{R_{Au}} + \frac{1}{R_{Ti}} \tag{4.1}$$

If you assumed the same thickness and compared the resistance of gold alone versus the equivalent circuit model, you obtain the following values:

- Au (solo): $20.5\,\mathrm{m\Omega}$
- Ti/Au : $19.5\,\mathrm{m\Omega}$

This shows, that more than 95% of the current would be conducted through the gold. Considering the difference in thickness between both layers it can be expected to be even more. In summary it can be concluded that the titanium layer is irrelevant when examing the electrical properties of the chip as assumed.

4.5.3 Ti/Au-MEA "V1" offers comparatively low resistance performance

In the next step, the conductivity of the sputtered thin film on the Ti/Au-MEA was investigated. Furthermore, the bulk conductivity was calculated and compared to the literature.

The layer thickness was measured with the Dektak, which revealed a total thickness of $175\,\mathrm{nm}$ of the combined Ti/Au-layer. The graph in Figure 4.28 shows a resistance measurement of $19.63\,\Omega$. The measured dimensions of the conduction line yielded a length $L = 23.5\,\mathrm{mm}$ and a cross-sectional area $A_{el} = 21.2\,\mathrm{\mu m}^2$, calculated by multiplying the average conduction layer thickness $h = 163.4\,\mathrm{nm}$, with the average width of the conduction line $w \approx 130\,\mathrm{\mu m}$.

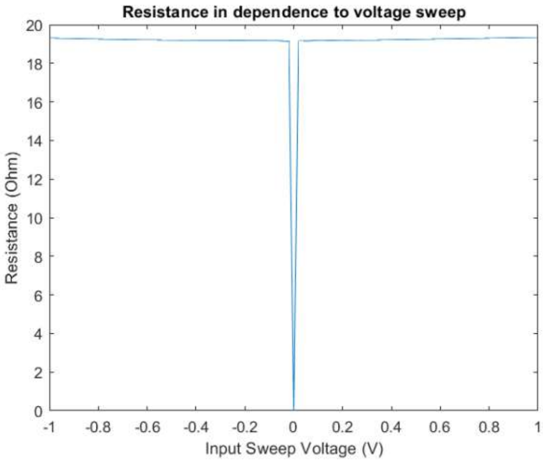

Figure 4.28: Voltage vs Resistance

According to Equation 3.1 this results in a specific bulk conduction of $0.0176\,\mathrm{\mu\Omega\,m}$, which is 19.7% worse than the literature data indicates ($0.022\,\mathrm{\mu\Omega\,m}$ at 20 ℃). Impurities of the crystal structure during the production process in the sputter device as well as flaws in the measurement method itself account for this. Here, one possible source of error could be generated by destroying the surface crystal structure when positioning the gold pins on top of the electrode tab. Also the application of the two-point probes measurement technique, where the contact resistances of the electrodes are not accounted for, will add to the error.

Additionally, it was observed that the pins of the MCS device used for the electrophysiological assessment buried themselves deep into the thin film on the chip and could be removed by wiping the chip carefully with a laboratory cloth drenched in isopropanol. In order to exclude a malfunctioning of the MEA, an updated production protocol for MEAs with thicker thin film layers and stronger resistance to mechanical damage was developed as a consequence.

Die approbierte gedruckte Originalversion dieser Diplomarbeit ist an der TU Wien Bibliothek verfügbar
The approved original version of this thesis is available in print at TU Wien Bibliothek.

4.5.4 Ti/Au-MEA "V2" displays the lowest resistance due to increased conduction layer thickness

In an attempt to improve the adhesion of the sputtered material, an updated production process of the Ti/Au MEA with thicker titanium and gold layers was executed and the resulting chips characterised as mentioned before.

The thickness measurement executed with the Dektak revealed a thickness of $186\,\mathrm{nm}$. This is only 6.2% higher than the MEA "V1" which can be explained by a deeper vacuum of factor two to four, which prevents the appearance of oxygen atoms in the reaction chamber. Oxygen atoms bond with the titanium layer during the sputter process forming titanium oxide, which appears in various polycrystalline formations. Hence, the resulting layer has an increased layer thickness and reduced layer quality.

The resistance measurement of the MEA "V2" was executed over a longer distance from two opposite electrodes and repeated for the MEA "V1" so that the results are comparable. The measurement revealed a resistance of $33.8\,\Omega$ for the "V2" and $44.5\,\Omega$ for the "V1". Therefore, the MEA "V2" has a conductance approximately 31.65% better than the MEA "V1".

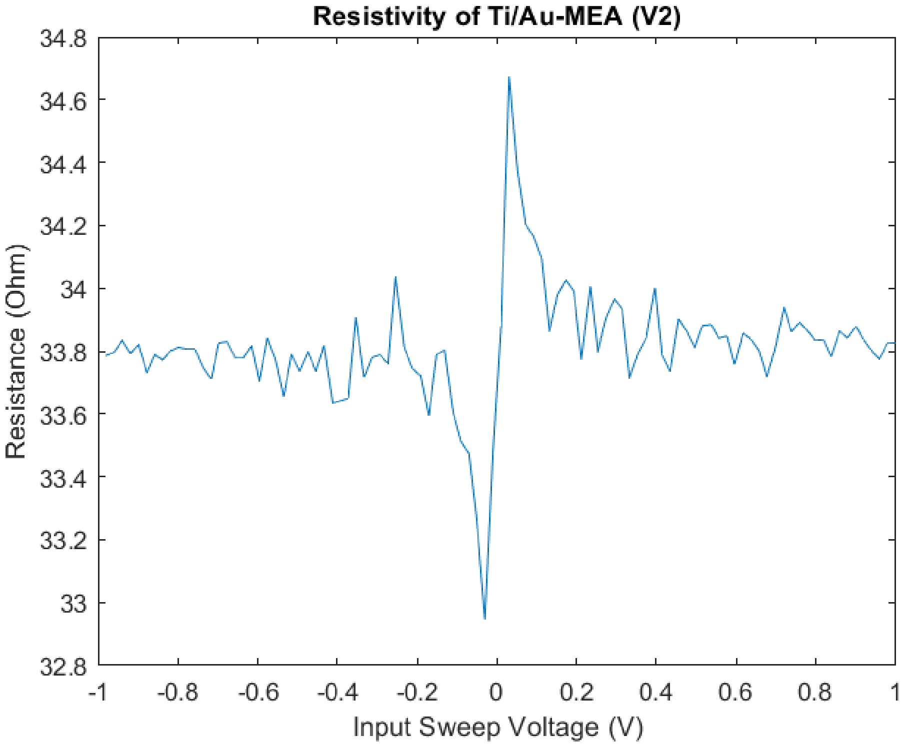

Figure 4.29: Resistivity of Ti/Au-MEA "V2" chip

4.5.5 Ti/ITO/Au-MEA offers tradeoff between transparency with high resistance

Lastly, one chip with indium tin oxide as the middle layer was produced. This material offers high transparency which makes the MEA useful for many biological applications, because this enables more possibilities for advanced spatiotemporal monitoring of cells. One example is the implementation of inverse illumination, which is a standard method in biological laboratory practice requiring transparency of the analyte carrier like the MEA. In return, ITO yields comparatively worse conductive properties because of its crystal structure with a specific resistance of $\approx 10 \times 10^{-4}\,\Omega\,\mathrm{cm}$. [174] A very thin layer of gold was added on top to improve the overall conductance of the chip. Since a trade-off between high conductivity and high transparency was seeked only a very

Die approbierte gedruckte Originalversion dieser Diplomarbeit ist an der TU Wien Bibliothek verfügbar
The approved original version of this thesis is available in print at TU Wien Bibliothek.

Die approbierte gedruckte Originalversion dieser Diplomarbeit ist an der TU Wien Bibliothek verfügbar
The approved original version of this thesis is available in print at TU Wien Bibliothek.

thin gold layer could be used, which is expected to result in higher resistivity than the Ti/Au-MEA. Figure 4.30 shows the resistance curve in dependence of the input voltage.

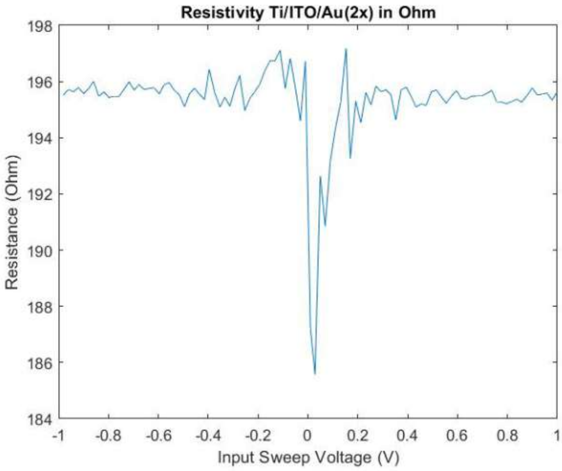

Figure 4.30: Voltage-current characteristics of the Ti/ITO/Au-MEA

The resistance measurement revealed an average resistance of $195.54\,\Omega$, which denotes a resistance that is approximately ten times higher than the Ti/Au-MEA "V1". Therefore, the Ti/ITO-chip is not expected to offer the ideal measurement conditions for assessment of action potentials in comparison to the other chips. On the other hand, it could offer the additional benefit of transparency. One suggestion would be the implementation of only a few ITO electrodes for advanced imaging among standard Ti/Au electrodes.

To summarise the primary results of the electrical characterisation, the three different resistances are depicted in the following Table 4.3 for a direct comparison.

	Ti/Au-"V1"	Ti/Au-"V2"	Ti/ITO/Au
Resistance (in Ohm)	44.5	33.8	195.54

Table 4.3: The measured resistances of the three different MEA designs

4.6 Electrophysiological assessment of P19 embryoid bodies on microfluidic platform resulted in inconclusive recordings

In the previous sections of this thesis, the electrical and fluid-mechanical functionalities of the developed neuron-on-a-chip device and the behaviour of the P19 ESC embryoid bodies in terms of size, growth and differentiation in dependence on their intial seeding density have been tested and characterised off-chip. Also, the ability of the cells to adhere, proliferate and to grow neurites on-chip was examined.

In a final experiment, electrophysiological activities derived by spontaneous electrical neural activity of the P19 ESC's on the chip-MEA-system were assessed. In case of successful assessment of signals, the activity or event rate of the different MEA designs and seeding densities can be linked and compared quantitatively. An overview of a typical recording with all sixty electrodes is presented below in Figure 4.31.

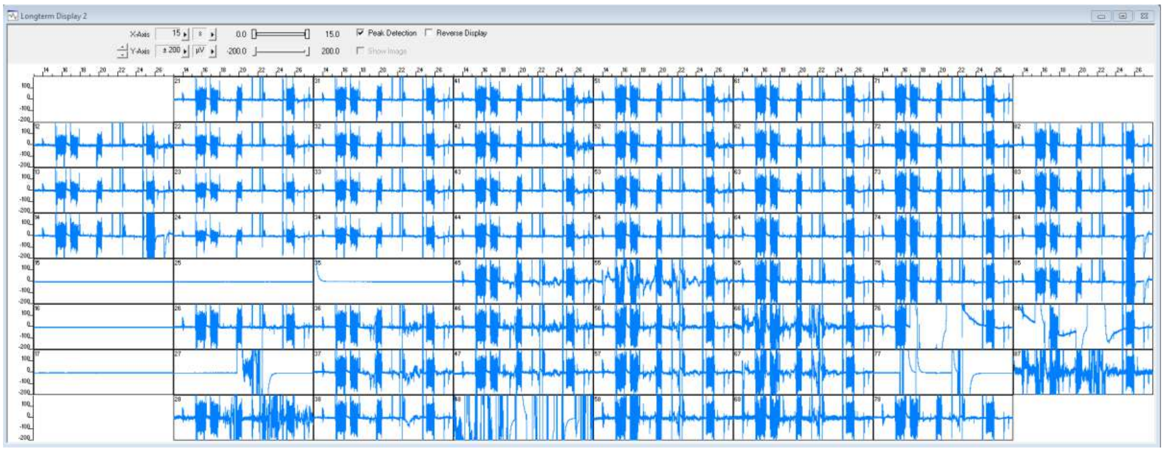

X-Axis 15 s 0.0 15.0 ☑ Peak Detection ☐ Reverse Display

Y-Axis ± 200 µV -200.0 200.0 ☐ Show Image

Figure 4.31: Depiction over the single channel electrodes in the software MC_Rack by Multichannel Systems

Two potential signalling events, which were recorded as part of the electrophysiological assessment, are presented below. All depicted peaks were recorded at only one single electrode, and events occurring at all channels were declared invalid, as due to the local confinement of action potentials, they can only be derived from signal artefacts.

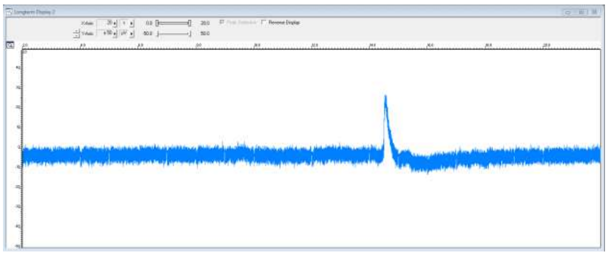

Figure 4.32: Potential peak, MEA: Ti/Au-"V2"

Figure 4.32 shows an exemplary event surpassing the signal noise, recorded on a Ti/Au-MEA "V2" and an EB of 2500 cells per well seeding density. After a depolarisation phase with a duration of approximately $40\,\mathrm{m\,sec}$, the voltage drops around $41.6\,\mathrm{mV}$ and reaches a local minimum. It returns to its baseline voltage after a repolarisation phase of around $310\,\mathrm{m\,sec}$ duration.

When comparing this specific peak to the hallmarks of a typical single action potential, one can observe a below-average but comparable amplitude of the peak. Also, the duration of the uprising to the peak and the downfall back to the offset voltage, equivalent to depolarisation- and repolarisation phase, are comparatively long. According to Hammond *et al.*, Ca2+-dependent action potentials via Ca2+ entry through voltage- and ligand-gated channels are characterised by relatively long peak duration and a low amplitude, which has been shown for some types of neuronal dendrites or certain endocrine cells. [175] The repolarisation phase of $310\,\mathrm{m\,sec}$ in contrast, is too long for most single action potentials. One possible assumption at this point could be a cascadic triggering of multiple neurons and a delayed repolarisation, since due to the electrode dimen-

Die approbierte gedruckte Originalversion dieser Diplomarbeit ist an der TU Wien Bibliothek verfügbar
The approved original version of this thesis is available in print at TU Wien Bibliothek.

sions a whole field potential is measured.

A similar event is depicted on the right in Figure 4.33, again recorded on a Ti/Au-MEA "V2" and an initial seeding density of 1000 cells/well. The amplitude of the local minimum stretches from a baseline of around $-6\,\mu$V to a minimum of $-41.4\,\mu$V, resulting in a peak of around $35\,\mu$V. It returns to its baseline value after $260\,\mathrm{m\,sec}$.

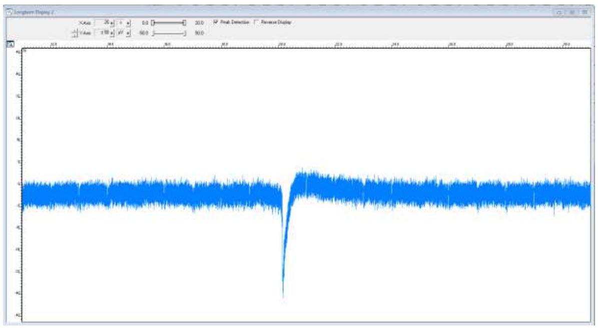

Figure 4.33: Potential peak, MEA: Ti/Au-"V2"

As very few signalling events were recorded, the embryoid bodies were subsequently investigated via brightfield microscopy. It could be observed that a comparatively low amount of neurites have been formed and cell debris was found in and outside the culturing wells. Two examples showing this issue are displayed below in Figure 4.34.

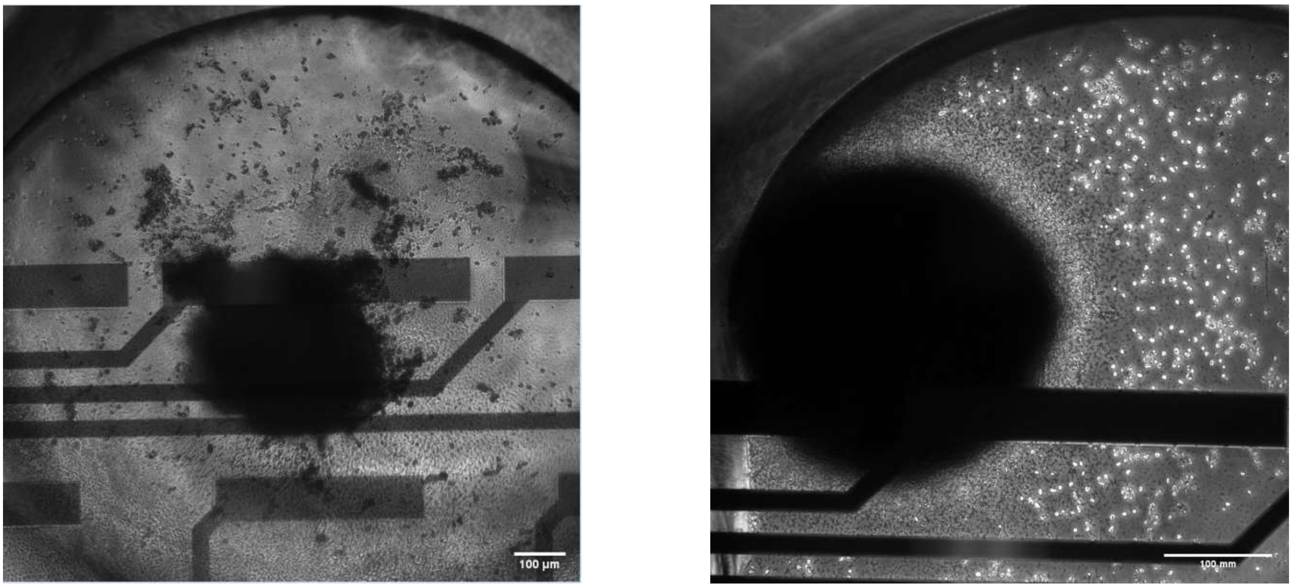

Figure 4.34: A depiction of two exemplary embryoid bodies showing malformed structures and dead cell debris surrounding them (left: ITO-MEA, D14, Density: 2500. Right: Ti/Au-MEA "V2", D15, Density: 1000)

Here it is evident that the strong appearance of cell debris and low expansion of neurites points towards low viability of the cells. This circumstance would explain the low electrophysiological signal rate in the recordings.

Additional chemical stimulation of the cells with $10\,\mu$M of adrenaline, which is common practice for verifying, that the measured signals are derived from biological activity of the cells, resulted in no further observable signal that could be classified as neural activity.

In summary, certain signalling patterns have been measured that slightly resemble typical action potential profiles in signal amplitude, duration and general signal morphology, but it could not be confirmed with the use of chemical stimulants. As a consequence, no information about the influence of initial seeding density, conduction line material and thickness on the signal could be derived. In previous sections, the cells have been demonstrated to display spontaneous neural activity by a calcium staining. Also the chip's ability to grow cells upon and conduct electrical current has been proven. In particular, the viability of multicellular spheroids as well as neural differentiation potential and neural activity of the P19 cells have been investigated both in a

Die approbierte gedruckte Originalversion dieser Diplomarbeit ist an der TU Wien Bibliothek verfügbar
The approved original version of this thesis is available in print at TU Wien Bibliothek.

standard culturing plate and on-a-chip.

The following error analysis showed that low viability of the embryoid bodies must play a main factor even after repetition of the experiment, although the exact reason for this issue is not known, as the cells displayed a different behaviour previously. Therefore, problems and difficulties around the manual handling are assumed to hold the most amount of potential for improvement. Therefore, possible pitfalls in the handling during cultivation and differentiation in the pre-seeding phase (D0-D7), EB-on-chip seeding (D7), post-seeding cultivation (after D7) and execution of the experiments. Further points of improvements beyond issues with the handling have been added to the list.

4.7 The PDMS-MEA-chip: problems and solutions

The problem analysis revealed several possible sites of optimisation with intent to improve cell viability and handling during execution of the experiments. Their problem sources and possible solutions are listed and discussed in the following chapter. The purpose of the list is to incentivise the investigation of the individual impact of these parameters to aid in optimising the presented sensor-integrated OOC-device for its use in future projects. In summary, five main problem sites have been examined.

Problem 1: Production process of the PDMS chip

Problem description: As described in the methods section, the PDMS chip, which is bonded upon the MEA, consists of several xurographically cut PDMS layers of 500 µm in thickness. This production approach is flexible, because requests for modification can be implemented straightforwardly, accelerating the iteration cycle of development. On the other hand, the layer production process of the chip requires manual labour and the production quality of the samples inherently differs slightly compared to an automated production process. More precisely, the positioning of the layers on top of each other is difficult to accomplish correctly and varies for each sample. In addition, this technique can only produce extrusions of two-dimensional structures.

Solution: As an alternative production process, 3D printing the microfluidic system would offer faster production times. Effective cell adhesion in combination with 3D printing techniques has been intensively described previously. [176] A second alternative would be the utilisation of a master mould. Samples would be produced by transfer of PDMS into the master mould, post-processed and bonded on top of the MEA. Both described processes would hereby provide more coherency in terms of sample quality and abate error-proneness. Also they offer the production of three-dimensional objects, e.g. cones or lateral cylinders.

Problem 2: Small well dimensions impede handling during seeding

Problem description: After cultivating the P19 embryoid bodies in a standard well plate, they are transferred in the chip, which has been filled with cell medium. The cells are susceptible to any kind of external mechanical stresses, so that this task needs to be executed very cautiously. Since the cells are introduced via the well opening and the small radius greatly aggravates the introduction of the pipette tip into the well, this task imposes a challenge in handling.

Solution: The simplest solution would be an increase of the dimensions of the wells in the next cycle of production. This facilitates the insertion of the pipette tip into the well and reduces unavoidable mechanical stress

Die approbierte gedruckte Originalversion dieser Diplomarbeit ist an der TU Wien Bibliothek verfügbar
The approved original version of this thesis is available in print at TU Wien Bibliothek.
TU Bibliothek WIEN Your knowledge hub

Die approbierte gedruckte Originalversion dieser Diplomarbeit ist an der TU Wien Bibliothek verfügbar
The approved original version of this thesis is available in print at TU Wien Bibliothek.
TU Bibliothek Your knowledge hub WIEN

on the cells. Also, introduction of a tapered design instead of a cylinder facilitates this, so that a truncated cone is used. This proposition creates another problem: the probability of embryoid bodies adhereing to electrodes is even more diminished. This issue is examined in Problem 4.

Problem 3: Suction of the coating agent and embryoid bodies inside the wells by capillary action in the bottleneck area

Problem description: During the cultivation and seeding it was observed that the surface coating agent with poly-l-lysine was sucked into the media channel, despite the partial obstacle wall. Additionally, it was noted that few embryoid bodies translocated intoF the channel far outside of the well after the seeding was finished via microscopic inspection.

Solution: This event is generated by capillary action or capillarity. Capillarity refers to the effect of liquid flowing into a narrow space, even in opposition to gravitational forces caused by the interaction of adhesive and cohesive forces within the fluid. Here, adhesive forces means the fluid-surface interaction and cohesive forces refer to surface tension within a fluid or interfluidic forces. The formula for the height h of the capillary rise in a cylindric pipe is given below in Equation 4.2:

$$h = \frac{2\sigma \cos\theta}{\rho g r} \tag{4.2}$$

Here, σ corresponds to surface tension, the angle θ is the contact angle, ρ corresponds to density, g gravitational force and r corresponds to radius.

Therefore, the capillary force can be directly reduced by increasing the radius or and decreasing the circumference of the medium channel. The bottleneck area, which is the narrowest and most critical area in the microfluidic chip, is recommended to be designed in a cylindric shape with an increased cross-sectional area.

Another alternative would be to decrease the surface tension with a hydrophobic and biocompatible reagent. In contrast, this interferes with the surface chemistry and might influence the cells' adhesive behaviour.

Problem 4: Inefficient EB positioning in wells over electrodes

Problem description: Since only a certain amount of the surface area on the MEA is covered by signal transducing electrodes, some embryoid bodies which have been cultivated and seeded successfully are not in contact with the recording electrodes and therefore, can not be investigated. Increasing the well-MEA surface area aggravates his problem.

Solution: One possible solution would be to implement an elliptic well form. This increases electrode coverage due to the electrode layout on the MEA. This way, a higher ratio of electrodes are in the area of interest. Another proposition would be to seed multiple EBs per well. Especially regarding a raise of well dimensions as proposed previously in Problem 2, which leads to a reduction of the ratio between electrode area (or area of interest) to the non-electrode area, due to the electrode layout. Since the exact position of an embryoid body on an electrode of the MEA can not be controlled, the seeding position can be viewed as a statistical event in dependence on the radius. Because of this, the probability of one embryoid body to adhere to an electrode as a crucial precondition for the experiment is reduced as a consequence. Utilisation multiple embryoid bodies in return increases the probability of low EB-electrode distance. This opens up new possibilities, as not only intra-, but also interspheroidal neural activity can be measured then. This decreases the demand of produced MEAs.

Another intricate alternative to increase cell-electrode contact would be a revision of the MEA-design, since less than 57%, or eight of fourteen of all electrodes per well are available for EBs to adhere to. In detail, the following three electrode parameters are recommended to be optimised for future projects:

1. Size: Smaller electrodes would decrease the amount of noise and increase the specificity of the measured signal. This also aids in distinguishing highly confined areas of interest from non-active areas.

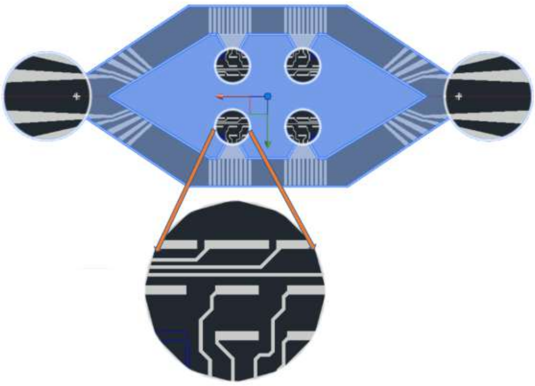

Figure 4.35: An overlay of the well over the MEA. Only eight of fourteen electrodes are (partially) in area of interest.

2. Positioning/Layout: Only few electrodes are within the area of interest, as presented in Figure 4.35. Better positioning of the electrodes with less distance from each other and a rectangular arrangement of the electrodes solves this problem.

3. Standardisation: It is recommended for a future design not to use two different electrode sizes, but to implement electrodes of the same size. Otherwise, the measured signals are not comparable directly as a result.

Problem 5: Evaporation

Problem description: One of the biggest problems during the execution of the experiments was the occurrence of evaporation and desiccation in the whole channel system and consequently the wells of the chip despite sealing of PCR foil. This results in increased cell necrosis. The evaporation effect is accelerated by two main factors: Firstly, the area that could be used to store medium is limited from the outside by the outer electrode tabs and from the centre caused by the electrode layout. Secondly, the capillary effect retents the medium from reentering the wells, as highlighted in problem 3.

Solution: The most straightforward solution would be to increase the overall volume so that more medium can enter the system. Moreover, scaling down the in-/outlets' radius and scaling up the channel dimensions decreases the medium-air surface area and as a consequence, slows the evaporation of the medium. Increasing the channel dimensions additionally facilitates the pumping of cell medium prior to the seeding step and prevents the formation of bubbles inside the channels.

Problem 6: Steady-state flow regime slowing nutrition supply

Problem description: As the presented microfluidic system constitutes a steady-state flow regime, it does not offer the possibility to externally generate fluid motion. This could foster a potential undersupply of nutrients in the embryoid bodies and decrease their viability.

Solution: Implementing a dynamic flow regime could aid the medium to flow back inside the well faster and increase the nutrient supply and medium turnover. This might positively influence the overall viability of the cells. Here it is important to keep the exposure of the EBs to an excess of fluid mechanical stress very low.

Moreover, introducing a flow regime aids in creating biochemical gradients, which in the case of neurons could aid in guiding neurite growth, as mentioned before. Also, flow with adaptable pump pressure is essential

Die approbierte gedruckte Originalversion dieser Diplomarbeit ist an der TU Wien Bibliothek verfügbar
The approved original version of this thesis is available in print at TU Wien Bibliothek.
TU Bibliothek WIEN Your knowledge hub

to mimic the physiological state of certain tissues ex vivo as well as possible. Brain tissue for example, would physiologically require comparatively low flow velocities.

Lastly, dynamic flow regime also opens up new experimental possibilities, as the investigation of the influence of flow regime on the neural activity of embryoid bodies is yet to be investigated.

A brief summary of the problems and solutions is provided in Table 4.4.

Problem	**Description of problem**	**Solution**
1	Xurographic production process requires manual, time-intensive, incoherent quality	3D printing or master mould production technique
2	Difficult pipetting during seeding step	Facilitation of handling by increasing well dimension
3	Suction of coating agent and EBs in channel	Capillary action decrease by bottleneck area redesign: 1. Implement cylindric shape, 2. Radius increase
4	Low cell-electrode contact	1. Seeding of multiple EBs per well 2. MEA electrode layout redesign: a) Size reduction, b) Electrode positioning, c) Size Standardisation
5	Evaporation of medium	Increasing channel dimensions & decreasing in-/outlet radius
6	Low medium turnover	Introduction of flow regime

Table 4.4: The problems and possible solutions of the current PDMS-MEA chip design

Die approbierte gedruckte Originalversion dieser Diplomarbeit ist an der TU Wien Bibliothek verfügbar
The approved original version of this thesis is available in print at TU Wien Bibliothek.

4.8 Alternative design proposition for microfluidic system

In a final step, an exemplary implementation of previously compiled suggestions for optimisation is presented as a possible alternative for the previous microfluidic chip design. Also, its performance in regard to suggested optimisations is quantified in Table 4.5 and compared to the old design that in previous electrophysiological assessments.

Generally, the total volume was increased by over 95% and the liquid-air surface was reduced by 20% to prevent medium evaporation and slow chip desiccation.

Also, the geometric shapes of the wells and the bottleneck have been changed for optimised fluid exchange, handling and MEA surface area coverage. The introduction of a cylindric bottleneck and an upside-down truncated elliptic cone as the well for cell seeds render a production process by 3D printing or master moulding necessary, as xurographic layer-by-layer production technique is restricted to vertically extruded two-dimensional structures.

The handling, especially for the EB-on-chip seeding step, was facilitated by increasing the top well surface by 220%. This surface increase does not count to the evaporation area, because the wells are sealed with an adhesive foil except for the direct introduction of fluids like chemical stimulants into the well.

The implementation of an elliptic base area on the MEA surface with increased dimensions (+80%) raises the number of accessible electrodes up to eleven out of fourteen. This facilitates seeding, growth and analysis of several EBs per well.

Additionally, the channel's shape is based on an arch instead of rounded rectangulars to avoid edges to subdue fluid turbulences.

Figure 4.36 shows a depiction of the resulting design with the fluid body in 3D on the left and a sketch of the outline in topview on the right.

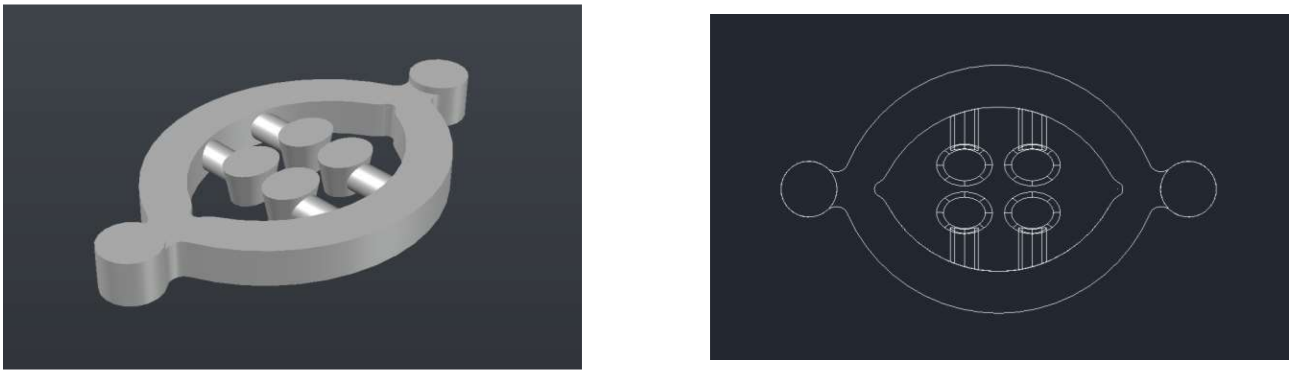

Figure 4.36: A depiction of an alternative design with implementation of suggested design optimisations

The following Table 4.5. lists the overall dimensions and optimisations of the alternative design and compares them to the old design.

Die approbierte gedruckte Originalversion dieser Diplomarbeit ist an der TU Wien Bibliothek verfügbar
The approved original version of this thesis is available in print at TU Wien Bibliothek.

Problem	Old Design	New Design
Overall dimensions	Width: 30,14 mm Length: 10,2 mm Height: 0,3 mm	Width: 31,233 mm Length: 20,429 mm Height: 0,35 mm
Difficult handling during seeding step	Top surface area of well : 3,1415 mm^2	Top surface area of well: 10,053 mm^2 (+220%)
Capillary effect Low medium turnover	Rectangular bottleneck cross section with high circumference and low cross-sectional area. Cross section: 1,178 mm^2	Increased bottleneck cross section for decreased capillary effect. Circular design for minimum circumference and adhesive retention. Cross section: 3.1415 mm^2 (+167%)
Electrode coverage	Accessible electrodes per well: 8/14	Accessible electrodes per well: 11/14 (+37,5%)
Desiccation	Low volume and high area of evaporation. Total volume: 294,1 mm^3 Evaporation area per in-/outlet: 15.71 mm^2	Total volume: 574,2 mm^3 (+ 95,24%) Evaporation area per in-/outlet: 12.56mm^2 (-20%)

Table 4.5: Quantified comparison of the performance of the alternative design to the old design used in electrophysiological measurements

Continuous Fluid Simulation

The varied geometrical shapes and increased dimensions of channels, wells and bottlenecks influence the behaviour of fluids heavily. In order to ensure low fluid mechanical forces on the embryoid bodies inside the wells, the fluid dynamics were analysed via CFD simulation again. The results are depicted in Figure 4.37 and show neglectable fluid shear stresses within the wells. Particle traces were added for demonstration. This means, that the elevation of the cross-sectional area of the bottleneck area connecting channels and wells up to 267% of the previous design did not impose any effect on the shear stresses inside the EB culturing wells.

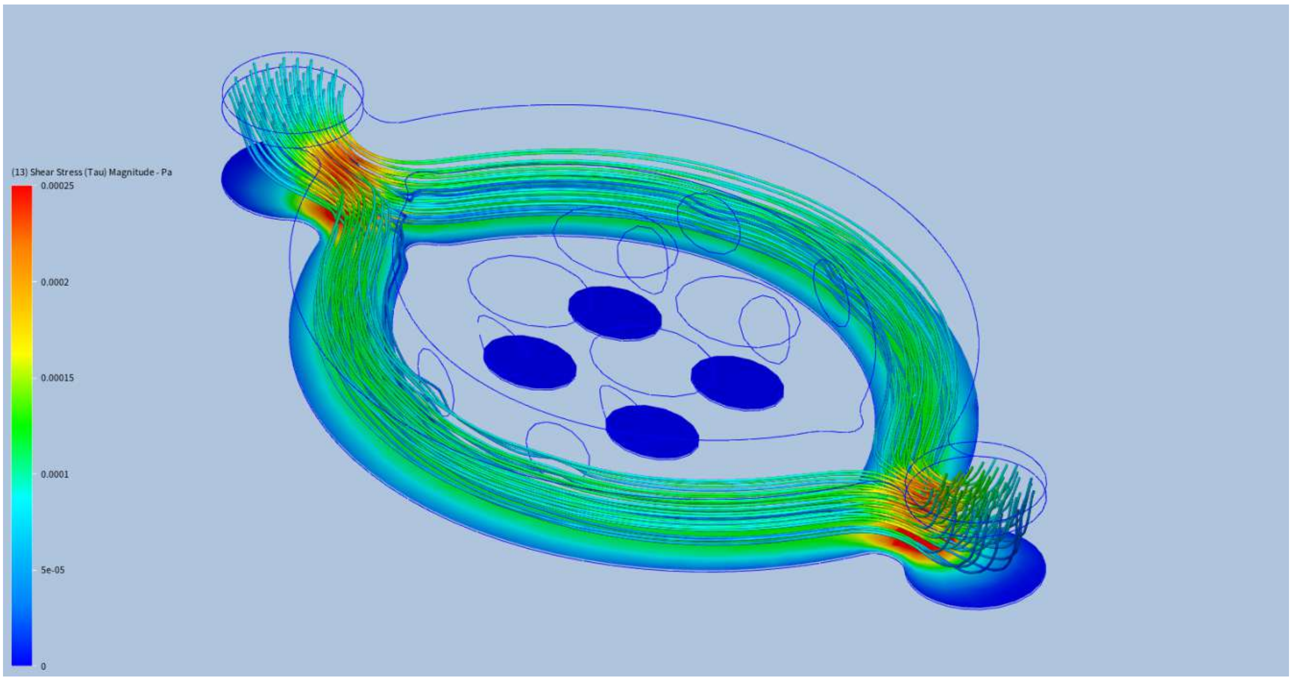

Figure 4.37: Depiction of the continuous fluid mechanical simulation of the alternative Design displays almost zero shear stress inside the wells

Die approbierte gedruckte Originalversion dieser Diplomarbeit ist an der TU Wien Bibliothek verfügbar
The approved original version of this thesis is available in print at TU Wien Bibliothek.

Die approbierte gedruckte Originalversion dieser Diplomarbeit ist an der TU Wien Bibliothek verfügbar
The approved original version of this thesis is available in print at TU Wien Bibliothek.

Die approbierte gedruckte Originalversion dieser Diplomarbeit ist an der TU Wien Bibliothek verfügbar
The approved original version of this thesis is available in print at TU Wien Bibliothek.

Chapter 5

Conclusion

In this thesis, a novel neuron-on-a-chip device for the growth, neuronal differentiation and proliferation of the P19 ESC line was developed. The correlations between cell seeding density, EB size, morphology and neuronal differentiation efficiency were investigated. The combination of the P19 ESC EBs grown in a sensor-integrated OOC platform comprises a versatile model of vertebrate embryo- and neurogenesis. This device may aid in the pursuit of developing early-stage treatments for neurodevelopmental diseases in the future.

In the first chapter, the motivation and the goals of this thesis were expounded. Then, a theoretical introduction to the cells of the CNS and stem cells was presented. The P19 embryonic carcinoma cell line as a pluripotent stem cell line, its properties and its importance as a model cell line due to the similarity to embryogenesis was elaborated. This was followed by an overview of current research models (in vivo, 2D in vitro, 3D in vitro) and current challenges around their use. Then, multicellular spheroids were introduced as a 3D in vitro culturing technique and research model with focus on properties and applications of neural P19 ESC embryoid bodies. Finally, the current state of the art of organ-on-a-chip applications for the investigation of neural tissue in biomedical sciences was discussed.

In the experimental results of chapter four, the initial characterisation of the P19 ESCs revealed high viability and the general capability to differentiate into neural tissue with the presented cultivation protocol. Furthermore, the differentiated P19 EBs exhibited calcium-dependent ion-channel activity, pointing towards the generatoin of spontaneous extracellular electrical activity. Image analysis of the growth and morphology of multicellular spheroids showed a dependence on the initial cell seeding density. A positive correlation between cell seeding density and EB size was found and analysed. Interestingly, the growth of embryoid bodies of P19 ESCs exceeding a seeding density of 5000 cells per well began to level off. Their viability rapidly diminished as high amounts of floating dead cell debris were generated and malformations in the overall spheroidal morphology occurred. In summary, an optimum range between 200 and 5000 cells per well reliably yielded EBs with low cell debris and high circularity. This interval of seeding densities is recommended for further investigations based on P19 embryoid bodies. The reasons for the appearance of malformations could not be clarified. It is proposed, that ineffective diffusive transport of gas or nutrients, strong concurrence for nutrients between the cells or mechanical forces contribute to the observed malformations.

Next, a positive correlation of the differentiation efficiency with increasing seeding densities was revealed. The variance of the differentiation efficiency within each density group increased strongly with rising cell seeding numbers. The highest ratio of differentiated to non-differentiated cells was achieved for a seeding density of 1000 cells per well, which was the middle of the tested densities. The embryoid bodies formed of this seeding density generated comparatively reproducible efficiencies. This means, that 1000 cells per well as the seeding density for the generation of embryoid bodies offers the highest differentiation efficiency with relatively high reproducibility. As a consequence, this density is the recommended starting point for applications with these

Die approbierte gedruckte Originalversion dieser Diplomarbeit ist an der TU Wien Bibliothek verfügbar
The approved original version of this thesis is available in print at TU Wien Bibliothek.

requirements. As a conclusion, it becomes apparent, that such embryoid bodies of medium size fulfil the trade-off between higher complexity of big spheroids and higher overall viability of small spheroids, which leads to the successful generation of complex neural networks in vitro. Moreover, it was observed, that differentiated neurons appeared preferably in regionally confined clusters. This cluster formation is analogous to the heterogeneous organisation of the human brain. Future investigation of this issue will improve our understanding of the generation of nervous systems in vitro and in vivo.

To address the research question stated in the aims of this thesis, the properties and design requirements of the components of the microfluidic PDMS chip and of the MEA were studied. A continuous fluid dynamic analysis was performed which revealed neglectable fluid mechanical shear stresses in proximity to the cells on-chip. The embryoid bodies were demonstrated to successfully adhere, grow and differentiate on the microfluidic OOC device. Moreover, growth of distinct neurite projections on glass and on chip has been achieved.

Next, the layout of the multielectrode array with purpose of measuring extracellular neural activity was investigated. An in-depth analysis of the electrical properties of the MEA with different conduction layer materials and thicknesses was performed. The electrical properties of the Ti/ITO/Au-MEA, which offers transparent electrodes for advanced high-resolution monitoring possibilities in real-time, showed diminished conductive power compared to the Ti/Au-MEA by a factor of 10. In contrast, increasing the thicknesses of the titanium and the gold layers improved the adhesion of the conduction material to the substrate and increased conductivity by 31.65%, which makes the Ti/Au-MEA with reinforced conduction material the preferred choice for future OOC applications in case electrode transparency is not required.

Finally, the electrophysiology of the P19 ESC embryoid bodies, seeded on the previously presented microfluidic PDMS-MEA-system, was assessed. The extracellular electrodes can only record whole-field potentials. This results in an unfavorable signal to noise ratio. Therefore, chemical stimulation is commonly used as a proof-of-concept to attribute signaling events to neural activity. The application of a chemical trigger could not verify a causal relation between the measured signals and neural activity of the P19 cells. Since the reasons for this could not be clarified, propositions for optimisation of the PDMS component design in terms of production process and dimensions were discussed to improve cell viability and handling. This was incorporated into a final iteration of the PDMS chip, which was compared to the old version and presented in the final section of the results and discussion chapter.

The biological and technical components of the system and their confluence have been thoroughly described in the course of this thesis. The ideal initial seeding size of P19 cells has been identified: 1000 cells per well generate healthy, well-differentiated and active embryoid bodies with reproducibly coherent properties. Calcium-dependent ion-channel activity pointing to generation of spontaneous action potentials was demonstrated, but this could not be confirmed by the electrophysiological recordings. The presented microfluidic OOC device offers a closed system for cultivation, adhesion and neural outgrowth of P19 embryoid bodies.

For future experiments, the successful recording of the electrophysiological cellular signals as a proof-of-concept for the complete functionality of the device in combination with the P19 ESCs would be desirable. Electrical activity is a key physiological parameter. Furthermore, the influence of the conductive material, of the initial seeding density and differentiation efficiency on the rate of electrical activity can be investigated. Also, transparent chips with a Ti/ITO/Au double layer as conduction material can be implemented. This opens new possibilities for biological investigation of simultaneous electrical recording and optical monitoring and analysis.Further ideas for future improvements would be the introduction of adjustable flow in the microfluidic system to reach more physiologic conditions on-a-chip and electrical stimulation of the cells, e.g. for controlled nerve growth conduction or electrical stimulation for triggering of action potentials via the MEA. As mentioned before, Park *et al.* already demonstrated a strong influence of interstitial levels of flow on the size, network formation and differentiation of neurospheres. [154] Also, future research around embryoid bodies' metabolism, the gene expression profiles and secretome analysis in dependence of the EBs size and cell location could deliver comprehensive insights into differentiation mechanics in embryoid bodies. An example of a promising methodology to improve control of differentiation rates of P19 ESCs with RA in embryoid bodies for future research efforts is the implementation of embryonal carcinoma cell encapsulation and bioreactor culture protocols, as reported previously with hematopoietic cells. [120]

To conclude, this thesis demonstrated that the developed microfluidic organ-on-a-chip device is capable of offering a low-cost, rapidly adaptible laboratory on-a-chip for the investigation of size-dependent differences in the efficiency of neuronal differentiation. The multicellular agglomeration of the P19 embryonal carcinoma cell line is a promising candidate for investigating vertebrate embryogenesis and specifically neurogenesis, which simulates certain aspects of human neurogenesis and exhibits similarity to human midbrain tissue. In this regard, this thesis demonstrated the conditions for the reliable generation of healthy and differentiated embryoid bodies as an advanced 3D in vitro model, which we use to model molecular and cellular aspects of the genesis of the human nervous system. The integration of microfluidics into a sensor-integrated OOC approach enables the real-time monitoring 2D monitoring of 3D tissue in high-resolution.

In future projects, the presented organ-on-a-chip approach in combination with the P19 cell line can be implemented for the investigation of early-stage embryonic development on a cellular and molecular level. It can also function as a model for ADME (absorption, distribution, metabolism and excretion) screenings for drug delivery systems in the preclinical phase of development. Also, other cell lines like transgenic cell lines or iPSC-derived tissues can be introduced. This could lead to pioneering new treatments for neurological diseases without the ethical and costly burdens that in vivo and current in vitro models inevitably constitute. This promises fascinating scientific discoveries, reduced necessity for animal models and finally relief for patients and health care systems.

Die approbierte gedruckte Originalversion dieser Diplomarbeit ist an der TU Wien Bibliothek verfügbar
The approved original version of this thesis is available in print at TU Wien Bibliothek.
TU Wien Bibliothek Your knowledge hub

Die approbierte gedruckte Originalversion dieser Diplomarbeit ist an der TU Wien Bibliothek verfügbar
The approved original version of this thesis is available in print at TU Wien Bibliothek.

Die approbierte gedruckte Originalversion dieser Diplomarbeit ist an der TU Wien Bibliothek verfügbar
The approved original version of this thesis is available in print at TU Wien Bibliothek.

Appendix

P19 cells

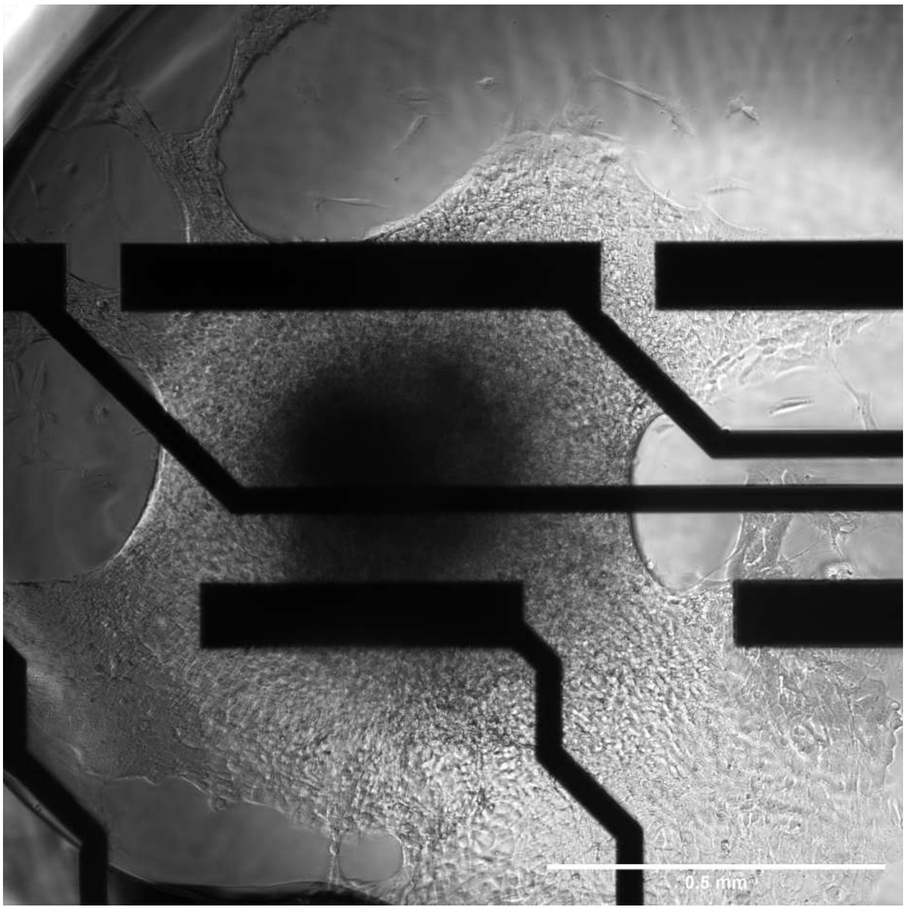

Figure 5.1: Embryoid body with strong projections on MEA-chip

Die approbierte gedruckte Originalversion dieser Diplomarbeit ist an der TU Wien Bibliothek verfügbar
The approved original version of this thesis is available in print at TU Wien Bibliothek.

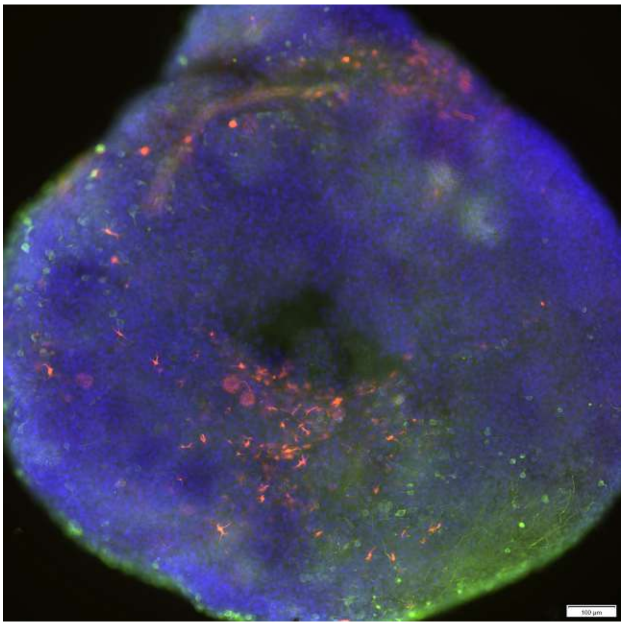

Figure 5.2: 2D-IHC-staining with astrocytes (red) and neurons (green) in wellplate

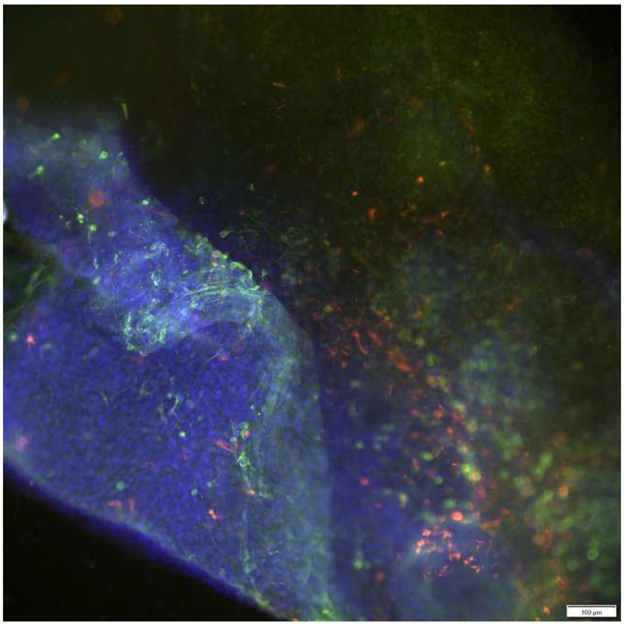

Figure 5.3: 3D-IHC-staining with astrocytes (red) and neurons (green) on-a-chip

Multielectrode array

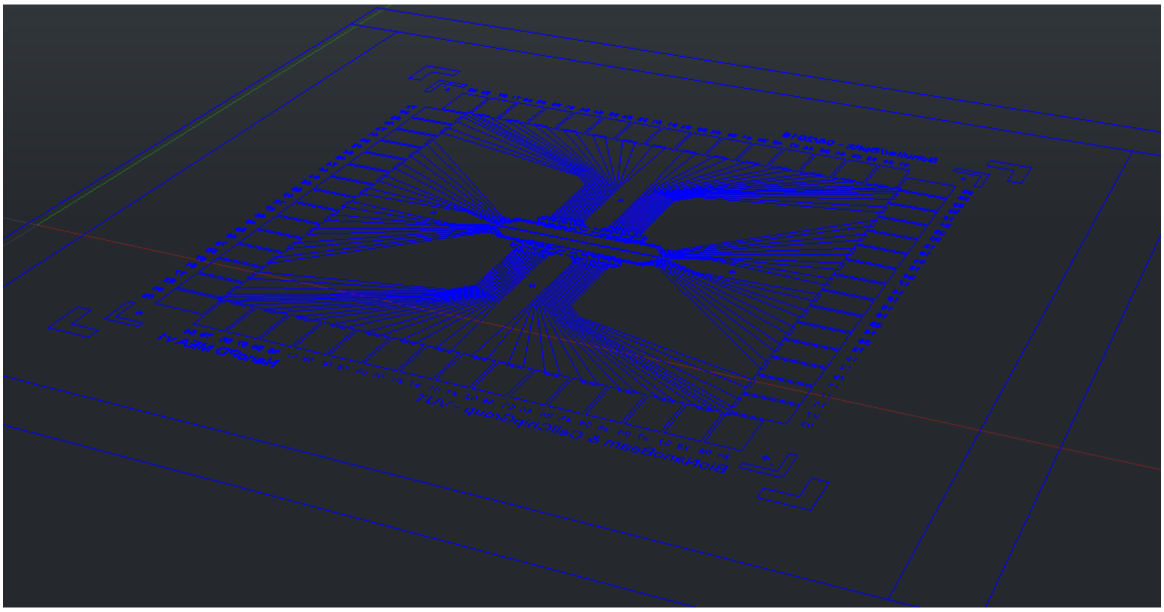

Figure 5.4: View of MEA in AutoCAD

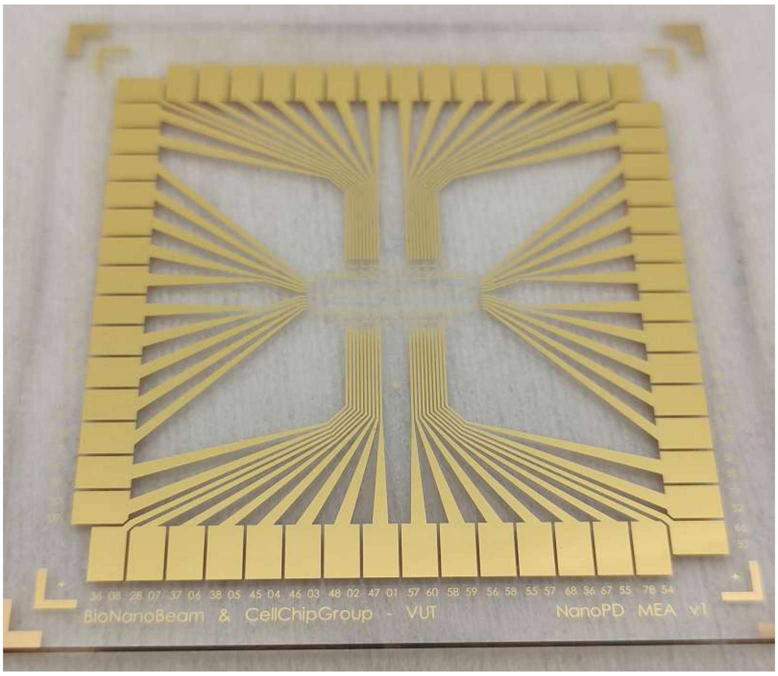

Figure 5.5: Picture of Ti/Au-MEA

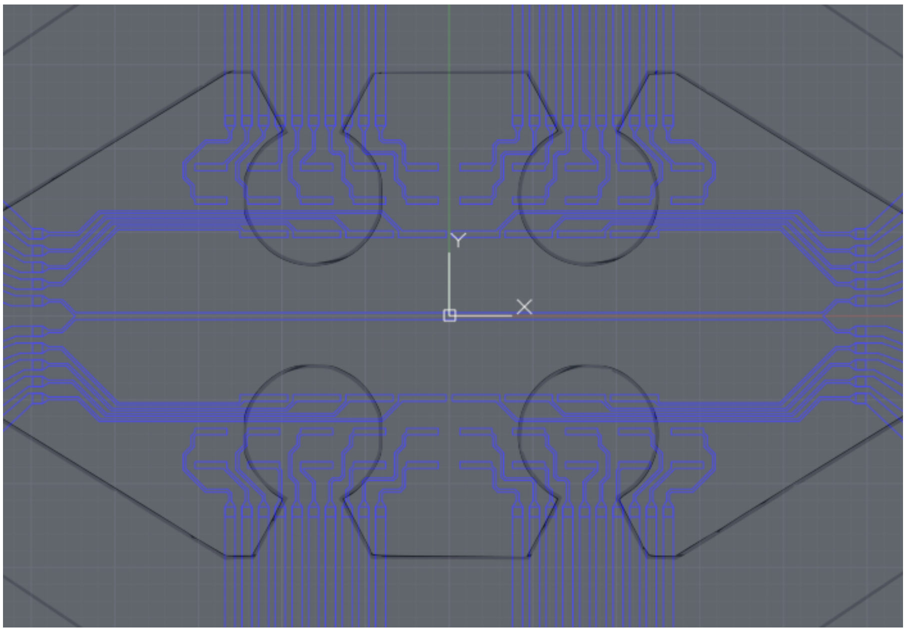

Figure 5.6: Sketched overlay of PDMS chip over MEA

Die approbierte gedruckte Originalversion dieser Diplomarbeit ist an der TU Wien Bibliothek verfügbar
The approved original version of this thesis is available in print at TU Wien Bibliothek.
TU WIEN Bibliothek Your knowledge hub

Figure 5.7: The loaded chip in petri dish before measurement (D9)

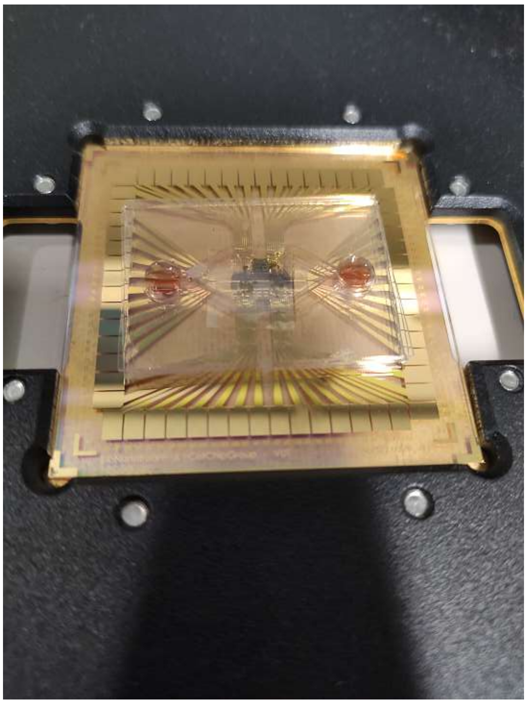

Figure 5.8: The chip layed onto the temperature platform of the MEA1060 by MCS

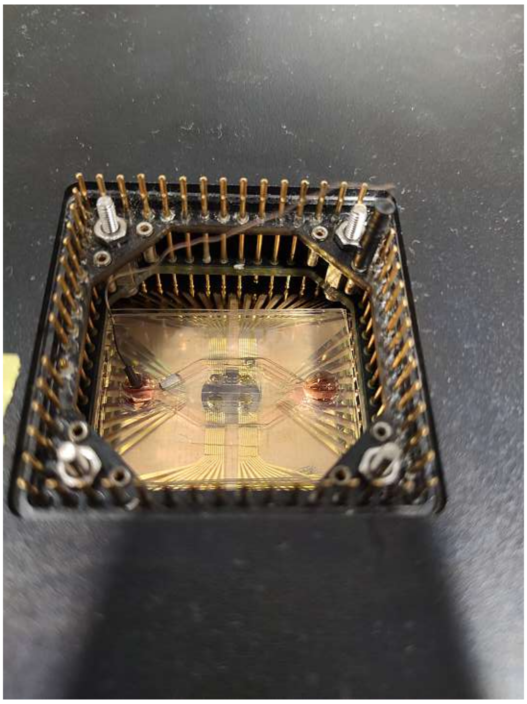

Figure 5.9: The chip clamped into interface with reference electrode inserted

Die approbierte gedruckte Originalversion dieser Diplomarbeit ist an der TU Wien Bibliothek verfügbar
The approved original version of this thesis is available in print at TU Wien Bibliothek.
TU WIEN Bibliothek Your knowledge hub

Die approbierte gedruckte Originalversion dieser Diplomarbeit ist an der TU Wien Bibliothek verfügbar
The approved original version of this thesis is available in print at TU Wien Bibliothek.

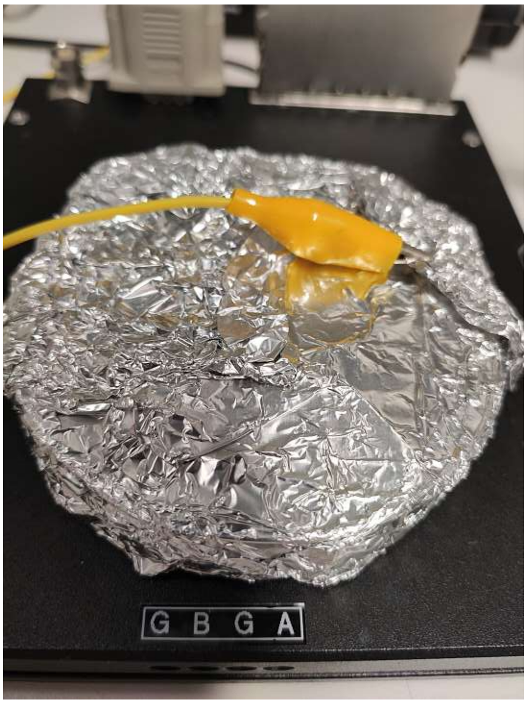

Figure 5.10: Aluminium shield over chip for prevention of capacitive coupling

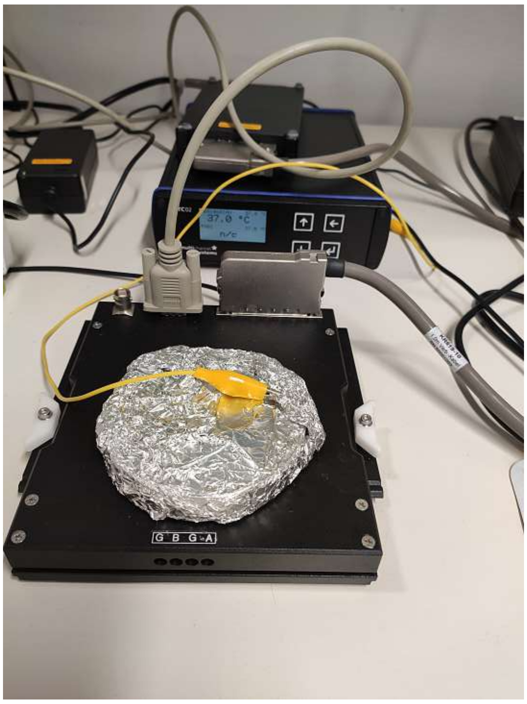

Figure 5.11: The whole MCS interface with the TC02 operator in the back for temperature control

Die approbierte gedruckte Originalversion dieser Diplomarbeit ist an der TU Wien Bibliothek verfügbar
The approved original version of this thesis is available in print at TU Wien Bibliothek.

Die approbierte gedruckte Originalversion dieser Diplomarbeit ist an der TU Wien Bibliothek verfügbar
The approved original version of this thesis is available in print at TU Wien Bibliothek.

Achnowledgements

In the past one and a half years, I was able to get deep insight into scientific research. It was extremely fascinating to see theory from books realised, be it during chip production in the cleanroom or seeing life proliferate through the microscope. Yet again, I learned how every little or big obstacle can be solved, as long as doubt and procrastination is overcome.

Firstly, I'd like to thank Prof. Peter Ertl and Prof. Heinz Wanzenböck for enabling the whole project and giving me valuable insights into scientific work, chip production and cleanroom work.

Secondly, I would like to thank Sarah Spitz from the Cell Chip Group of the Institute of technical chemistry for her unbelievable patience, professionalism and guidance. I learnt a lot about cell culturing and biological methodology. Her passion for science, systematic project work, biology and the mysteries of life they comprise were an inspiration to me in times, when it seemed to me like this project was a road to nowhere. I could not have found a more fitting teacher.

Also, I would like to thank Philipp, Markus, Sebastian, Sonia and Chris for their help in the laboratory. Generally, I'd like to thank all member of the BMMS and especially in my bureau CH 02 14A to make the experimental, administrative and writing work more enjoyable. Zoom meetings ended up funnier than coffee breaks, which non-the-less brightened the day.

Lastly, I would like to thank my family and friends for always supporting me in every dimension possible. This project would not have been possible by any means without them.

Die approbierte gedruckte Originalversion dieser Diplomarbeit ist an der TU Wien Bibliothek verfügbar
The approved original version of this thesis is available in print at TU Wien Bibliothek.

Die approbierte gedruckte Originalversion dieser Diplomarbeit ist an der TU Wien Bibliothek verfügbar
The approved original version of this thesis is available in print at TU Wien Bibliothek.
TU WIEN Bibliothek Your knowledge hub

Bibliography

[1] Gao Liyang et al. “Neural Commitment of Embryonic Stem Cells through the Formation of Embryoid Bodies (EBs)”. In: *The Malaysian Journal of Medical Sciences : MJMS* 21.5 (2014), p. 8. ISSN: 21804303. URL: `/pmc/articles/PMC4418120/%20/pmc/articles/PMC4418120/?report=abstract%20https://www.ncbi.nlm.nih.gov/pmc/articles/PMC4418120/`.

[2] Lisa M. Smits et al. “Modeling Parkinson’s disease in midbrain-like organoids”. In: *npj Parkinson’s Disease* 5.1 (Dec. 2019). ISSN: 23738057. DOI: `10.1038/s41531-019-0078-4`.

[3] Marcel A.G. Van Der Heyden and Libert H.K. Defize. “Twenty one years of P19 cells: What an embryonal carcinoma cell line taught us about cardiomyocyte differentiation”. In: *Cardiovascular Research* 58.2 (May 2003), pp. 292–302. ISSN: 00086363. DOI: `10.1016/S0008-6363(02)00771-X/2/58-2-292-FIG1.GIF`. URL: `https://academic.oup.com/cardiovascres/article/58/2/292/340911`.

[4] Alessandra Livigni et al. “Differentiation of Embryonic Stem Cells into Anterior Definitive Endoderm”. In: *Current Protocols in Stem Cell Biology* 10.1 (Sept. 2009), pp. 1–1. ISSN: 1938-8969. DOI: `10.1002/9780470151808.SC01G03S10`. URL: `https://onlinelibrary.wiley.com/doi/full/10.1002/9780470151808.sc01g03s10%20https://onlinelibrary.wiley.com/doi/abs/10.1002/9780470151808.sc01g03s10%20https://currentprotocols.onlinelibrary.wiley.com/doi/10.1002/9780470151808.sc01g03s10`.

[5] Kira Zeevaert et al. “Cell Mechanics in Embryoid Bodies”. In: *Cells 2020, Vol. 9, Page 2270* 9.10 (Oct. 2020), p. 2270. ISSN: 2073-4409. DOI: `10.3390/CELLS9102270`. URL: `https://www.mdpi.com/2073-4409/9/10/2270/htm%20https://www.mdpi.com/2073-4409/9/10/2270`.

[6] Dale Purves et al. *Neuroscience (Sixth Edition) | Veronica Jimenez - Academia.edu*. Ed. by George Augustine. 6th ed. July 2018. ISBN: 978-1605353807. URL: `https://www.academia.edu/43014289/Neuroscience_by_Dale_Purves_et_al_eds_z_lib_org_`.

[7] *Image of CNS. "central-nervous-system_G_160935779.jpg (2000×1765)". URL: https://pgneet.co/wp-content/uploads/2020/03/central-nervous-system_G_160935779.jpg*. URL: `https://pgneet.co/wp-content/uploads/2020/03/central-nervous-system_G_160935779.jpg`.

[8] Lawrence S. Sherman William James Larsen. *Human Embryology - Third Edition*. 3rd ed. Churchill Livingstone, July 2001. ISBN: 978-0443065835. URL: `https://books.google.at/books?vid=ISBN0443065837&redir_esc=y`.

[9] Schwartz JH Kandel ER. *Principles of Neural Science, Fifth Edition | AccessNeurology | McGraw Hill Medical*. 2013. URL: `https://neurology.mhmedical.com/content.aspx?bookid=1049&sectionid=59138139`.

[10] Dale Purves et al. “Neuroscience (Second Edition)”. In: *Sinauer Associates, Inc.* (2001), pp. 1–2. URL: `https://www.ncbi.nlm.nih.gov/books/NBK10799/`.

[11] Christopher S. von Bartheld, Jami Bahney, and Suzana Herculano-Houzel. “The Search for True Numbers of Neurons and Glial Cells in the Human Brain: A Review of 150 Years of Cell Counting”. In: *The Journal of comparative neurology* 524.18 (Dec. 2016), p. 3865. ISSN: 10969861. DOI: `10.1002/CNE.24040`. URL: `/pmc/articles/PMC5063692/%20/pmc/articles/PMC5063692/?report=abstract%20https://www.ncbi.nlm.nih.gov/pmc/articles/PMC5063692/`.

[12] R. Douglas Fields et al. “Glial biology in learning and cognition”. In: *Neuroscientist* 20.5 (Oct. 2014), pp. 426–431. ISSN: 10894098. DOI: `10.1177/1073858413504465`. URL: `https://journals.sagepub.com/doi/full/10.1177/1073858413504465`.

[13] Sarah Knapp. *Glia Cell*. Oct. 2020. URL: `https://biologydictionary.net/glial-cells/`.

[14] Brian A. Macvicar and Eric A. Newman. “Astrocyte regulation of blood flow in the brain”. In: *Cold Spring Harbor perspectives in biology* 7.5 (2015), pp. 1–15. ISSN: 1943-0264. DOI: `10.1101/CSHPERSPECT.A020388`. URL: `https://pubmed.ncbi.nlm.nih.gov/25818565/`.

[15] Alexander V. Gourine et al. “Astrocytes control breathing through pH-dependent release of ATP.” In: *Science (New York, N.Y.)* 329.5991 (July 2010), pp. 571–575. ISSN: 0036-8075. DOI: `10.1126/SCIENCE.1190721`. URL: `https://www.ncbi.nlm.nih.gov/pmc/articles/pmid/20647426/?tool=EBI%20https://europepmc.org/article/MED/20647426`.

[16] Pasko Rakic. “Mode of cell migration to the superficial layers of fetal monkey neocortex”. In: *The Journal of comparative neurology* 145.1 (1972), pp. 61–83. ISSN: 0021-9967. DOI: `10.1002/CNE.901450105`. URL: `https://pubmed.ncbi.nlm.nih.gov/4624784/`.

[17] Junyu Mai et al. “Axon Initiation and Growth Cone Turning on Bound Protein Gradients”. In: *Journal of Neuroscience* 29.23 (June 2009), pp. 7450–7458. ISSN: 0270-6474. DOI: `10.1523/JNEUROSCI.1121-09.2009`. URL: `https://www.jneurosci.org/content/29/23/7450%20https://www.jneurosci.org/content/29/23/7450.abstract`.

[18] Colleen Macpherson. *The accidental discovery of stem cells - University of Saskatchewan - Arts & Science: The Magazine*. May 2018. URL: `https://artsandscience.usask.ca/news/magazine/Spring_2018/stem-cells.php`.

[19] R. P. (Robert Paul) Lanza and Anthony Atala. “Handbook of stem cells. Volume 2, Adult and fetal stem cells”. In: *Elsevier* (2012). URL: `https://play.google.com/store/books/details/Handbook_of_Stem_Cells_Edition_2?id=wm-K_dKpjBAC&hl=de&gl=DE`.

[20] Evan Y. Snyder and Stephen Yip. “Stem Cell Biology”. In: *Fetal and Neonatal Physiology: Third Edition* 1-2 (Jan. 2004), pp. 57–65. DOI: `10.1016/B978-0-7216-9654-6.50009-6`.

[21] Michaela Prochazkova et al. “Embryonic Versus Adult Stem Cells”. In: *Stem Cell Biology and Tissue Engineering in Dental Sciences* (Jan. 2015), pp. 249–262. DOI: `10.1016/B978-0-12-397157-9.00020-5`.

[22] Philip Roelandt and Catherine M. Verfaillie. “Multipotent Adult Progenitor Cells”. In: *Principles of Regenerative Medicine* (2011), pp. 263–272. DOI: `10.1016/B978-0-12-381422-7.10015-X`.

[23] M. J. Evans and M. H. Kaufman. “Establishment in culture of pluripotential cells from mouse embryos”. In: *Nature 1981 292:5819* 292.5819 (1981), pp. 154–156. ISSN: 1476-4687. DOI: `10.1038/292154a0`. URL: `https://www.nature.com/articles/292154a0`.

[24] James A. Thomson. “Embryonic stem cell lines derived from human blastocysts”. In: *Science* 282.5391 (Nov. 1998), pp. 1145–1147. ISSN: 00368075. DOI: `10.1126/SCIENCE.282.5391.1145/ASSET/4FA17082-B65A-4ACF-9EC3-0AD6579B0CB6/ASSETS/GRAPHIC/SE4686988004.JPEG`. URL: `https://www.science.org/doi/abs/10.1126/science.282.5391.1145`.

Die approbierte gedruckte Originalversion dieser Diplomarbeit ist an der TU Wien Bibliothek verfügbar
The approved original version of this thesis is available in print at TU Wien Bibliothek.
TU WIEN Bibliothek Your knowledge hub

[25] Kazutoshi Takahashi et al. “Induction of Pluripotent Stem Cells from Adult Human Fibroblasts by Defined Factors”. In: *Cell* 131.5 (Nov. 2007), pp. 861–872. ISSN: 0092-8674. DOI: `10.1016/J.CELL.2007.11.019`.

[26] Jane Lebkowski. “GRNOPC1: the world’s first embryonic stem cell-derived therapy”. In: *http://dx.doi.org/10.2217/rme* 6.6 Suppl (Oct. 2011), pp. 11–13. ISSN: 1746076X. DOI: `10.2217/RME.11.77`. URL: `https://www.futuremedicine.com/doi/abs/10.2217/rme.11.77`.

[27] Eric W. Esch, Anthony Bahinski, and Dongeun Huh. “Organs-on-chips at the frontiers of drug discovery”. In: *Nature Reviews Drug Discovery 2015 14:4* 14.4 (Mar. 2015), pp. 248–260. ISSN: 1474-1784. DOI: `10.1038/nrd4539`. URL: `https://www.nature.com/articles/nrd4539`.

[28] Hiroshi Kawasaki et al. “Induction of Midbrain Dopaminergic Neurons from ES Cells by Stromal Cell–Derived Inducing Activity”. In: *Neuron* 28.1 (Oct. 2000), pp. 31–40. ISSN: 0896-6273. DOI: `10.1016/S0896-6273(00)00083-0`.

[29] Colin W. Pouton and John M. Haynes. “Embryonic stem cells as a source of models for drug discovery”. In: *Nature Reviews Drug Discovery 2007 6:8* 6.8 (Aug. 2007), pp. 605–616. ISSN: 1474-1784. DOI: `10.1038/nrd2194`. URL: `https://www.nature.com/articles/nrd2194`.

[30] John McNeish. “Embryonic stem cells in drug discovery”. In: *Nature Reviews Drug Discovery 2004 3:1* 3.1 (2004), pp. 70–80. ISSN: 1474-1784. DOI: `10.1038/nrd1281`. URL: `https://www.nature.com/articles/nrd1281`.

[31] Hynek Wichterle et al. “Directed differentiation of embryonic stem cells into motor neurons”. In: *Cell* 110.3 (Aug. 2002), pp. 385–397. ISSN: 00928674. DOI: `10.1016/S0092-8674(02)00835-8/ATTACHMENT/03A66480-5654-425E-9EA5-405DA1F61987/MMC1.PDF`. URL: `http://www.cell.com/article/S0092867402008358/fulltext%20http://www.cell.com/article/S0092867402008358/abstract%20https://www.cell.com/cell/abstract/S0092-8674(02)00835-8`.

[32] Fred H. Gage. “Mammalian neural stem cells”. In: *Science (New York, N.Y.)* 287.5457 (Feb. 2000), pp. 1433–1438. ISSN: 0036-8075. DOI: `10.1126/SCIENCE.287.5457.1433`. URL: `https://pubmed.ncbi.nlm.nih.gov/10688783/`.

[33] E. Mezey et al. “Turning blood into brain: cells bearing neuronal antigens generated in vivo from bone marrow”. In: *Science (New York, N.Y.)* 290.5497 (Dec. 2000), pp. 1779–1782. ISSN: 0036-8075. DOI: `10.1126/SCIENCE.290.5497.1779`. URL: `https://pubmed.ncbi.nlm.nih.gov/11099419/`.

[34] Isha Verma and Polani B. Seshagiri. “Directed differentiation of mouse P19 embryonal carcinoma cells to neural cells in a serum- and retinoic acid-free culture medium”. In: *In Vitro Cellular and Developmental Biology - Animal* 54.8 (Sept. 2018), pp. 567–579. ISSN: 10712690. DOI: `10.1007/S11626-018-0275-1/FIGURES/6`. URL: `https://link.springer.com/article/10.1007/s11626-018-0275-1`.

[35] M. W. McBurney. “P19 embryonal carcinoma cells.” In: *International Journal of Developmental Biology* 37.1 (Feb. 2003), pp. 135–140. ISSN: 0214-6282. DOI: `10.1387/IJDB.8507558`. URL: `http://www.ijdb.ehu.es/web/paper/8507558`.

[36] Susanne Bremer and Richard Vogel. “Pluripotent stem cells of the mouse as a potential in vitro model for mammalian germ cells. Sister chromatid exchanges induced by MMC and ENU in undifferentiated cell lines compared to differentiated cell lines”. In: *Mutation Research/Genetic Toxicology and Environmental Mutagenesis* 444.1 (July 1999), pp. 97–102. ISSN: 1383-5718. DOI: `10.1016/S1383-5718(99)00090-X`.

[37] Gail R. Martin. “Teratocarcinomas as a model system for the study of embryogenesis and neoplasia”. In: *Cell* 5.3 (July 1975), pp. 229–243. ISSN: 0092-8674. DOI: `10.1016/0092-8674(75)90098-7`. URL: `https://pubmed.ncbi.nlm.nih.gov/1097123/`.

TU WIEN Bibliothek Your knowledge hub
Die approbierte gedruckte Originalversion dieser Diplomarbeit ist an der TU Wien Bibliothek verfügbar
The approved original version of this thesis is available in print at TU Wien Bibliothek.

[38] Francois Artzt Karen; Jacob. "Absence of serologically detectable H-2 on primitive teratocarcinoma cells in culture". In: *Transplantation* 17.6 (June 1974), pp. 632–634.

[39] M. Edidin et al. "Embryonic and Fetal Antigens in Cancer". In: (1971), pp. 239–248.

[40] Marcel A.G. Van Der Heyden et al. "P19 embryonal carcinoma cells: a suitable model system for cardiac electrophysiological differentiation at the molecular and functional level". In: *Cardiovascular Research* 58.2 (Jan. 2003), pp. 410–422. ISSN: 00086363. DOI: `10.1016/S0008-6363(03)00247-5`. URL: `https://www.academia.edu/27761514/P19_embryonal_carcinoma_cells_a_suitable_model_system_for_cardiac_electrophysiological_differentiation_at_the_molecular_and_functional_level`.

[41] Charles E. Murry and Gordon Keller. "Differentiation of Embryonic Stem Cells to Clinically Relevant Populations: Lessons from Embryonic Development". In: *Cell* 132.4 (Feb. 2008), pp. 661–680. ISSN: 0092-8674. DOI: `10.1016/J.CELL.2008.02.008`.

[42] Elizabeth M.V. Jones-Villeneuve et al. "Retinoic acid induces embryonal carcinoma cells to differentiate into neurons and glial cells." In: *Journal of Cell Biology* 94.2 (Aug. 1982), pp. 253–262. ISSN: 0021-9525. DOI: `10.1083/JCB.94.2.253`. URL: `http://rupress.org/jcb/article-pdf/94/2/253/1076189/253.pdf`.

[43] Randal W. Berg and Michael W. McBurney. "Cell density and cell cycle effects on retinoic acid-induced embryonal carcinoma cell differentiation". In: *Developmental Biology* 138.1 (Mar. 1990), pp. 123–135. ISSN: 0012-1606. DOI: `10.1016/0012-1606(90)90182-I`.

[44] Sherry A. Tanumihardjo. "Vitamin A: biomarkers of nutrition for development". In: *The American Journal of Clinical Nutrition* 94.2 (Aug. 2011), 658S. ISSN: 00029165. DOI: `10.3945/AJCN.110.005777`. URL: `/pmc/articles/PMC3142734/%20/pmc/articles/PMC3142734/?report=abstract%20https://www.ncbi.nlm.nih.gov/pmc/articles/PMC3142734/`.

[45] PotukuchiVenkata Gurunadha Krishna Sarma et al. "In vitro differentiation of cultured human CD34+ cells into astrocytes". In: *Neurology India* 61.4 (July 2013), p. 383. ISSN: 0028-3886. DOI: `10.4103/0028-3886.117615`. URL: `http://www.neurologyindia.com/text.asp?2013/61/4/383/117615`.

[46] Gregg Duester. "Retinoic Acid Synthesis and Signaling during Early Organogenesis". In: *Cell* 134.6 (Sept. 2008), p. 921. ISSN: 00928674. DOI: `10.1016/J.CELL.2008.09.002`. URL: `/pmc/articles/PMC2632951/%20/pmc/articles/PMC2632951/?report=abstract%20https://www.ncbi.nlm.nih.gov/pmc/articles/PMC2632951/`.

[47] Linda Z. Holland. "A chordate with a difference". In: *Nature 2007 447:7141* 447.7141 (May 2007), pp. 153–154. ISSN: 1476-4687. DOI: `10.1038/447153a`. URL: `https://www.nature.com/articles/447153a`.

[48] Julie Marill et al. "Retinoic Acid Metabolism and Mechanism of Action: A Review". In: *Current Drug Metabolism* 4.1 (Mar. 2005), pp. 1–10. ISSN: 13892002. DOI: `10.2174/1389200033336900`.

[49] *Depiction of molecular structure of retinoic acid. URL: https://www.stemcell.com/all-trans-retinoic-acid.html Copyright © 2022 by STEMCELL Technologies Inc.* 2022. URL: `https://www.stemcell.com/all-trans-retinoic-acid.html`.

[50] abcam.cn. *All-Trans-Retinol Molecular Structure*. 2022. URL: `https://www.abcam.cn/products/biochemicals/all-trans-retinol-vitamin-a-retinoic-acid-receptor-ligand-ab141962.html`.

[51] Atsushi Morii, Syouichi Katayama, and Tetsuya Inazu. "Establishment of a Simple Method for Inducing Neuronal Differentiation of P19 EC Cells without Embryoid Body Formation and Analysis of the Role of Histone Deacetylase 8 Activity in This Differentiation". In: *Biological and Pharmaceutical Bulletin* 43.7 (July 2020), pp. 1096–1103. ISSN: 0918-6158. DOI: `10.1248/BPB.B20-00091`.

Die approbierte gedruckte Originalversion dieser Diplomarbeit ist an der TU Wien Bibliothek verfügbar
The approved original version of this thesis is available in print at TU Wien Bibliothek.

Die approbierte gedruckte Originalversion dieser Diplomarbeit ist an der TU Wien Bibliothek verfügbar
The approved original version of this thesis is available in print at TU Wien Bibliothek.

[52] M. W. McBurney et al. “Control of muscle and neuronal differentiation in a cultured embryonal carcinoma cell line”. In: *Nature 1982 299:5879* 299.5879 (1982), pp. 165–167. ISSN: 1476-4687. DOI: `10.1038/299165a0`. URL: `https://www.nature.com/articles/299165a0`.

[53] Mary K.S. Edwards and Michael W. McBurney. “The concentration of retinoic acid determines the differentiated cell types formed by a teratocarcinoma cell line”. In: *Developmental Biology* 98.1 (July 1983), pp. 187–191. ISSN: 0012-1606. DOI: `10.1016/0012-1606(83)90348-2`.

[54] Michael F.A. Finley, Nita Kulkarni, and James E. Huettner. “Synapse formation and establishment of neuronal polarity by P19 embryonic carcinoma cells and embryonic stem cells”. In: *The Journal of neuroscience : the official journal of the Society for Neuroscience* 16.3 (Feb. 1996), pp. 1056–1065. ISSN: 0270-6474. DOI: `10.1523/JNEUROSCI.16-03-01056.1996`. URL: `https://pubmed.ncbi.nlm.nih.gov/8558234/%20https://pubmed.ncbi.nlm.nih.gov/8558234/?dopt=Abstract`.

[55] Li-Ying Wu et al. “The Role of Hypoxia in the Differentiation of P19 Embryonal Carcinoma Cells into Dopaminergic Neurons”. In: *Neurochemical Research 2008 33:10* 33.10 (May 2008), pp. 2118–2125. ISSN: 1573-6903. DOI: `10.1007/S11064-008-9728-3`. URL: `https://link.springer.com/article/10.1007/s11064-008-9728-3`.

[56] P. A. MacPherson et al. “P19 cells differentiate into glutamatergic and glutamate-responsive neurons in vitro”. In: *Neuroscience* 80.2 (July 1997), pp. 487–499. ISSN: 0306-4522. DOI: `10.1016/S0306-4522(97)00102-4`. URL: `https://pubmed.ncbi.nlm.nih.gov/9284351/`.

[57] Anna C. Svensson et al. “Expression of functional CB1 cannabinoid receptors in retinoic acid-differentiated P19 embryonal carcinoma cells”. In: *Journal of neuroscience research* 83.6 (May 2006), pp. 1128–1140. ISSN: 0360-4012. DOI: `10.1002/JNR.20792`. URL: `https://pubmed.ncbi.nlm.nih.gov/16477621/%20https://pubmed.ncbi.nlm.nih.gov/16477621/?dopt=Abstract`.

[58] David S.K. Magnuson et al. “In vivo electrophysiological maturation of neurons derived from a multipotent precursor (embryonal carcinoma) cell line”. In: *Brain research. Developmental brain research* 84.1 (Jan. 1995), pp. 130–141. ISSN: 0165-3806. DOI: `10.1016/0165-3806(94)00166-W`. URL: `https://pubmed.ncbi.nlm.nih.gov/7720212/%20https://pubmed.ncbi.nlm.nih.gov/7720212/?dopt=Abstract`.

[59] Hirotada Akiyama et al. “Implication of Trip15/CSN2 in early stage of neuronal differentiation of P19 embryonal carcinoma cells”. In: *Brain research. Developmental brain research* 140.1 (Jan. 2003), pp. 45–56. ISSN: 0165-3806. DOI: `10.1016/S0165-3806(02)00574-6`. URL: `https://pubmed.ncbi.nlm.nih.gov/12524175/%20https://pubmed.ncbi.nlm.nih.gov/12524175/?dopt=Abstract`.

[60] Raphaël Rouget et al. “Characterization of the survival motor neuron (SMN) promoter provides evidence for complex combinatorial regulation in undifferentiated and differentiated P19 cells”. In: *Biochemical Journal* 385.2 (Jan. 2005), pp. 433–443. ISSN: 0264-6021. DOI: `10.1042/BJ20041024`. URL: `/biochemj/article/385/2/433/41732/Characterization-of-the-survival-motor-neuron-SMN`.

[61] Yosuke Tanaka et al. “Chronological expression of microtubule-associated proteins (MAPs) in EC cell P19 after neuronal induction by retinoic acid”. In: *Brain Research* 596.1-2 (Nov. 1992), pp. 269–278. ISSN: 0006-8993. DOI: `10.1016/0006-8993(92)91557-U`.

[62] David S.K. Magnuson et al. “Neurons derived from P19 embryonal carcinoma cells develop responses to excitatory and inhibitory neurotransmitters”. In: *Brain research. Developmental brain research* 90.1-2 (Dec. 1995), pp. 141–150. ISSN: 0165-3806. DOI: `10.1016/0165-3806(96)83494-8`. URL: `https://pubmed.ncbi.nlm.nih.gov/8719337/`.

[63] Dina Popova, Jessica Karlsson, and Stig O.P. Jacobsson. “Comparison of neurons derived from mouse P19, rat PC12 and human SH-SY5Y cells in the assessment of chemical- and toxin-induced neurotoxicity”. In: *BMC Pharmacology and Toxicology* 18.1 (June 2017), pp. 1–11. ISSN: 20506511. DOI: `10.1186/S40360-017-0151-8/FIGURES/5`. URL: `https://link.springer.com/articles/10.1186/s40360-017-0151-8%20https://link.springer.com/article/10.1186/s40360-017-0151-8`.

[64] Robert L. Perlman. “Mouse models of human disease: An evolutionary perspective”. In: *Evolution, Medicine, and Public Health* 2016.1 (Apr. 2016), p. 170. ISSN: 2050-6201. DOI: `10.1093/EMPH/EOW014`. URL: `/pmc/articles/PMC4875775/%20/pmc/articles/PMC4875775/?report=abstract%20https://www.ncbi.nlm.nih.gov/pmc/articles/PMC4875775/`.

[65] Aaron C Ericsson et al. “A Brief History of Animal Modeling”. In: *Missouri Medicine* 110.3 (2013), p. 201. ISSN: 00266620. URL: `https://www.ncbi.nlm.nih.gov/pmc/articles/PMC3979591/`.

[66] S. Blair Hedges. “The origin and evolution of model organisms”. In: *Nature Reviews Genetics 2002 3:11* 3.11 (Nov. 2002), pp. 838–849. ISSN: 1471-0064. DOI: `10.1038/nrg929`. URL: `https://www.nature.com/articles/nrg929`.

[67] E. O. Wiley and Bruce S. Lieberman. “Phylogenetics: Theory and Practice of Phylogenetic Systematics: Second Edition”. In: *Phylogenetics: Theory and Practice of Phylogenetic Systematics: Second Edition* (Apr. 2011). DOI: `10.1002/9781118017883`. URL: `https://onlinelibrary.wiley.com/doi/book/10.1002/9781118017883`.

[68] Gastone G. Celesia. “Alcmaeon of Croton’s observations on health, brain, mind, and soul”. In: *Journal of the history of the neurosciences* 21.4 (Oct. 2012), pp. 409–426. ISSN: 1744-5213. DOI: `10.1080/0964704X.2011.626265`. URL: `https://pubmed.ncbi.nlm.nih.gov/22947382/`.

[69] Andreas Keller. “Drosophila melanogaster’s history as a human commensal”. In: *Current Biology* 17.3 (Feb. 2007), R77–R81. ISSN: 0960-9822. DOI: `10.1016/J.CUB.2006.12.031`.

[70] Nicholas S. Tolwinski. “Introduction: Drosophila—A Model System for Developmental Biology”. In: *Journal of Developmental Biology* 5.3 (Sept. 2017). ISSN: 22213759. DOI: `10.3390/JDB5030009`. URL: `/pmc/articles/PMC5831767/%20https://www.ncbi.nlm.nih.gov/pmc/articles/PMC5831767/`.

[71] Vittoria Mariano et al. “Modelling Learning and Memory in Drosophila to Understand Intellectual Disabilities”. In: *Neuroscience* 445 (Oct. 2020), pp. 12–30. ISSN: 1873-7544. DOI: `10.1016/J.NEUROSCIENCE.2020.07.034`. URL: `https://pubmed.ncbi.nlm.nih.gov/32730949/`.

[72] Margret H. Bülow, Brendon D. Parsons, and Francesca Di Cara. “The Drosophila melanogaster as Genetic Model System to Dissect the Mechanisms of Disease that Lead to Neurodegeneration in Adrenoleukodystrophy”. In: *Advances in experimental medicine and biology* 1299 (2020), pp. 145–159. ISSN: 0065-2598. DOI: `10.1007/978-3-030-60204-8{\_}11`. URL: `https://pubmed.ncbi.nlm.nih.gov/33417213/`.

[73] Zhasmine Mirzoyan et al. “Drosophila melanogaster: A model organism to study cancer”. In: *Frontiers in Genetics* 10 (2019), p. 51. ISSN: 16648021. DOI: `10.3389/FGENE.2019.00051/BIBTEX`.

[74] Karen C.M. Moraes and Jacques Montagne. “Drosophila melanogaster: A Powerful Tiny Animal Model for the Study of Metabolic Hepatic Diseases”. In: *Frontiers in Physiology* 12 (Sept. 2021), p. 1577. ISSN: 1664042X. DOI: `10.3389/FPHYS.2021.728407/BIBTEX`.

[75] Volker Hartenstein. “The neuroendocrine system of invertebrates: a developmental and evolutionary perspective”. In: *The Journal of endocrinology* 190.3 (Sept. 2006), pp. 555–570. ISSN: 0022-0795. DOI: `10.1677/JOE.1.06964`. URL: `https://pubmed.ncbi.nlm.nih.gov/17003257/%20https://pubmed.ncbi.nlm.nih.gov/17003257/?dopt=Abstract`.

TU Bibliothek WIEN Your knowledge hub
Die approbierte gedruckte Originalversion dieser Diplomarbeit ist an der TU Wien Bibliothek verfügbar
The approved original version of this thesis is available in print at TU Wien Bibliothek.

[76] Aniket V. Gore et al. “The zebrafish: A fintastic model for hematopoietic development and disease”. In: *Wiley interdisciplinary reviews. Developmental biology* 7.3 (May 2018). ISSN: 1759-7692. DOI: `10.1002/WDEV.312`. URL: `https://pubmed.ncbi.nlm.nih.gov/29436122/`.

[77] Björn Busse et al. “Zebrafish: An Emerging Model for Orthopedic Research”. In: *Journal of orthopaedic research : official publication of the Orthopaedic Research Society* 38.5 (May 2020), pp. 925–936. ISSN: 1554-527X. DOI: `10.1002/JOR.24539`. URL: `https://pubmed.ncbi.nlm.nih.gov/31773769/`.

[78] Marta D’Amora and Silvia Giordani. “The utility of zebrafish as a model for screening developmental neurotoxicity”. In: *Frontiers in Neuroscience* 12 (Dec. 2018), p. 976. ISSN: 1662453X. DOI: `10.3389/FNINS.2018.00976/BIBTEX`.

[79] Geoff Spencer. *Background on Mouse as a Model Organism*. May 2012. URL: `https://www.genome.gov/10005834/background-on-mouse-as-a-model-organism`.

[80] Guido Hermey. “Transgene Tiermodelle”. In: *Der Experimentator: Neurowissenschaften* (2010), pp. 157–177. DOI: `10.1007/978-3-8274-2369-6{\_}8`. URL: `https://link.springer.com/chapter/10.1007/978-3-8274-2369-6_8`.

[81] Michel A. Duchosal et al. “Transfer of human systemic lupus erythematosus in severe combined immunodeficient (SCID) mice”. In: *The Journal of experimental medicine* 172.3 (Sept. 1990), pp. 985–988. ISSN: 0022-1007. DOI: `10.1084/JEM.172.3.985`. URL: `https://pubmed.ncbi.nlm.nih.gov/2388039/`.

[82] Amos Gilhar et al. “Autoimmune hair loss (alopecia areata) transferred by T lymphocytes to human scalp explants on SCID mice.” In: *The Journal of Clinical Investigation* 101.1 (Jan. 1998), pp. 62–67. ISSN: 0021-9738. DOI: `10.1172/JCI551`. URL: `http://www.jci.org`.

[83] Xinhua Yu, Qiaoniang Huang, and Frank Petersen. “History and milestones of mouse models of autoimmune diseases”. In: *Current pharmaceutical design* 21.18 (May 2015), pp. 2308–2319. ISSN: 1873-4286. DOI: `10.2174/1381612821666150316115412`. URL: `https://pubmed.ncbi.nlm.nih.gov/25777764/`.

[84] Markel Olabarria et al. “Concomitant astroglial atrophy and astrogliosis in a triple transgenic animal model of Alzheimer’s disease”. In: *Glia* 58.7 (May 2010), pp. 831–838. ISSN: 1098-1136. DOI: `10.1002/GLIA.20967`. URL: `https://onlinelibrary.wiley.com/doi/full/10.1002/glia.20967%20https://onlinelibrary.wiley.com/doi/abs/10.1002/glia.20967%20https://onlinelibrary.wiley.com/doi/10.1002/glia.20967`.

[85] Elmira Anderzhanova, Thomas Kirmeier, and Carsten T. Wotjak. “Animal models in psychiatric research: The RDoC system as a new framework for endophenotype-oriented translational neuroscience”. In: *Neurobiology of Stress* 7 (Dec. 2017), pp. 47–56. ISSN: 2352-2895. DOI: `10.1016/J.YNSTR.2017.03.003`.

[86] Ted M. Dawson, Todd E. Golde, and Clotilde Lagier-Tourenne. “Animal models of neurodegenerative diseases”. In: *Nature Neuroscience 2018 21:10* 21.10 (Sept. 2018), pp. 1370–1379. ISSN: 1546-1726. DOI: `10.1038/s41593-018-0236-8`. URL: `https://www.nature.com/articles/s41593-018-0236-8`.

[87] Valerie C. Henderson et al. “Threats to validity in the design and conduct of preclinical efficacy studies: a systematic review of guidelines for in vivo animal experiments”. In: *PLoS medicine* 10.7 (July 2013). ISSN: 1549-1676. DOI: `10.1371/JOURNAL.PMED.1001489`. URL: `https://pubmed.ncbi.nlm.nih.gov/23935460/`.

[88] Rebecca G. Bagley. “Commentary on Folkman: “Tumor Angiogenesis Factor””. In: *Cancer Research* 76.7 (Apr. 2016), pp. 1673–1674. ISSN: 0008-5472. DOI: `10.1158/0008-5472.CAN-16-0675`. URL: `https://cancerres.aacrjournals.org/content/76/7/1673%20https://cancerres.aacrjournals.org/content/76/7/1673.abstract`.

TU Bibliothek WIEN Your knowledge hub
Die approbierte gedruckte Originalversion dieser Diplomarbeit ist an der TU Wien Bibliothek verfügbar
The approved original version of this thesis is available in print at TU Wien Bibliothek.

[89] Isabella W.Y. Mak, Nathan Evaniew, and Michelle Ghert. “Lost in translation: animal models and clinical trials in cancer treatment”. In: *American Journal of Translational Research* 6.2 (2014), p. 114. ISSN: 19438141. URL: `/pmc/articles/PMC3902221/%20/pmc/articles/PMC3902221/?report=abstract%20https://www.ncbi.nlm.nih.gov/pmc/articles/PMC3902221/`.

[90] Charis P. Segeritz and Ludovic Vallier. “Cell Culture: Growing Cells as Model Systems In Vitro”. In: *Basic Science Methods for Clinical Researchers* (Apr. 2017), p. 151. DOI: `10.1016/B978-0-12-803077-6.00009-6`. URL: `/pmc/articles/PMC7149418/%20/pmc/articles/PMC7149418/?report=abstract%20https://www.ncbi.nlm.nih.gov/pmc/articles/PMC7149418/`.

[91] Tomasz Kolenda et al. “State of the art paper 2D and 3D cell cultures-a comparison of different types of cancer cell cultures”. In: (2016). DOI: `10.5114/aoms.2016.63743`. URL: `https://doi.org/10.5114/aoms.2016.63743`.

[92] Michele A. Wozniak et al. “Focal adhesion regulation of cell behavior”. In: *Biochimica et biophysica acta* 1692.2-3 (July 2004), pp. 103–119. ISSN: 0006-3002. DOI: `10.1016/J.BBAMCR.2004.04.007`. URL: `https://pubmed.ncbi.nlm.nih.gov/15246682/`.

[93] Sudipa June Chatterjee, Ruba Halaoui, and Luke McCaffrey. “Apical–Basal Polarity as a Sensor for Epithelial Homeostasis: A Matter of Life and Death”. In: *Current Pathobiology Reports* 4.3 (Sept. 2016), pp. 99–106. ISSN: 2167485X. DOI: `10.1007/S40139-016-0107-5/FIGURES/1`. URL: `https://link.springer.com/article/10.1007/s40139-016-0107-5`.

[94] Brendon M. Baker and Christopher S. Chen. “Deconstructing the third dimension-how 3D culture microenvironments alter cellular cues”. In: *Journal of Cell Science* 125.13 (July 2012), pp. 3015–3024. ISSN: 00219533. DOI: `10.1242/JCS.079509/258092/AM/DECONSTRUCTING-THE-THIRD-DIMENSION-HOW-3D-CULTURE`.

[95] Claudia Fischbach et al. “Engineering tumors with 3D scaffolds”. In: *Nature methods* 4.10 (Oct. 2007), pp. 855–860. ISSN: 1548-7091. DOI: `10.1038/NMETH1085`. URL: `https://pubmed.ncbi.nlm.nih.gov/17767164/`.

[96] Francesco Pampaloni, Emmanuel G. Reynaud, and Ernst H.K. Stelzer. “The third dimension bridges the gap between cell culture and live tissue”. In: *Nature reviews. Molecular cell biology* 8.10 (Oct. 2007), pp. 839–845. ISSN: 1471-0080. DOI: `10.1038/NRM2236`. URL: `https://pubmed.ncbi.nlm.nih.gov/17684528/`.

[97] Klaus Von Der Mark et al. “Relationship between cell shape and type of collagen synthesised as chondrocytes lose their cartilage phenotype in culture”. In: *Nature 1977 267:5611* 267.5611 (1977), pp. 531–532. ISSN: 1476-4687. DOI: `10.1038/267531a0`. URL: `https://www.nature.com/articles/267531a0`.

[98] Gi Seok Jeong et al. “Networked neural spheroid by neuro-bundle mimicking nervous system created by topology effect”. In: *Molecular Brain* 8 (Mar. 2015). ISSN: 17566606. DOI: `10.1186/S13041-015-0109-Y`.

[99] Nicole Prior, Patricia Inacio, and Meritxell Huch. “Liver organoids: from basic research to therapeutic applications”. In: *Gut* 68.12 (Dec. 2019), pp. 2228–2237. ISSN: 0017-5749. DOI: `10.1136/GUTJNL-2019-319256`. URL: `https://gut.bmj.com/content/68/12/2228%20https://gut.bmj.com/content/68/12/2228.abstract`.

[100] Marta Kapałczyńska et al. “2D and 3D cell cultures - a comparison of different types of cancer cell cultures”. In: *Archives of medical science : AMS* 14.4 (2018), pp. 910–919. ISSN: 1734-1922. DOI: `10.5114/AOMS.2016.63743`. URL: `https://pubmed.ncbi.nlm.nih.gov/30002710/`.

Die approbierte gedruckte Originalversion dieser Diplomarbeit ist an der TU Wien Bibliothek verfügbar
The approved original version of this thesis is available in print at TU Wien Bibliothek.
TU WIEN Bibliothek Your knowledge hub

[101] Leoni A. Kunz-Schughart et al. “The use of 3-D cultures for high-throughput screening: The multicellular spheroid model”. In: *Journal of Biomolecular Screening* 9.4 (June 2004), pp. 273–285. ISSN: 10870571. DOI: `10.1177/1087057104265040`. URL: `https://journals.sagepub.com/doi/abs/10.1177/1087057104265040`.

[102] Zeynep Dereli-Korkut et al. “Three dimensional microfluidic cell arrays for ex vivo drug screening with mimicked vascular flow”. In: *Analytical Chemistry* 86.6 (Mar. 2014), pp. 2997–3004. ISSN: 15206882. DOI: `10.1021/AC403899J/SUPPL{\_}FILE/AC403899J{\_}SI{\_}002.PDF`. URL: `https://pubs.acs.org/doi/abs/10.1021/ac403899j`.

[103] Chia Hsun Hsieh et al. “The effect of primary cancer cell culture models on the results of drug chemosensitivity assays: The application of perfusion microbioreactor system as cell culture vessel”. In: *BioMed Research International* 2015 (Jan. 2015). ISSN: 23146141. DOI: `10.1155/2015/470283`. URL: `https://www.hindawi.com/journals/bmri/2015/470283/`.

[104] Benedikt W. Graf and Stephen A. Boppart. “Imaging and analysis of three-dimensional cell culture models.” In: *Methods in molecular biology (Clifton, N.J.)* 591 (2010), pp. 211–227. ISSN: 19406029. DOI: `10.1007/978-1-60761-404-3{\_}13/COVER`. URL: `https://link.springer.com/protocol/10.1007/978-1-60761-404-3_13`.

[105] Joshua M. Brickman and Palle Serup. “Properties of embryoid bodies”. In: *Wiley Interdisciplinary Reviews: Developmental Biology* 6.2 (Mar. 2017), e259. ISSN: 1759-7692. DOI: `10.1002/WDEV.259`. URL: `https://onlinelibrary.wiley.com/doi/full/10.1002/wdev.259%20https://onlinelibrary.wiley.com/doi/abs/10.1002/wdev.259%20https://wires.onlinelibrary.wiley.com/doi/10.1002/wdev.259`.

[106] Qi Long Ying et al. “Conversion of embryonic stem cells into neuroectodermal precursors in adherent monoculture”. In: *Nature Biotechnology 2003 21:2* 21.2 (Jan. 2003), pp. 183–186. ISSN: 1546-1696. DOI: `10.1038/nbt780`. URL: `https://www.nature.com/articles/nbt780`.

[107] Ruei Zhen Lin and Hwan You Chang. “Recent advances in three-dimensional multicellular spheroid culture for biomedical research”. In: *Biotechnology journal* 3.9-10 (2008), pp. 1172–1184. ISSN: 1860-7314. DOI: `10.1002/BIOT.200700228`. URL: `https://pubmed.ncbi.nlm.nih.gov/18566957/`.

[108] Ruei Zeng Lin et al. “Dynamic analysis of hepatoma spheroid formation: Roles of E-cadherin and β1-integrin”. In: *Cell and Tissue Research* 324.3 (June 2006), pp. 411–422. ISSN: 0302766X. DOI: `10.1007/S00441-005-0148-2/FIGURES/8`. URL: `https://link.springer.com/article/10.1007/s00441-005-0148-2`.

[109] Gwon Soo Jung et al. “Morphogenetic and neuronal characterization of human neuroblastoma multicellular spheroids cultured under undifferentiated and all-trans-retinoic acid-differentiated conditions”. In: *BMB Reports* 46.5 (2013), p. 276. ISSN: 19766696. DOI: `10.5483/BMBREP.2013.46.5.196`. URL: `/pmc/articles/PMC4133894/%20/pmc/articles/PMC4133894/?report=abstract%20https://www.ncbi.nlm.nih.gov/pmc/articles/PMC4133894/`.

[110] John M. Yuhas et al. “A Simplified Method for Production and Growth of Multicellular Tumor Spheroids”. In: *Cancer Research* 37.10 (1977).

[111] Jin Zhou et al. “Embryoid bodies formation and differentiation from mouse embryonic stem cells in collagen/Matrigel scaffolds”. In: *Journal of Genetics and Genomics* 37.7 (July 2010), pp. 451–460. ISSN: 1673-8527. DOI: `10.1016/S1673-8527(09)60064-3`.

[112] Liz Y. Wu, Dino Di Carlo, and Luke P. Lee. “Microfluidic self-assembly of tumor spheroids for anticancer drug discovery”. In: *Biomedical Microdevices* 10.2 (Apr. 2008), pp. 197–202. ISSN: 13872176. DOI: `10.1007/s10544-007-9125-8`.

TU WIEN Bibliothek Your knowledge hub
Die approbierte gedruckte Originalversion dieser Diplomarbeit ist an der TU Wien Bibliothek verfügbar
The approved original version of this thesis is available in print at TU Wien Bibliothek.

[113] Scott L. Nyberg et al. “Rapid, large-scale formation of porcine hepatocyte spheroids in a novel spheroid reservoir bioartificial liver”. In: *Liver Transplantation* 11.8 (Aug. 2005), pp. 901–910. ISSN: 1527-6473. DOI: `10.1002/LT.20446`. URL: `https://onlinelibrary.wiley.com/doi/full/10.1002/lt.20446%20https://onlinelibrary.wiley.com/doi/abs/10.1002/lt.20446%20https://aasldpubs.onlinelibrary.wiley.com/doi/10.1002/lt.20446`.

[114] Valerie M. Weaver et al. “β4 integrin-dependent formation of polarized three-dimensional architecture confers resistance to apoptosis in normal and malignant mammary epithelium”. In: *Cancer Cell* 2.3 (Sept. 2002), pp. 205–216. ISSN: 1535-6108. DOI: `10.1016/S1535-6108(02)00125-3`.

[115] Bin Kim Jong. “Three-dimensional tissue culture models in cancer biology”. In: *Seminars in Cancer Biology* 15.5 (Oct. 2005), pp. 365–377. ISSN: 1044-579X. DOI: `10.1016/J.SEMCANCER.2005.05.002`.

[116] Maria Wartenberg et al. “Tumor-induced angiogenesis studied in confrontation cultures of multicellular tumor spheroids and embryoid bodies grown from pluripotent embryonic stem cells”. In: *The FASEB Journal* 15.6 (Apr. 2001), pp. 995–1005. ISSN: 1530-6860. DOI: `10.1096/FSB2FJ000350COM`. URL: `https://onlinelibrary.wiley.com/doi/full/10.1096/fsb2fj000350com%20https://onlinelibrary.wiley.com/doi/abs/10.1096/fsb2fj000350com%20https://faseb.onlinelibrary.wiley.com/doi/10.1096/fsb2fj000350com`.

[117] Patricio Godoy et al. “Recent advances in 2D and 3D in vitro systems using primary hepatocytes, alternative hepatocyte sources and non-parenchymal liver cells and their use in investigating mechanisms of hepatotoxicity, cell signaling and ADME”. In: *Archives of Toxicology* 87.8 (Aug. 2013), p. 1315. ISSN: 03405761. DOI: `10.1007/S00204-013-1078-5`. URL: `/pmc/articles/PMC3753504/%20/pmc/articles/PMC3753504/?report=abstract%20https://www.ncbi.nlm.nih.gov/pmc/articles/PMC3753504/`.

[118] Achilles A. Demetriou et al. “Prospective, Randomized, Multicenter, Controlled Trial of a Bioartificial Liver in Treating Acute Liver Failure”. In: *Annals of Surgery* 239.5 (May 2004), p. 660. ISSN: 00034932. DOI: `10.1097/01.SLA.0000124298.74199.E5`. URL: `/pmc/articles/PMC1356274/%20/pmc/articles/PMC1356274/?report=abstract%20https://www.ncbi.nlm.nih.gov/pmc/articles/PMC1356274/`.

[119] Gail R. Martin and Martin J. Evans. “The morphology and growth of a pluripotent teratocarcinoma cell line and its derivatives in tissue culture”. In: *Cell* 2.3 (July 1974), pp. 163–172. ISSN: 0092-8674. DOI: `10.1016/0092-8674(74)90090-7`.

[120] Stephen M. Dang et al. “Controlled, Scalable Embryonic Stem Cell Differentiation Culture”. In: *STEM CELLS* 22.3 (May 2004), pp. 275–282. ISSN: 1549-4918. DOI: `10.1634/STEMCELLS.22-3-275`. URL: `https://onlinelibrary.wiley.com/doi/full/10.1634/stemcells.22-3-275%20https://onlinelibrary.wiley.com/doi/abs/10.1634/stemcells.22-3-275%20https://stemcellsjournals.onlinelibrary.wiley.com/doi/10.1634/stemcells.22-3-275`.

[121] Steven C Petrovic and Rani H Hammericksen. “Determination of Ferrocene Solubility by Normalized Chronoamperometry: An Evaluation of Experimental Constraints”. In: *Electroanalysis* (2002), pp. 599–604. DOI: `10.1002/1521-4109`.

[122] Guoqing Hu and Dongqing Li. “Three-dimensional modeling of transport of nutrients for multicellular tumor spheroid culture in a microchannel”. In: *Biomedical Microdevices* 9.3 (June 2007), pp. 315–323. ISSN: 13872176. DOI: `10.1007/S10544-006-9035-1/FIGURES/6`. URL: `https://link.springer.com/article/10.1007/s10544-006-9035-1`.

[123] W. Mueller-Klieser. “Method for the determination of oxygen consumption rates and diffusion coefficients in multicellular spheroids”. In: *Biophysical Journal* 46.3 (Sept. 1984), pp. 343–348. ISSN: 0006-3495. DOI: `10.1016/S0006-3495(84)84030-8`.

Die approbierte gedruckte Originalversion dieser Diplomarbeit ist an der TU Wien Bibliothek verfügbar
The approved original version of this thesis is available in print at TU Wien Bibliothek.
TU WIEN Bibliothek Your knowledge hub

[124] Efrem Curcio et al. “Mass transfer and metabolic reactions in hepatocyte spheroids cultured in rotating wall gas-permeable membrane system”. In: *Biomaterials* 28.36 (Dec. 2007), pp. 5487–5497. ISSN: 0142-9612. DOI: `10.1016/J.BIOMATERIALS.2007.08.033`.

[125] Jose Alvarez-Pérez, Paloma Ballesteros, and Sebastián Cerdán. “Microscopic images of intraspheroidal pH by 1H magnetic resonance chemical shift imaging of pH sensitive indicators”. In: *Magnetic Resonance Materials in Physics, Biology and Medicine* 18.6 (Dec. 2005), pp. 293–301. ISSN: 09685243. DOI: `10.1007/s10334-005-0013-z`.

[126] Wenjie Wang et al. “3D spheroid culture system on micropatterned substrates for improved differentiation efficiency of multipotent mesenchymal stem cells”. In: *Biomaterials* 30.14 (May 2009), pp. 2705–2715. ISSN: 01429612. DOI: `10.1016/j.biomaterials.2009.01.030`. URL: `https://linkinghub.elsevier.com/retrieve/pii/S0142961209000519`.

[127] Filip Laco et al. “Unraveling the Inconsistencies of Cardiac Differentiation Efficiency Induced by the GSK3β Inhibitor CHIR99021 in Human Pluripotent Stem Cells”. In: *Stem Cell Reports* 10.6 (June 2018), pp. 1851–1866. ISSN: 22136711. DOI: `10.1016/j.stemcr.2018.03.023`. URL: `https://linkinghub.elsevier.com/retrieve/pii/S2213671118301504`.

[128] Hiroshi Kitani et al. “Efficiency of neural differentiation of mouse P19 embryonal carcinoma cells is dependent on the seeding density”. In: *Cell Transplantation* 6.5 (Sept. 1997), pp. 521–525. ISSN: 0963-6897. DOI: `10.1016/S0963-6897(97)00071-7`.

[129] Dorit Parnas and Michal Linial. “Acceleration of neuronal maturation of P19 cells by increasing culture density”. In: *Developmental Brain Research* 101.1-2 (July 1997), pp. 115–124. ISSN: 0165-3806. DOI: `10.1016/S0165-3806(97)00057-6`.

[130] Matthias Löhle et al. “Differentiation Efficiency of Induced Pluripotent Stem Cells Depends on the Number of Reprogramming Factors”. In: *STEM CELLS* 30.3 (Mar. 2012), pp. 570–579. ISSN: 1549-4918. DOI: `10.1002/STEM.1016`. URL: `https://onlinelibrary.wiley.com/doi/full/10.1002/stem.1016%20https://onlinelibrary.wiley.com/doi/abs/10.1002/stem.1016%20https://stemcellsjournals.onlinelibrary.wiley.com/doi/10.1002/stem.1016`.

[131] Fuad Gandhi Torizal et al. “Size-dependent hepatic differentiation of human induced pluripotent stem cells spheroid in suspension culture”. In: *Regenerative Therapy* 12 (Dec. 2019), pp. 66–73. ISSN: 2352-3204. DOI: `10.1016/J.RETH.2019.04.011`.

[132] Bing Song et al. “Improved Hematopoietic Differentiation Efficiency of Gene-Corrected Beta-Thalassemia Induced Pluripotent Stem Cells by CRISPR/Cas9 System”. In: *https://home.liebertpub.com/scd* 24.9 (Dec. 2014), pp. 1053–1065. ISSN: 15578534. DOI: `10.1089/SCD.2014.0347`. URL: `https://www.liebertpub.com/doi/abs/10.1089/scd.2014.0347`.

[133] Jaimeson Veldhuizen et al. “Engineering anisotropic human stem cell-derived three-dimensional cardiac tissue on-a-chip”. In: *Biomaterials* 256 (Oct. 2020), p. 120195. ISSN: 0142-9612. DOI: `10.1016/J.BIOMATERIALS.2020.120195`.

[134] Jesus Shrestha et al. “Lung-on-a-chip: the future of respiratory disease models and pharmacological studies”. In: *Critical reviews in biotechnology* 40.2 (Feb. 2020), pp. 213–230. ISSN: 1549-7801. DOI: `10.1080/07388551.2019.1710458`. URL: `https://pubmed.ncbi.nlm.nih.gov/31906727/`.

[135] Aleksander Skardal et al. “Multi-tissue interactions in an integrated three-tissue organ-on-a-chip platform”. In: *Scientific Reports 2017 7:1* 7.1 (Aug. 2017), pp. 1–16. ISSN: 2045-2322. DOI: `10.1038/s41598-017-08879-x`. URL: `https://www.nature.com/articles/s41598-017-08879-x`.

[136] Aung K. Soe, Saeid Nahavandi, and Khashayar Khoshmanesh. “Neuroscience goes on a chip”. In: *Biosensors and Bioelectronics* 35.1 (May 2012), pp. 1–13. ISSN: 0956-5663. DOI: `10.1016/J.BIOS.2012.02.012`.

Die approbierte gedruckte Originalversion dieser Diplomarbeit ist an der TU Wien Bibliothek verfügbar
The approved original version of this thesis is available in print at TU Wien Bibliothek.

[137] Todd M. Squires and Stephen R. Quake. “Microfluidics: Fluid physics at the nanoliter scale”. In: *Reviews of Modern Physics* 77.3 (July 2005), pp. 977–1026. ISSN: 00346861. DOI: `10.1103/REVMODPHYS.77.977/FIGURES/47/MEDIUM`. URL: `https://journals.aps.org/rmp/abstract/10.1103/RevModPhys.77.977`.

[138] Justin Bobo et al. “3D In Vitro Neuron on a Chip for Probing Calcium Mechanostimulation”. In: *Advanced Biosystems* 4.10 (Oct. 2020), p. 2000080. ISSN: 2366-7478. DOI: `10.1002/ADBI.202000080`. URL: `https://onlinelibrary.wiley.com/doi/full/10.1002/adbi.202000080%20https://onlinelibrary.wiley.com/doi/abs/10.1002/adbi.202000080%20https://onlinelibrary.wiley.com/doi/10.1002/adbi.202000080`.

[139] Stefania Torino et al. “PDMS-Based Microfluidic Devices for Cell Culture”. In: *Inventions 2018, Vol. 3, Page 65* 3.3 (Sept. 2018), p. 65. DOI: `10.3390/INVENTIONS3030065`. URL: `https://www.mdpi.com/2411-5134/3/3/65/htm%20https://www.mdpi.com/2411-5134/3/3/65`.

[140] Yu Huang, Justin C. Williams, and Stephen M. Johnson. “Brain slice on a chip: opportunities and challenges of applying microfluidic technology to intact tissues”. In: *Lab on a Chip* 12.12 (May 2012), pp. 2103–2117. ISSN: 14730189. DOI: `10.1039/C2LC21142D`. URL: `https://pubs.rsc.org/en/content/articlehtml/2012/lc/c2lc21142d%20https://pubs.rsc.org/en/content/articlelanding/2012/lc/c2lc21142d`.

[141] Pamela G. Gross et al. “Applications of microfluidics for neuronal studies”. In: *Journal of the Neurological Sciences* 252.2 (Jan. 2007), pp. 135–143. ISSN: 0022-510X. DOI: `10.1016/J.JNS.2006.11.009`.

[142] Thomas M. Pearce and Justin C. Williams. “Microtechnology: Meet neurobiology”. In: *Lab on a Chip* 7.1 (Dec. 2006), pp. 30–40. ISSN: 1473-0189. DOI: `10.1039/B612856B`. URL: `https://pubs.rsc.org/en/content/articlehtml/2007/lc/b612856b%20https://pubs.rsc.org/en/content/articlelanding/2007/lc/b612856b`.

[143] Rosanne van de Wijdeven et al. “A novel lab-on-chip platform enabling axotomy and neuromodulation in a multi-nodal network”. In: *Biosensors & bioelectronics* 140 (Sept. 2019). ISSN: 1873-4235. DOI: `10.1016/J.BIOS.2019.111329`. URL: `https://pubmed.ncbi.nlm.nih.gov/31163396/`.

[144] Shawn Mikula, Jonas Binding, and Winfried Denk. “Staining and embedding the whole mouse brain for electron microscopy”. In: *Nature Methods 2012 9:12* 9.12 (Oct. 2012), pp. 1198–1201. ISSN: 1548-7105. DOI: `10.1038/nmeth.2213`. URL: `https://www.nature.com/articles/nmeth.2213`.

[145] Johannes Niediek et al. “Reliable Analysis of Single-Unit Recordings from the Human Brain under Noisy Conditions: Tracking Neurons over Hours”. In: *PLOS ONE* 11.12 (Dec. 2016), e0166598. ISSN: 1932-6203. DOI: `10.1371/JOURNAL.PONE.0166598`. URL: `https://journals.plos.org/plosone/article?id=10.1371/journal.pone.0166598`.

[146] Gaute T. Einevoll et al. “Towards reliable spike-train recordings from thousands of neurons with multielectrodes”. In: *Current Opinion in Neurobiology* 22.1 (Feb. 2012), pp. 11–17. ISSN: 0959-4388. DOI: `10.1016/J.CONB.2011.10.001`.

[147] György Buzsáki, Costas A. Anastassiou, and Christof Koch. “The origin of extracellular fields and currents — EEG, ECoG, LFP and spikes”. In: *Nature Reviews Neuroscience 2012 13:6* 13.6 (May 2012), pp. 407–420. ISSN: 1471-0048. DOI: `10.1038/nrn3241`. URL: `https://www.nature.com/articles/nrn3241`.

[148] Raha M. Dastgheyb, Seung Wan Yoo, and Norman J. Haughey. “MEAnalyzer – a Spike Train Analysis Tool for Multi Electrode Arrays”. In: *Neuroinformatics* 18.1 (Jan. 2020), pp. 163–179. ISSN: 15590089. DOI: `10.1007/S12021-019-09431-0/FIGURES/7`. URL: `https://link.springer.com/article/10.1007/s12021-019-09431-0`.

Die approbierte gedruckte Originalversion dieser Diplomarbeit ist an der TU Wien Bibliothek verfügbar
The approved original version of this thesis is available in print at TU Wien Bibliothek.
TU WIEN Bibliothek Your knowledge hub

[149] Makoto. Taketani and M. Baudry. *Advances in network electrophysiology : using multi-electrode arrays*. Springer, 2006. ISBN: 978-0-387-25857-7. URL: `https://link.springer.com/book/10.1007/b136263`.

[150] Peter B. Allen et al. “Single-synapse ablation and long-term imaging in live C. elegans”. In: *Journal of Neuroscience Methods* 173.1 (Aug. 2008), pp. 20–26. ISSN: 0165-0270. DOI: `10.1016/J.JNEUMETH.2008.05.007`.

[151] Christophe Py et al. “A novel silicon patch-clamp chip permits high-fidelity recording of ion channel activity from functionally defined neurons”. In: *Biotechnology and Bioengineering* 107.4 (Nov. 2010), pp. 593–600. ISSN: 1097-0290. DOI: `10.1002/BIT.22834`. URL: `https://onlinelibrary.wiley.com/doi/full/10.1002/bit.22834%20https://onlinelibrary.wiley.com/doi/abs/10.1002/bit.22834%20https://onlinelibrary.wiley.com/doi/10.1002/bit.22834`.

[152] Heather A. Enright et al. “Functional and transcriptional characterization of complex neuronal co-cultures”. In: *Scientific Reports 2020 10:1* 10.1 (July 2020), pp. 1–14. ISSN: 2045-2322. DOI: `10.1038/s41598-020-67691-2`. URL: `https://www.nature.com/articles/s41598-020-67691-2`.

[153] Geon Hui Lee et al. “Bottom-Up Engineering of Well-Defined 3D Microtissues Using Microplatforms and Biomedical Applications”. In: *Advanced Healthcare Materials* 5.1 (Jan. 2016), pp. 56–74. ISSN: 2192-2659. DOI: `10.1002/ADHM.201500107`. URL: `https://onlinelibrary.wiley.com/doi/full/10.1002/adhm.201500107%20https://onlinelibrary.wiley.com/doi/abs/10.1002/adhm.201500107%20https://onlinelibrary.wiley.com/doi/10.1002/adhm.201500107`.

[154] Jisoo Park et al. “Three-dimensional brain-on-a-chip with an interstitial level of flow and its application as an in vitro model of Alzheimer’s disease”. In: *Lab on a Chip* 15.1 (Dec. 2014), pp. 141–150. ISSN: 14730189. DOI: `10.1039/C4LC00962B`. URL: `https://pubs.rsc.org/en/content/articlehtml/2015/lc/c4lc00962b%20https://pubs.rsc.org/en/content/articlelanding/2015/lc/c4lc00962b`.

[155] Siran Wang et al. “In vitro 3D corneal tissue model with epithelium, stroma, and innervation”. In: *Biomaterials* 112 (Jan. 2017), pp. 1–9. ISSN: 0142-9612. DOI: `10.1016/J.BIOMATERIALS.2016.09.030`.

[156] Xiaochuan Dai et al. “Three-dimensional mapping and regulation of action potential propagation in nanoelectronics-innervated tissues”. In: *Nature Nanotechnology 2016 11:9* 11.9 (June 2016), pp. 776–782. ISSN: 1748-3395. DOI: `10.1038/nnano.2016.96`. URL: `https://www.nature.com/articles/nnano.2016.96`.

[157] Midori Kato-Negishi et al. “A neurospheroid network-stamping method for neural transplantation to the brain”. In: *Biomaterials* 31.34 (Dec. 2010), pp. 8939–8945. ISSN: 0142-9612. DOI: `10.1016/J.BIOMATERIALS.2010.08.008`.

[158] Sahba Mobini et al. “Advances in ex vivo models and lab-on-a-chip devices for neural tissue engineering”. In: *Biomaterials* 198 (Apr. 2019), pp. 146–166. ISSN: 0142-9612. DOI: `10.1016/J.BIOMATERIALS.2018.05.012`.

[159] Wei Zhou et al. “Ultrasound neuro-modulation chip: activation of sensory neurons in Caenorhabditis elegans by surface acoustic waves”. In: *Lab on a Chip* 17.10 (May 2017), pp. 1725–1731. ISSN: 14730189. DOI: `10.1039/C7LC00163K`. URL: `https://pubs.rsc.org/en/content/articlehtml/2017/lc/c7lc00163k%20https://pubs.rsc.org/en/content/articlelanding/2017/lc/c7lc00163k`.

[160] Rosanne van de Wijdeven et al. “Structuring a multi-nodal neural network in vitro within a novel design microfluidic chip”. In: *Biomedical microdevices* 20.1 (Mar. 2018). ISSN: 1572-8781. DOI: `10.1007/S10544-017-0254-4`. URL: `https://pubmed.ncbi.nlm.nih.gov/29294210/`.

TU WIEN Bibliothek Your knowledge hub
Die approbierte gedruckte Originalversion dieser Diplomarbeit ist an der TU Wien Bibliothek verfügbar
The approved original version of this thesis is available in print at TU Wien Bibliothek.

[161] Olaf Sporns. “The human connectome: a complex network”. In: *Annals of the New York Academy of Sciences* 1224.1 (Apr. 2011), pp. 109–125. ISSN: 1749-6632. DOI: 10.1111/J.1749-6632.2010.05888.X. URL: https://onlinelibrary.wiley.com/doi/full/10.1111/j.1749-6632.2010.05888.x%20https://onlinelibrary.wiley.com/doi/abs/10.1111/j.1749-6632.2010.05888.x%20https://nyaspubs.onlinelibrary.wiley.com/doi/10.1111/j.1749-6632.2010.05888.x.

[162] Hongjun Song et al. “A microfluidic impedance flow cytometer for identification of differentiation state of stem cells”. In: *Lab on a Chip* 13.12 (May 2013), pp. 2300–2310. ISSN: 14730189. DOI: 10.1039/C3LC41321G. URL: https://pubs.rsc.org/en/content/articlehtml/2013/lc/c3lc41321g%20https://pubs.rsc.org/en/content/articlelanding/2013/lc/c3lc41321g.

[163] Choong Kim et al. “3-Dimensional cell culture for on-chip differentiation of stem cells in embryoid body”. In: *Lab on a Chip* 11.5 (Mar. 2011), pp. 874–882. ISSN: 14730189. DOI: 10.1039/C0LC00516A. URL: https://pubs.rsc.org/en/content/articlehtml/2011/lc/c0lc00516a%20https://pubs.rsc.org/en/content/articlelanding/2011/lc/c0lc00516a.

[164] International Organization for Standardization. *ISO Reinraumklassen*. 2015. URL: https://www.iso.org/obp/ui/#iso:std:iso:14644:-1:ed-2:v1:en.

[165] Pamela A. Mosier-Boss and Steven H. Lieberman. “Comparison of Three Methods to Improve Adherence of Thin Gold Films to Glass Substrates and Their Effect on the SERS Response:” in: *http://dx.doi.org/10.1366/00* 53.7 (Aug. 2016), pp. 862–873. DOI: 10.1366/0003702991947469. URL: https://journals.sagepub.com/doi/abs/10.1366/0003702991947469.

[166] Wayne Rasband. *Software: Circularity Fiji Plugin*. Aug. 2000. URL: https://imagej.nih.gov/ij/plugins/circularity.html.

[167] Chiara Moriconi et al. “INSIDIA: A FIJI Macro Delivering High-Throughput and High-Content Spheroid Invasion Analysis”. In: *Biotechnology journal* 12.10 (Oct. 2017). ISSN: 1860-7314. DOI: 10.1002/BIOT.201700140. URL: https://pubmed.ncbi.nlm.nih.gov/28786556/.

[168] Bastian R. Brückner and Andreas Janshoff. “Elastic properties of epithelial cells probed by atomic force microscopy”. In: *Biochimica et Biophysica Acta (BBA) - Molecular Cell Research* 1853.11 (Nov. 2015), pp. 3075–3082. ISSN: 0167-4889. DOI: 10.1016/J.BBAMCR.2015.07.010.

[169] Abolfazl Barzegari et al. “The role of Hippo signaling pathway and mechanotransduction in tuning embryoid body formation and differentiation”. In: *Journal of Cellular Physiology* 235.6 (June 2020), pp. 5072–5083. ISSN: 1097-4652. DOI: 10.1002/JCP.29455. URL: https://onlinelibrary.wiley.com/doi/full/10.1002/jcp.29455%20https://onlinelibrary.wiley.com/doi/abs/10.1002/jcp.29455%20https://onlinelibrary.wiley.com/doi/10.1002/jcp.29455.

[170] K. C. Hribar et al. “Nonlinear 3D projection printing of concave hydrogel microstructures for long-term multicellular spheroid and embryoid body culture”. In: *Lab on a Chip* 15.11 (June 2015), pp. 2412–2418. ISSN: 14730189. DOI: 10.1039/C5LC00159E. URL: https://pubs.rsc.org/en/content/articlehtml/2015/lc/c5lc00159e%20https://pubs.rsc.org/en/content/articlelanding/2015/lc/c5lc00159e.

[171] Jaesung Park et al. “Microfabrication-based modulation of embryonic stem cell differentiation”. In: *Lab on a Chip* 7.8 (July 2007), pp. 1018–1028. ISSN: 1473-0189. DOI: 10.1039/B704739H. URL: https://pubs.rsc.org/en/content/articlehtml/2007/lc/b704739h%20https://pubs.rsc.org/en/content/articlelanding/2007/lc/b704739h.

[172] Katherine W. Rogers and Alexander F. Schier. “Morphogen Gradients: From Generation to Interpretation”. In: *http://dx.doi.org/10.1146/annurev-cellbio-092910-154148* 27 (Oct. 2011), pp. 377–407. ISSN: 10810706. DOI: 10.1146/ANNUREV-CELLBIO-092910-154148. URL: https://www.annualreviews.org/doi/abs/10.1146/annurev-cellbio-092910-154148.

Die approbierte gedruckte Originalversion dieser Diplomarbeit ist an der TU Wien Bibliothek verfügbar
The approved original version of this thesis is available in print at TU Wien Bibliothek.

[173] David R. Lide. *Handbook of Chemistry and Physics, Edition 88th*. 88th ed. CRC Press, 2007. ISBN: 0849304881. URL: `https://vdoc.pub/documents/crc-handbook-of-chemistry-and-physics-88th-edition-672937loskn0`.

[174] Zhangxian Chen et al. "Fabrication of highly transparent and conductive indium-tin oxide thin films with a high figure of merit via solution processing". In: *Langmuir* 29.45 (Nov. 2013), pp. 13836–13842. ISSN: 07437463. DOI: `10.1021/LA4033282/SUPPL{\_}FILE/LA4033282{\_}SI{\_}001.PDF`. URL: `https://pubs.acs.org/doi/abs/10.1021/la4033282`.

[175] Constance Hammond and François Michel. *The voltage-gated channels of Ca2+ action potentials: Generalization*. Elsevier Inc., Jan. 2015, pp. 93–120. ISBN: 9780123970329. DOI: `10.1016/B978-0-12-397032-9.00005-4`.

[176] Veli Ozbolat et al. "3D Printing of PDMS Improves Its Mechanical and Cell Adhesion Properties". In: *ACS biomaterials science & engineering* 4.2 (Feb. 2018), pp. 682–693. ISSN: 2373-9878. DOI: `10.1021/ACSBIOMATERIALS.7B00646`. URL: `https://pubmed.ncbi.nlm.nih.gov/33418756/`.

Die approbierte gedruckte Originalversion dieser Diplomarbeit ist an der TU Wien Bibliothek verfügbar
The approved original version of this thesis is available in print at TU Wien Bibliothek.
TU WIEN Bibliothek Your knowledge hub

Die approbierte gedruckte Originalversion dieser Diplomarbeit ist an der TU Wien Bibliothek verfügbar
The approved original version of this thesis is available in print at TU Wien Bibliothek.